DYNAMIC SOIL-STRUCTURE INTERACTION:
PILE FOUNDATIONS AND RETAINING STRUCTURES

By

Guoxi WU

B.Eng. Nanjing Institute of Architectural Engineering, 1984

M.A.Sc. Tongji University, Shanghai, PRC, 1987

M.A.Sc. The University of British Columbia, Canada, 1992

A THESIS SUBMITTED IN PARTIAL FULFILLMENT OF

THE REQUIREMENTS FOR THE DEGREE OF

DOCTOR OF PHILOSOPHY

in

THE FACULTY OF GRADUATE STUDIES

CIVIL ENGINEERING

We accept this thesis as conforming

to the required standard

THE UNIVERSITY OF BRITISH COLUMBIA

August 10, 1994

(Signature)

Department of ___Civil Engineering___

The University of British Columbia
Vancouver, Canada

Date ___Oct. 7, 1994___

DE-6 (2/88)

ABSTRACT

This thesis deals with two important topics in soil-structure interaction: seismic earth pressures against rigid walls and the seismic response of pile foundations. These two disparate problems are linked by a common method of solution which is an approximation to the response of the half-space, either linear or non-linear.

The approximate formulation permits analytical solutions against rigid walls when the backfill is uniform and elastic. The solution agrees very closely with an existing exact solution. For elastic non-homogeneous backfills and for non-linear soil response the approximate formulation is expressed using the finite element method.

An efficient computer program SPAW has been developed to determine dynamic thrusts and moments against rigid walls for arbitrary non-homogeneous soil layers. Results of analyses show that the peak dynamic thrusts are larger for a uniform soil profile than when the shear modulus of the soil varies linearly or parabolically with depth. The program SPAW also possesses the ability of modelling the effect of soil non-linearity on dynamic thrusts. Studies showed that an increase of peak dynamic thrust may be expected due to soil non-linearity, compared with results from a linear elastic analysis.

A quasi-3D finite element method of analysis has been proposed to determine dynamic response of pile foundations subjected to horizontal loading. A computer program PILIMP has been developed for the analyses of elastic response of pile foundations including the determination of pile impedances as a function of frequency. The analysis

is conducted in the frequency domain. The program can analyze single piles and pile groups in arbitrary non-homogeneous soil layers.

Another quasi-3D finite element computer program PILE3D has been developed for the analysis of non-linear response of pile foundations in the time domain. The program is suitable of dynamic analyses of single piles and pile groups. The soil non-linearity during shaking is modelled using a modified equivalent linear method. Yielding of the soil is taken into account and there is a no-tension option controlling the analysis.

The proposed quasi-3D model has been validated using the elastic solutions from Kaynia and Kausel (1982), Novak and Nogami (1977) and Novak (1974), Fan et al. (1991), data from full scale vibration tests of a single pile and a 6-pile group, and data from centrifuge tests of a single pile and a 2x2 pile group under strong shaking from simulated earthquake. Excellent results have been obtained using the proposed method. Time-dependent variations of dynamic impedances of pile foundations during shaking have been evaluated for the model pile foundations used in the centrifuge tests. The analyses quantify the reduction in the stiffnesses of the pile foundations with the increased level of shaking. The translational stiffness k_{vv} decreases the most during strong shaking; the rotational stiffness $k_{\theta\theta}$ decreases the least. However, the damping of pile foundations increases with the level of shaking.

Table of Contents

List of Tables

List of Figures

x

Acknowledgement

The author sincerely thanks his research supervisor, Professor W.D. Liam Finn, for his guidance, suggestions and encouragement during the course of research and preparation of this thesis.

The author also wishes to thank Professors P.M. Byrne, Y.P. Vaid, Dr. R. J. Fannin of UBC and Dr. M. K. Lee of B. C. Hydro for serving as members of the supervisory committee and for reviewing the manuscript. Appreciation is also extended to other faculty members in the Dept. of Civil Engineering for offering many excellent courses which established the cornerstone of this research.

The postgraduate fellowship awarded by the Canadian National Science and Engineering Research Council and the research assistantship provided by the University of British Columbia are gratefully acknowledged.

Finally, the author would like to thank his wife Lillian for her love and faithful support over the course of preparation of this thesis. This thesis is dedicated to her and our sons, Galen and Allan.

Chapter 1

Introduction

This thesis deals with two important topics in soil-structure interaction: seismic earth pressures against rigid walls and the seismic response of pile foundations. These two disparate problems are linked by a common method of solution based on an approximation to the response of the half-space, either linear or non-linear. In the case of the pile foundations, the piles are modelled as linear beam element inclusions in the half space.

The rigid wall solution has important applications: seismic earth pressures against deep basement walls, buried containment structures and the wingwalls of dams. The seismic analysis of pile foundations remains a challenging problem both in engineering practice and in research. The action of pile foundations is a key element in evaluating properly the response of pile-supported buildings, bridges and offshore platforms to earthquake loading. Characterization of the stiffness and damping of pile foundations is a complex major task for large bridges with multiple points of seismic input. The method developed in this thesis for solving these two major soil-structure interaction problems is capable of simulating important features of seismic interaction.

The methodology used for solving the rigid-wall problem is essentially a 2-D plane strain application of the quasi-3D theory developed for dealing with more general 3-D soil-structure systems subjected to horizontal shaking. The basic idea of the proposed quasi-3D theory is that the dynamic motions excited in a 3-D half-space by shear waves

propagating vertically is governed primarily by compression waves propagating in the principal shaking direction and shear waves propagating in the two other directions. Other types of waves in the 3-D half-space are ignored in the analysis because they are assumed to be less significant. This assumption will be validated later using elastic solution based on a full 3-D formulation.

In the seismic analysis and design of rigid-wall systems, the basic challenge is to evaluate the magnitude and distribution of dynamic soil pressures against the walls induced by ground shaking. In addition to the evaluation of dynamic soil pressures against rigid walls with elastic homogeneous soil backfills, there are two important issues relative to rigid walls. The first issue is the accurate evaluation of dynamic soil pressures against rigid walls with arbitrary non-homogeneous backfills. The second issue is the appropriate modelling of soil non-linearity under relatively strong shaking. Therefore, a portion of this thesis is devoted to developing a cost-effective method for dealing with arbitrary non-homogeneous soil profile and soil non-linearity.

In the first part of this thesis, the 2-D plane strain formulation of the quasi-3D theory is used to obtain solutions of dynamic soil pressures against rigid walls with uniform backfills. Then the theory is implemented into an effective finite element program. The finite element method of analysis is used to explore the effect of soil non-homogeneity on dynamic pressures on rigid walls. Effect of soil non-linearity under strong shaking is also investigated.

The second part of this thesis is devoted to dynamic response of pile foundations subjected to horizontal shaking. Pile foundations are widely used in civil engineering

works. Pile-group foundations are used to support important structures such as high-rise buildings, bridges, and large power transmission towers. When these pile-supported structures are located in a seismic active zone, concerns arise on how piles, either individually or in groups, respond to earthquake loading. Many studies have been conducted on the dynamic response of pile foundations, most of which are restricted to elastic response.

This thesis describes the development of a cost-effective and reliable numerical procedure which can be used to study dynamic response of pile foundations when foundation soils are non-linear and nonhomogeneous. The quasi-3D theory is adopted to the dynamic analyses of pile foundations. A number of solutions for elastic homogeneous response have been developed in order to validate the proposed quasi-3D method by comparing the results with the published elastic solutions based on full-3D formulation.

OUTLINE OF THE THESIS

Chapter 2 gives a review of existing methods for determining dynamic soil pressures on rigid walls and presents objectives of the present research study.

Chapter 3 gives a simplified method of analysis for rigid wall-soil systems subjected to horizontal dynamic loads assuming linear elastic response of the soil. Analytical solutions of dynamic soil pressures against rigid walls with homogeneous soil backfills are derived first. Dynamic thrusts against rigid walls are determined using both sinusoidal motions and earthquake motions as input. The results from the present analysis are validated by comparison with the published results developed from full 2-D elastic response analysis by Wood (1973). Studies are made to examine the accuracy of the response spectrum method for determining peak dynamic thrust against rigid walls.

Chapter 4 extends the method of analysis to deal with rigid walls with an arbitrary nonhomogeneous soil profile. Analyses are performed to study the pattern of dynamic thrusts against rigid walls for nonhomogeneous soil profiles. Finally the effect of soil non-linearity on dynamic response of rigid walls is explored by using the equivalent linear approach (Seed and Idriss, 1967).

Chapter 5 gives a review for current methods of dynamic response analysis of pile foundations and outlines the objectives of this thesis for the analysis of pile foundations.

Chapter 6 presents a quasi-3D finite element method for dynamic response analysis of pile foundations assuming elastic response of soil and piles. The proposed model is verified first against elastic solutions of single piles by Kaynia and Kausel (1982). Then the proposed model is calibrated using data from a full-scale vibration test on a single pile.

Chapter 7 applies the proposed quasi-3D theory to the dynamic analysis of elastic response of pile groups. The proposed model for pile groups is verified first against elastic solutions by Kaynia and Kausel (1982) and then against results of a field vibration test on a 6-pile group by Crouse and Cheang (1987).

Chapter 8 applies the proposed quasi-3D theory to the dynamic analysis of pile foundations under earthquake loading taking the non-linear response of the soil into account. The non-linear finite element analysis is conducted in the time domain. Procedures for modelling non-linear soil response are also described in this chapter.

Chapter 9 describes the validation of the proposed model for non-linear dynamic response of pile foundations using data from centrifuge tests of a single pile and a 2x2 pile group. The variations of dynamic impedances of pile foundations with time during shaking are also evaluated and demonstrated for the model pile foundations.

Chapter 10 summarizes the developments described in earlier chapters and presents the conclusions arising from the various studies.

Part I

Dynamic Thrusts on Rigid Walls

Chapter 2

Dynamic analyses of rigid walls

2.1 Literature review

For seismic design of a rigid wall it is important to know the magnitude and distribution of seismic pressure on the wall induced by earthquake motion. Probably the earliest researches dealing with seismic induced earth pressure on retaining structures were those of Mononobe (1929) and Okabe (1926). The Mononobe-Okabe method is the modification of Coulomb's classic earth pressure theory which takes into account the inertia forces caused by earthquake accelerations. Seed and Whitman (1970) made a detailed evaluation of the Mononobe-Okabe method. One of the basic requirements of applying the Mononobe - Okabe method is that the wall has to move sufficiently to create a limit equilibrium state in the backfill. This condition is not satisfied in most rigid wall cases.

Several researchers have used elastic wave theory to derive seismic backfill pressure against a rigid wall. Matuo and Ohara (1960) obtained an approximate elastic solution for the dynamic soil pressure on a rigid wall using a two-dimensional analytical model. They simplified the problem by assuming zero vertical displacement in the soil mass. This simplification leads to infinitely large wall pressure when Poisson's ratio of the soil is equal to 0.5 as in a fully saturated undrained backfill. Scott (1973) used a one-dimensional elastic shear beam connected to the wall by Winkler springs to model the problem. The advantage of this model is that close-form solutions can easily be obtained.

The disadvantage is that his solution requires a representative value of the Winkler spring constant. Scott used Wood's (1973) solutions to define the characteristics of the Winkler spring constant. However, the Winkler spring constant was determined only for the first-mode motion. For a wall with relatively long backfill ($L^*/H > 4$), the accuracy of Scott's first-mode solution deteriorates rapidly with the increase of L^*/H ratio.

Wood (1973) made a comprehensive study on the behaviour of the rigid soil-retaining structures subjected to earthquake motions. His work is considered to be one of the more important contributions to understanding of this problem.

Wood's solution of rigid-wall problem. In Wood's solution, the soil is assumed to be an isotropic homogeneous elastic material. The wall-soil system was assumed to satisfy the condition of plane strain. The analytical solutions were obtained assuming a smooth contact between the wall and the backfill; that is, the vertical boundaries are assumed to be free from shear stresses. Figure 2.1 shows the rigid-wall soil system used in Wood's study and the associated boundary conditions.

The modal frequencies ω_{nm} for the wall-soil system shown in Figure 2.1 are not explicitly expressed in Wood's solution. For the homogeneous backfill, the modal frequency ω_{nm} is governed by

$$\alpha^2 = r^2 - \frac{\omega_{nm}^2}{V_p^2} \qquad (2.1)$$
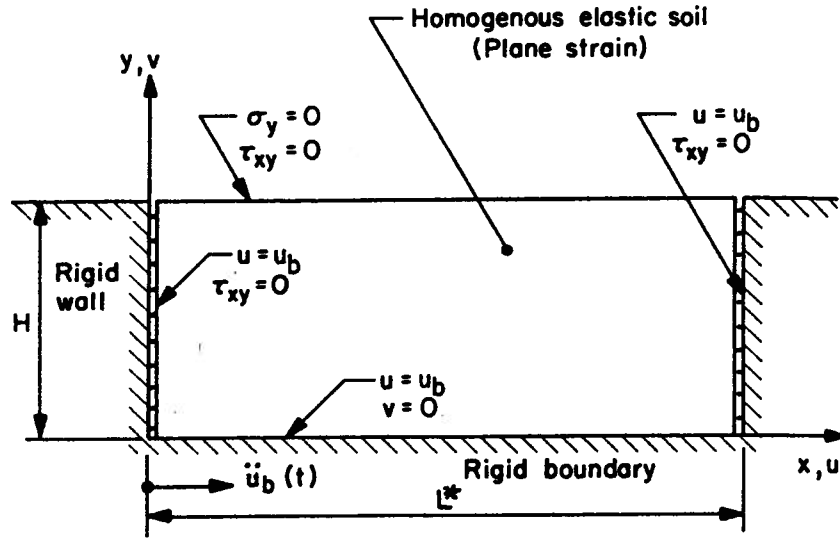
RIGID WALL PROBLEM

Figure 2.1: Wall-soil system used in Wood's study (after Wood, 1973)

and

$$\beta^2 = r^2 - \frac{\omega_{nm}^2}{V_s^2} \tag{2.2}$$

where V_p, V_s are the compression wave velocity and shear wave velocity of soil, $r = \frac{n\pi}{L^*}$, and parameters α, β have particular values for each mode. They must satisfy the following equation

$$\{4\alpha\beta + \frac{(r^2 + \beta^2)^2}{\alpha\beta}\} \sinh \alpha H \cdot \sinh \beta H -$$
$$\{4r^2 + \frac{(r^2 + \beta^2)^2}{r^2}\} \cosh \alpha H \cdot \cosh \beta H + 4(r^2 + \beta^2) = 0 \tag{2.3}$$

The roots of the frequency equations were numerically evaluated using Newton's method on a digital computer. An iterative process was used to compute the roots indicated by sign changes in the frequency equations.

It can be seen that the frequency solution is too complicated to apply in practice. Although graphic solutions of modal frequency were given by Wood, these solutions are limited to particular values of Poisson's ratio. Furthermore modal frequencies are not available when the soil backfill is non-homogeneous, which is normally the case encountered in reality.

The complex-amplitudes of steady-state wall force for a one-g-amplitude harmonic base forcing were presented in Wood's study as

$$F_r'(\omega) = \Sigma\Sigma \frac{F_{nm}}{(1 - \frac{\omega^2}{\omega_{nm}^2}) + 2i\lambda_{nm}\frac{\omega}{\omega_{nm}}} \tag{2.4}$$

where F_{nm} is the static-one-g modal force per unit length. Mathematical expression of F_{nm} is not available in Wood's solution, but graphic results of F_{nm} were presented.

The one-g static force per unit length of wall was obtained by applying a static horizontal acceleration of one-g throughout the soil layer. The static force acting on the wall due to 1-g static horizontal loading, F_{sr}, is expressed as

$$\frac{F_{sr}}{\gamma H^2} = \frac{4}{\pi^3 k^2}(\frac{L^*}{H})^2 \Sigma_{n=1,3,5,\dots} \frac{1}{n^3} \{2B_n \sinh rH + C_n(2rH + k' + 1)e^{rH}$$
$$+D_n(-2rH + k' + 1)e^{-rH} - (C_n + D_n)(k' + 1) - k^2 rH\} \tag{2.5}$$

Where constants C_n, D_n, B_n are parameters associated with the nth mode and properties of soil. Their detailed formulations can be found in Wood (1973).

For a L^*/H ratio of 5.0, the force F_{sr} can be approximated satisfactorily using about 20 terms in Eq.2.5. A smaller number of terms are required for L^*/H less than 5.0 and

a larger number for L^*/H greater than 5.0.

Wood's solution is quite complicated even under very idealistic conditions of a homogeneous soil layer under harmonic loading. Therefore, in engineering practice Wood's solution is applied approximately. The dynamic thrust is approximately taken as $\gamma H^2 A$ (Whitman, 1991) for a horizontal acceleration Ag, which is the static force for a wall-soil system with $L^*/H{=}10$ and $\nu = 0.4$. The use of this expression must be justified in many cases especially at resonance when the fundamental frequency of the wall-soil system is very close to the predominant frequency of the excitation motion. At resonant condition the dynamic thrust are likely to be much greater than the static force.

For earthquake type of loading, Wood (1973) states " In view of the uncertainties inherent in the estimation of earthquake-induced pressures on walls, computation of the response time-history is probably not warranted and approximate evaluation may often be satisfactory". Wood proposed that the response spectrum method is applied to estimate the peak dynamic thrust on the wall for earthquake loading.

Although Wood's solution for dynamic thrust on rigid walls is mathematically correct for harmonic loading, uncertainties and difficulties arise when his method is applied in practice to the wall-soil system under earthquake loading. Significant errors of dynamic thrusts may be caused by using the response spectrum method proposed by Wood.

The other restriction of Wood's solution is that his method is not capable of dealing with rigid walls having arbitrarily nonhomogeneous backfills. In addition the effect of soil non-linearity on the dynamic thrust under strong motions cannot be assessed using Wood's method.

2.2 Objectives of current research

Due to the limitations of Wood's solution in engineering practice, the current research is targeted to find an effective method for determining the dynamic thrusts on rigid walls subjected to horizontal dynamic loads. A proposed method is used to analyze wall-soil systems with nonhomogeneous soil profiles and to study the effect of soil non-linearity on dynamic response.

The method of analysis is formulated based on simplified elastic wave equations. The equations of motion are established considering dynamic force equilibrium in the horizontal direction only. An analytical solution for dynamic pressures against rigid walls is derived first for homogeneous backfills. Under harmonic horizontal loading, peak dynamic thrusts against rigid walls are determined.

For earthquake loading, time-history response of dynamic thrust is determined using the mode-superposition method. The time-history response of each mode is added up in phase. The commonly used Response Spectrum method is also used to predict the peak dynamic thrust. The accuracy of the response spectrum method is evaluated against the rigorous mode-superposition method.

The proposed method is then applied to the wall-soil systems with nonhomogeneous backfills. A finite element program SPAW (Seismic Pressures Against Rigid Walls) was developed to implement the analysis. The computational time and cost for time-history analysis is negligible using SPAW. The dynamic analyses of nonhomogenous soil profiles

are illustrated through two types of soil profiles, soil profiles with linear and parabolic variations of shear moduli with depth. Analyses are performed for both harmonic loading and earthquake loading assuming elastic response.

The effect of soil non-linearity on dynamic thrusts against rigid walls was also studied. The equivalent linear approach (Seed and Idriss, 1967) is used to model non-linear soil response. The effect of the intensity of shaking on dynamic thrusts against rigid walls is investigated for soil profiles with parabolic variations of shear moduli with depth.

Chapter 3

Dynamic Thrusts on Rigid Walls with Uniform Elastic Backfills

3.1 Introduction

A method is proposed for determining the dynamic thrust against a rigid soil-retaining structure subjected to horizontal dynamic loads. The method is based on simplified elastic wave equations. The equation of motion is derived from dynamic force equilibrium in the horizontal direction only. Two types of waves, shear waves and compression waves, are considered to define the horizontal motions of the backfills.

The dynamic equation of motion is solved analytically taking into account the boundary conditions of the problem. The solution is applied first to obtain the total thrust acting on the wall due to horizontal one-g static loading to estimate the accuracy of the approximate solutions against Wood's exact solutions from the 2-D plane strain analysis.

Simple explicit expressions for computing the dynamic thrusts are presented for both sinusoidal motion and earthquake motion. Time history solutions of the dynamic thrusts for earthquake motions can be readily obtained using the mode superposition method. Studies were made to examine the different patterns of dynamic thrusts for harmonic loading and earthquake loading.

Finally the response spectrum method is applied to obtain the peak dynamic thrusts

for earthquake motions. The accuracy of the response spectrum method is also investigated.

3.2   Dynamic analysis of rigid wall-soil system

Figure 3.1(a) shows the geometry of the problem and its boundary conditions. A uniform elastic soil layer is confined by two vertical rigid walls at its two side boundaries and a rigid base. The soil layer has a total length of 2L and height of H. Subjected to horizontal seismic body force, the soil layer in the system generates an antisymmetric field of horizontal normal stresses σ_x with zero stresses $\sigma_x=0$ at x = L. The original wall-soil problem can be equivalently represented by half of its geometry using this antisymmetric condition. The equivalent problem is shown in Figure 3.1(b), and this is the physical model that will be analyzed. The ground acceleration is input at the base of the wall-soil system.

The soil is assumed to be a homogeneous, isotropic, visco-elastic solid with a shear modulus G and Poisson's ratio ν. The equations of dynamic force equilibrium for the backfill in the horizontal and vertical directions are written as

$$\frac{\partial \sigma_x}{\partial x} + \frac{\partial \tau_{xy}}{\partial y} = \rho \frac{\partial^2 u}{\partial t^2} \tag{3.1}$$

$$\frac{\partial \tau_{xy}}{\partial x} + \frac{\partial \sigma_y}{\partial y} = \rho \frac{\partial^2 v}{\partial t^2} \tag{3.2}$$

where σ_x and σ_y are the normal stresses in the X and Y directions, respectively, and τ_{xy} is the shear stress in the x-y plane. u and v are the displacements in the X and Y directions, respectively.

(a)

(b)
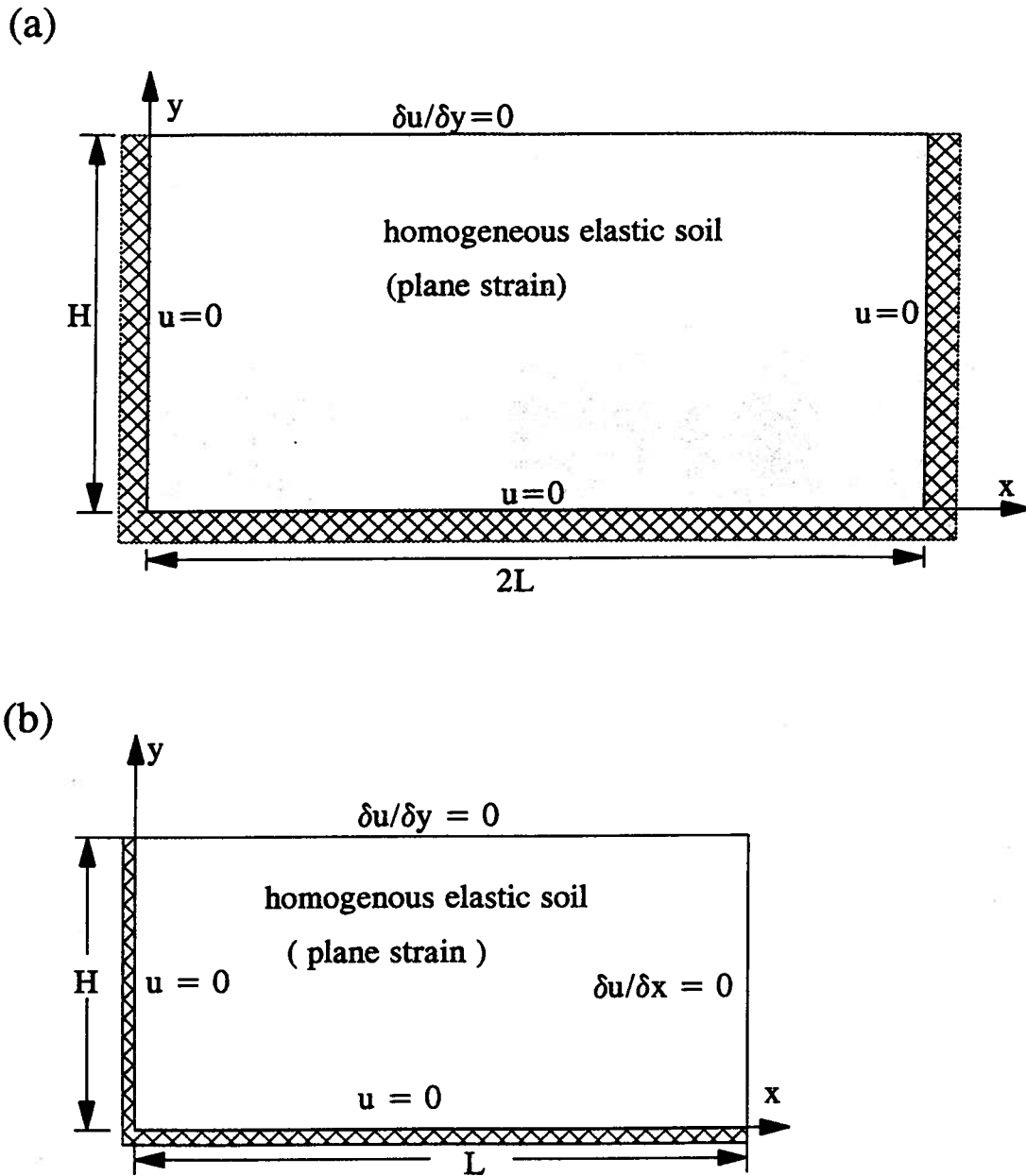
Figure 3.1: Definition of rigid-wall problem (a) original problem (b) equivalent problem by using antisymmetric condition

For the two-dimensional plane strain conditions, the stress components are related to the displacements by

$$\sigma_x = \frac{2G}{1 - 2\nu}[(1 - \nu)\frac{\partial u}{\partial x} + \nu\frac{\partial v}{\partial y}] \tag{3.3}$$

$$\sigma_y = \frac{2G}{1 - 2\nu}[(1 - \nu)\frac{\partial v}{\partial y} + \nu\frac{\partial u}{\partial x}] \tag{3.4}$$

$$\tau_{xy} = G(\frac{\partial u}{\partial y} + \frac{\partial v}{\partial x}) \tag{3.5}$$

Although the problem involves two displacement components u and v, only the horizontal displacement u is taken into account in the analysis to simply the solution of the problem. The equation of dynamic force equilibrium in the horizontal direction Eq.3.1 is used in the analysis. Considering various forms of approximation to the problem, the governing equation of the undamped free vibration of the backfill in the horizontal direction can be written as

$$\theta G\frac{\partial^2 u}{\partial x^2} + G\frac{\partial^2 u}{\partial y^2} = \rho\frac{\partial^2 u}{\partial t^2} \tag{3.6}$$

and the normal stress σ_x is given by

$$\sigma_x = \beta G\frac{\partial u}{\partial x} \tag{3.7}$$

where ρ is the mass density of the soil backfill, t is time, θ and β are functions of Poisson's ratio ν.

Eq. 3.6 suggests that the dynamic response of the backfill is governed by two types of waves: the shear wave and the compression wave. The compression wave in the backfill produces the dynamic earth pressure against the rigid wall given by Eq. 3.7.

The precise expressions for θ and β depend on the approximations used to model the wall-soil system. Three cases are examined and their corresponding expressions for θ and β are given below.

(i). $v=0$ assumption. In this case, the displacements in the vertical direction Y are assumed to be zero.

Using this assumption, σ_x and τ_{xy} are obtained from Eq. 3.3 and Eq. 3.5 as

$$\sigma_x = \frac{2(1-\nu)}{1-2\nu}G\frac{\partial u}{\partial x} \tag{3.8}$$

$$\tau_{xy} = G\frac{\partial u}{\partial y} \tag{3.9}$$

Substituting Eq. 3.8 and Eq. 3.9 into Eq. 3.1 and comparing with Eq. 3.6, one finds

$$\theta = \beta = \frac{2(1-\nu)}{1-2\nu} \tag{3.10}$$

(ii). $\sigma_y=0$ assumption. In this case, the normal stresses in the vertical direction Y are assumed to be zero.

Applying the assumption to Eq. 3.4, one finds that

$$\frac{\partial v}{\partial y} = -\frac{\nu}{1-\nu}\frac{\partial u}{\partial x} \tag{3.11}$$

Therefore, σ_x and $\partial \tau_{xy}/\partial y$ are obtained from Eq. 3.3 and Eq. 3.5 as

$$\sigma_x = \frac{2}{1-\nu}G\frac{\partial u}{\partial x} \tag{3.12}$$

$$\frac{\partial \tau_{xy}}{\partial y} = G\frac{\partial^2 u}{\partial y^2} - G\frac{\nu}{1-\nu}\frac{\partial^2 u}{\partial x^2} \qquad (3.13)$$

Substituting Eq. 3.12 and Eq. 3.13 into Eq. 3.1 and comparing with Eq. 3.6, one finds

$$\theta = \frac{2-\nu}{1-\nu} \qquad (3.14)$$

$$\beta = \frac{2}{1-\nu} \qquad (3.15)$$

(iii). the proposed model. In this case, the shear stresses are modelled using the shear beam analogy(see Appendix 1 for detail).

In this model, the shear stress τ_{xy} is given by

$$\tau_{xy} = G\frac{\partial u}{\partial y} \qquad (3.16)$$

The normal stress σ_x is found by assuming $\sigma_y=0$ in the backfill

$$\sigma_x = \frac{2}{1-\nu}G\frac{\partial u}{\partial x} \qquad (3.17)$$

Substituting Eq. 3.16 and Eq. 3.17 into Eq. 3.1 and comparing with Eq. 3.6, one finds

$$\theta = \beta = \frac{2}{1-\nu}$$

Three different models yield three different expressions for the coefficient θ in Eq. 3.6. However the dynamic response of the wall-soil system for these three cases can be represented by the same equation, Eq. 3.6. Therefore the general derivation of dynamic

solutions proceeds from Eq. 3.6.

Assume the displacement solution has the form

$$u(x, y, t) = \Sigma\Sigma(A \cdot \sin a_m x + B \cdot \cos a_m x)(C \cdot \sin b_n y + D \cdot \cos b_n y) \cdot Y_{mn}(t)$$

Applying the boundary conditions

$$u = 0......at..y = 0$$

$$u = 0......at..x = 0$$

The constants B and D are determined to be zero.

$$u(x, y, t) = \Sigma\Sigma C_1 \cdot \sin a_m x \cdot \sin b_n y \cdot Y_{mn}(t)$$

$$\frac{\partial u}{\partial x} = \Sigma\Sigma C_1 a_m \cdot \cos a_m x \cdot \sin b_n y \cdot Y_{mn}(t)$$

$$\frac{\partial u}{\partial y} = \Sigma\Sigma C_1 b_n \cdot \sin a_m x \cdot \cos b_n y \cdot Y_{mn}(t)$$

Applying the other two boundary conditions

$$\frac{\partial u}{\partial x} = 0......at..x = L$$

$$\frac{\partial u}{\partial y} = 0......at..y = H$$

one obtains

$$a_m \cdot \cos a_m L = 0$$

$$b_n \cdot \cos b_n H = 0$$

therefore

$$b_n = \frac{(2n-1)\pi}{2H} \tag{3.18}$$

$$a_m = \frac{(2m-1)\pi}{2L} \tag{3.19}$$

The mode shape functions are written as

$$\Phi_{mn}(x,y) = C_1 \sin b_n y \cdot \sin a_m x \tag{3.20}$$

and the displacement solution becomes

$$u(x,y,t) = \Sigma\Sigma\Phi_{mn}(x,y) \cdot Y_{mn}(t) \tag{3.21}$$

Substituting Eq. (3.21) into 3.6, one obtains

$$-G(\theta a_m^2 + b_n^2) \cdot Y_{mn}(t) = \rho \ddot{Y}_{mn}(t)$$

$$-\frac{G}{\rho}(\theta a_m^2 + b_n^2) = \frac{\ddot{Y}_{mn}(t)}{Y_{mn}(t)} = -\omega_{mn}^2$$

the natural frequencies of the system are found to be

$$\omega_{mn}^2 = \frac{G}{\rho}(b_n^2 + \theta a_m^2) \tag{3.22}$$

the frequency of the first mode is

$$\omega_{11}^2 = \frac{G\pi^2}{4\rho H^2}(1 + \theta\frac{H^2}{L^2}) \tag{3.23}$$

In the case of an undamped forced vibration subjected to a ground acceleration $\ddot{u}_0(t)$, the governing equation becomes

$$\rho\frac{\partial^2 u}{\partial t^2} - (\theta G\frac{\partial^2 u}{\partial x^2} + G\frac{\partial^2 u}{\partial y^2}) = -\rho\ddot{u}_0(t) \tag{3.24}$$

Substituting Eq. (3.21) into Eq. (3.24), multiplying the equation by the mode shape functions, and integrating over the domain, one obtains that

$$\int\int \rho \Sigma\Sigma\Phi_{ij}\ddot{Y}_{ij}(t)\cdot\Phi_{mn}dxdy + \int\int \Sigma\Sigma G(\theta a_i^2 + b_j^2)\Phi_{ij}Y_{ij}\cdot\Phi_{mn}dxdy = -\ddot{u}_0(t)\int\int \rho\Phi_{mn}(x,y)\cdot dxdy$$

Applying the orthogonality conditions and recalling Eq. (3.22), one obtains

$$\int\int \rho\Phi_{mn}^2 dxdy \cdot \ddot{Y}_{mn}(t) + \int\int \rho\Phi_{mn}^2 dxdy \cdot \omega_{mn}^2 Y_{mn}(t) = -\ddot{u}_0(t)\int\int \rho\Phi_{mn}(x,y)\cdot dxdy$$

$$\ddot{Y}_{mn}(t) + \omega_{mn}^2 \cdot Y_{mn}(t) = -\ddot{u}_0(t)\cdot\alpha_{mn}$$

where

$$\alpha_{mn} = \frac{\int\int \rho\sin(a_m x)\cdot\sin(b_n y)dx.dy}{\int\int \rho\sin^2(a_m x)\cdot\sin^2(b_n y)dx.dy}$$

$$\alpha_{mn} = \frac{16}{(2m-1)(2n-1)\pi^2} \tag{3.25}$$

Let $Y_{mn}(t) = \alpha_{mn}\cdot f_{mn}(t)$,

$$\ddot{f}_{mn}(t) + \omega_{mn}^2 \cdot f_{mn}(t) = -\ddot{u}_0(t) \tag{3.26}$$

For a damped forced vibration of the wall-soil system, a constant modal damping ratio λ is introduced

$$\ddot{f}_{mn}(t) + 2\lambda\omega_{mn}\cdot\dot{f}_{mn}(t) + \omega_{mn}^2 \cdot f_{mn}(t) = -\ddot{u}_0(t) \tag{3.27}$$

For a given ground excitation $\ddot{u}_0(t)$, a close-form solution of the displacement u is found to be

$$u(x,y,t) = \Sigma\Sigma \sin a_m x \cdot \sin b_n y \cdot \alpha_{mn}\cdot f_{mn}(t)$$

where $f_{mn}(t)$ is the time history solution of Eq. (3.27) corresponding to a particular modal frequency ω_{mn}. It is noted that Eq. (3.27) is the standard damped vibration equation of a single degree of freedom system.

The dynamic earth pressure acting on the wall is determined to be the normal stress σ_x at x=0. The dynamic pressure distribution along the wall is

$$\sigma_x(x,y,t)_{x=0} = \beta G \frac{\partial u}{\partial x}|_{x=0}$$

$$\sigma_x(x,y,t)_{x=0} = \beta G \Sigma \Sigma a_m \alpha_{mn} \cdot \sin(b_n y) \cdot f_{mn}(t)$$

The total dynamic thrust acting on the wall is

$$P(t) = \int_0^H \sigma_x(x,y,t)_{x=0} \cdot dy$$

$$P(t) = \beta G \cdot \Sigma \Sigma \frac{a_m \cdot \alpha_{mn}}{b_n} f_{mn}(t)$$

$$P(t) = \beta G \cdot \Sigma \Sigma \frac{16 f_{mn}(t)}{\pi^2 (2n-1)^2 L/H} \qquad (3.28)$$

The total dynamic moment acting at the base of the wall is

$$M(t) = \int_0^H y \cdot \sigma_x(x,y,t)_{x=0} \cdot dy$$

$$M(t) = \beta G \cdot \Sigma \Sigma \frac{a_m \cdot \alpha_{mn} \cdot \sin(b_n H)}{b_n^2} f_{mn}(t) \qquad (3.29)$$

For a harmonic input $\ddot{u}_0(t) = A_{max} \cdot e^{i\omega t}$, the amplitude of the steady-state response $f_{mn}(t)$ is found from Eq. 3.27 to be

$$f_{mn} = -\frac{A_{max}}{(\omega_{mn}^2 - \omega^2) + 2i \cdot \lambda \omega_{mn} \cdot \omega} \qquad (3.30)$$

For any excitation $\ddot{u}_0(t)$ the time history of the modal dynamic thrust associated with a particular mode is obtained using Eq. (3.28). The time-history of the dynamic thrust for the desired number of modes are then determined using the mode-superposition method. Therefore the peak dynamic thrust acting on the wall can be determined exactly for any type of input motion.

For earthquake motion the peak modal thrust acting on the wall associated with the modal frequency ω_{mn} could be determined using the pseudo-spectral velocity S_v^{mn}. The pseudo-spectral velocity S_v^{mn} is derived from response spectral displacement S_d^{mn} by

$$S_v^{mn} = \omega_{mn} \cdot S_d^{mn} \tag{3.31}$$

where S_d^{mn} is also the peak of $f_{mn}(t)$ corresponding to an excitation frequency ω_{mn}. From Eq. 3.28 the peak modal thrust P_{mn} is determined as

$$P_{mn} = \beta G \frac{16}{\pi^2 (2n-1)^2 L/H} \frac{S_v^{mn}}{\omega_{mn}} \tag{3.32}$$

Estimation of the peak dynamic thrust is made by combining the individual peak modal thrusts by some approximate method. Either the absolute summation or the root square summation of the peak modal thrust is commonly used.

3.3   Static 1-g solution: Validation of model

In the previous section, three models namely, $v = 0$, $\sigma_y = 0$, and the proposed model, were presented which yielded different expressions for the coefficient θ in Eq. 3.6. It is necessary to examine the accuracy of solution provided by each model. Wood's rigorous solution (Wood, 1973) provides a measure for evaluating the accuracy of the approximate

solutions. Wood's solution for 1-g static horizontal loading is given in Eq. 2.5.

To allow a measure of the accuracy of the approximate solutions, a 1-g static solution is derived using the proposed approximate method. The 1-g static solution is the limit dynamic solution when the period of the dynamic motion becomes infinitely long. From Eq. 3.27 the static deflection produced by a 1-g static force is given by

$$f_{mn}(t) = \frac{g}{\omega_{mn}^2} \tag{3.33}$$

The corresponding 1-g static thrust is obtained by substituting Eq. 3.33 into Eq. 3.28

$$P_{st} = G\beta g \Sigma\Sigma \frac{16}{\pi^2 (2n-1)^2 \omega_{mn}^2 L/H} \tag{3.34}$$

The 1-g static moment acting at the base of the wall is obtained from Eq. 3.29

$$M_{st} = G\beta g \Sigma\Sigma \frac{a_m \cdot \alpha_{mn} \cdot \sin(b_n H)}{b_n^2 \omega_{mn}^2} \tag{3.35}$$

The total thrust against the wall due to 1-g static horizontal force is determined by doing a double summation for modes m and n from Eq. (3.34). A normalized thrust ratio is introduced and defined as

$$THRUST \cdot RATIO = \frac{TOTAL \cdot THRUST}{\rho H^2 A_{max}} \tag{3.36}$$

where A_{max} is the peak ground acceleration in m/sec^2, ft/sec^2 or other consistent unit.

Comparison of the accuracy of approximate solutions The approximate solutions are used to obtain the total 1-g static force for two wall-soil systems: one with a

semi-infinite backfill and the other one with a finite backfill. The semi-infinite backfill is approximated by using L/H=5.0 and the finite backfill is represented by using L/H=1.5. Results from the different analyses are compared in Figure 3.2 (a) and 3.2 (b) for L/H=5.0 and L/H=1.5, respectively. The following observations may be made based on the results.

The proposed model gives results that are in very good agreement with Wood's exact results for both L/H=5.0 and L/H=1.5. The approximation of the proposed model works even better for walls retaining finite backfill (L/H=1.5). Usually this model gives total force slightly less than the exact total force.

The $\sigma_y=0$ model yields results that are in very good agreement with the exact results for L/H=5.0. For wall-soil systems with L/H=5.0, the accuracy of the $\sigma_y=0$ model is comparable to that of the proposed model. The difference between the two models is that the $\sigma_y=0$ model overestimates the response but the proposed model underestimates the response slightly.

However for L/H=1.5, the $\sigma_y=0$ model does not give as good results as the proposed model does. The solutions from the proposed model are much closer to the exact solutions than those from the $\sigma_y=0$ model. The $\sigma_y=0$ model may overestimate the total force by about 18%. The proposed model only underestimates the total force by 4%.

When the $v=0$ model is applied, the accuracy of the solution is very good provided $\nu < 0.3$. As ν exceeds 0.3, the solutions start to deviate from the exact solutions. For L/H=5.0, the accuracy of the solution from the $v=0$ model becomes unacceptable as $\nu > 0.4$.

Recently Veletsos and Younan (1994) made studies on rigid walls with horizontally
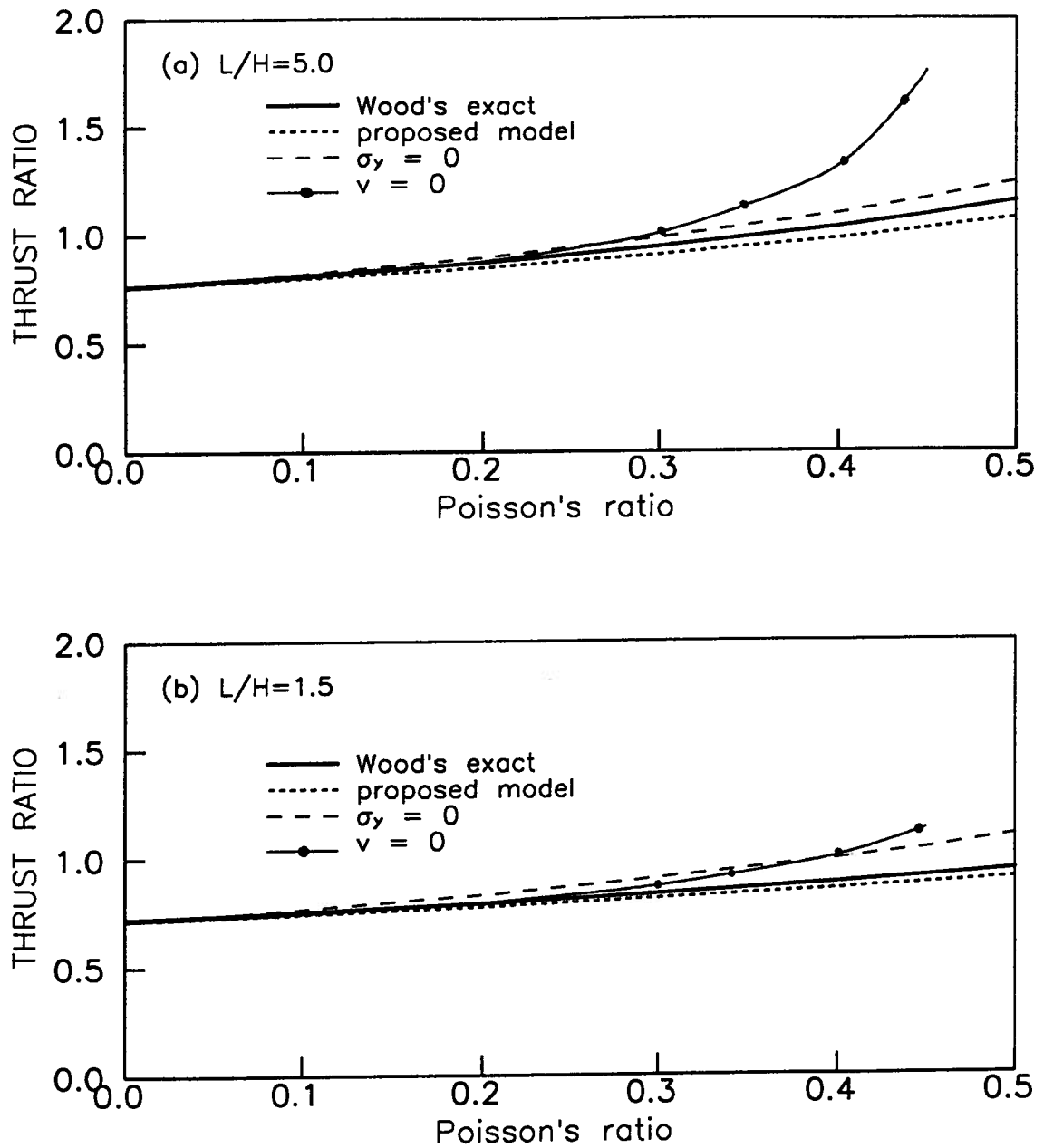
Figure 3.2: Comparison of the accuracy of approximate solutions for rigid-wall systems (a) L/H=5.0 (b) L/H=1.5

semi-infinite backfills. The accuracy of the $\sigma_y=0$ model and $v=0$ model were examined in that paper against Wood's rigorous solution. They reached similar conclusions to the above regarding the accuracy of these two models. Their conclusions were made for the semi-infinite backfills only, which is similar to the case with L/H=5.0.

The studies presented conclude that the proposed model gives the best approximation to solutions for the rigid-wall systems with infinite backfills and finite backfills. Therefore, the proposed model will be used for all further studies with $\theta = \beta = 2/(1 - \nu)$.

Static 1-g solution using $\theta = 2/(1 - \nu)$ Additional analyses were carried to study the accuracy of the solution for the entire range of L/H ratios. Figure 3.3(a) and Figure 3.3(b) show the relationship between the normalized thrust ratios and the L/H ratios for $\nu = 0.3$, 0.4 and 0.5. The results from Wood's study (Wood, 1973) are shown in Figure 3.3(a), and the results from this study are shown in Figure 3.3(b). The two solutions agree fairly well for the entire range of L/H ratio. In general, the thrust ratios determined from this study are about 5 % less than that predicted by Wood. Although Wood's solution that was obtained from a 2-dimensional plane strain analysis is more accurate than that from this study, the small amount of error in the thrust ratio is compensated for by the convenience of using the much simpler expression of the total thrust shown in Eq. (3.34). The simplicity in determination of the total thrust leads to ready application in engineering.

The thrust ratios plotted in Figure 3.3 are found to be independent of the shear modulus G of the backfill. The total thrusts increase with the increase of L/H ratio, but they approach steady values for L/H > 4. For L/H=5.0 and $\nu = 0.4$, the total thrust under
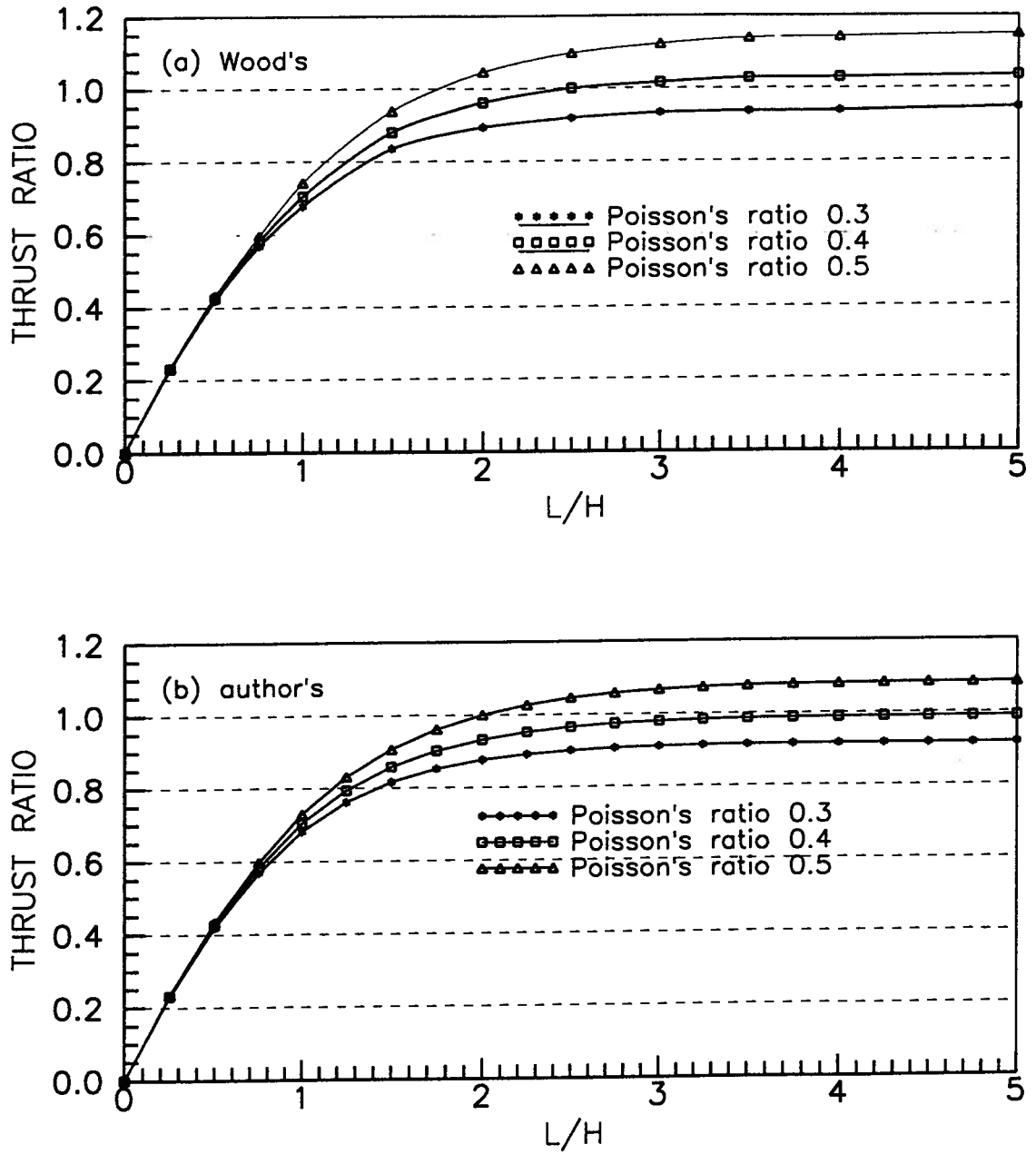
Figure 3.3: Normalized thrust ratios for 1-g static solution(a) Wood's solution (b) author's solution
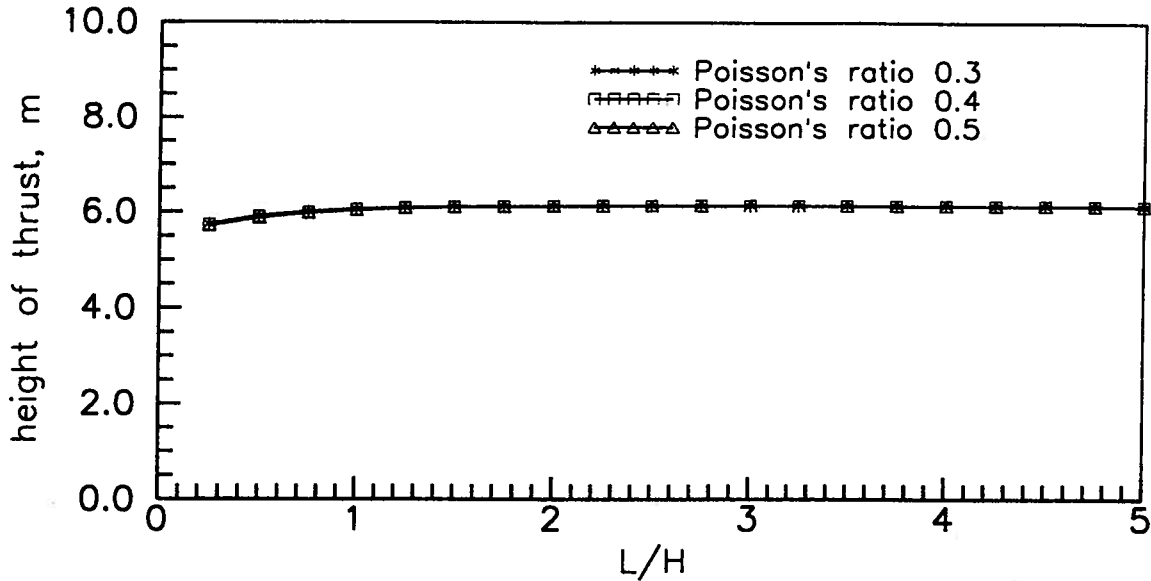
Figure 3.4: Heights of thrusts due to 1-g static horizontal force (wall height H=10m)

1-g static horizontal force is estimated to be $1.0\ \gamma H^2$. For a 10m high wall and a backfill with unit weight $\gamma=19.6\ kN/m^3$, the total thrust is calculated to be 1960 kN for per unit wide wall. For values of ν other than 0.3, 0.4 and 0.5, the 1-g static thrusts are easily obtained using Eq. (3.34).

The height of the resultant thrust above the base of the wall due to the 1-g static horizontal force is plotted in Figure 3.4 against the L/H ratio for $\nu = 0.3$, 0.4 and 0.5. The heights of resultant thrusts are identical for $\nu = 0.3$, 0.4 and 0.5. They remain constant when L/H is greater than 1.0. The heights of the resultant thrusts are about 0.6H above the base of the wall.

3.4 Dynamic thrusts under sinusoidal motions

Dynamic amplification of structural response depends on the ratio of the frequency of the input excitation to the fundamental frequency of the structure. Resonant response occurs when the excitation frequency matches the fundamental frequency. For wall-soil systems, a simple approach is to take the fundamental frequency of the backfill ω_s to approximate the frequency of the system. This representation is especially useful for wall-soil systems with long backfills, where the fundamental frequency of the wall-soil system is very close to the fundamental frequency of the backfill. However, for wall-soil systems with finite backfills, the fundamental frequency of the combined wall-soil system ω_{11} is more critical.

Therefore, two frequency ratios f_{R1} and f_{R2} are used to investigate the dynamic amplification of the wall-soil systems. The frequency ratio f_{R1} is defined by the ratio between the angular frequency ω of the input motion and the natural angular frequency ω_s of the fundamental mode of the infinite horizontal backfill. The frequency ratio f_{R1} is quantitatively expressed as

$$f_{R1} = \omega/\omega_s \qquad (3.37)$$

For a uniform soil profile, ω_s is determined by $\omega_s = V_s\pi/2H$, in which V_s is the shear wave velocity of the backfill.

The frequency ratio f_{R2} is defined by the ratio between the angular frequency of the input motion (ω) and the fundamental angular frequency (ω_{11}) of the wall-soil system. The frequency ratio f_{R2} is expressed as

$$f_{R2} = \omega/\omega_{11} \qquad (3.38)$$
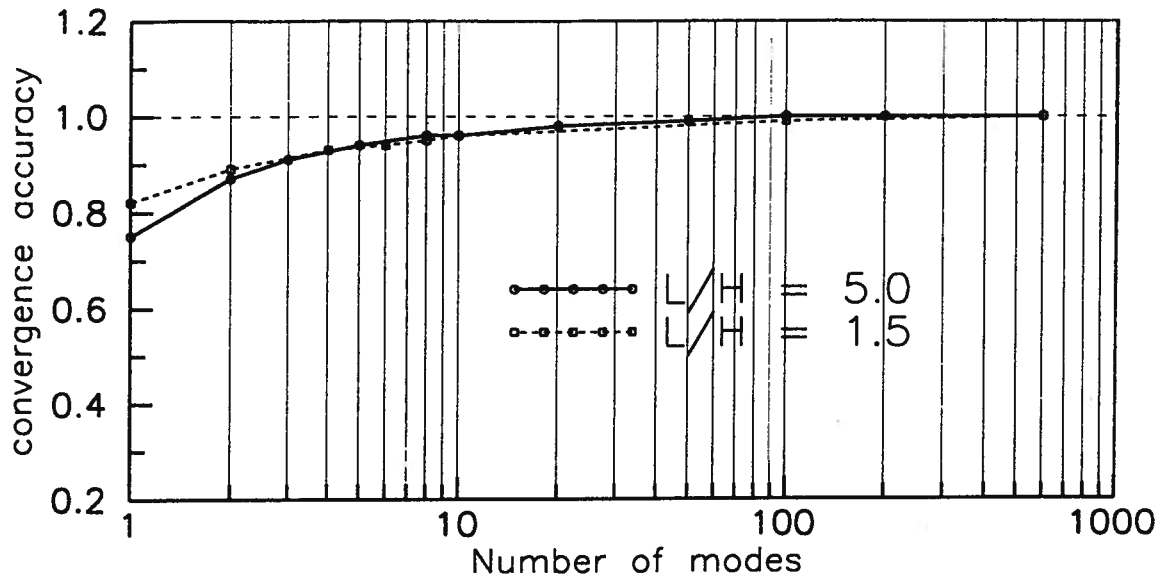
Figure 3.5: Accuracy of solutions versus number of modes used

For a uniform soil profile, the fundamental angular frequency ω_{11} of the wall-soil system can be determined by using Eq. 3.23.

Before proceeding with the analysis of dynamic amplification as a function of frequency ratio, studies were made first to examine the relationship between the accuracy of solutions and the number of modes used. Figure 3.5 shows the accuracy of dynamic thrust obtained using increasing number of modes in the dynamic solution. Analyses were carried out at one randomly selected frequency for each L/H ratio. Frequencies corresponding to $f_{R1} = 1.0$ and $f_{R1} = 1.14$ were used for L/H = 5.0 and L/H = 1.5, respectively. For all analyses $\nu = 0.4$ and $\lambda = 10\%$ were used.

The solutions converged very fast for the problems investigated. By just using the first mode, about 75% accuracy in the solutions was achieved for L/H=5.0 and 82% for L/H=1.5. Excellent accuracy (95%) was obtained by using the first 10 modes. Although

a much smaller number of modes could be used to compute the dynamic response adequately for engineering purpose, 600 modes were used here to get an 'exact' solution for assessing the accuracy of the results. From Eq. 3.28, it can be seen that the solution converges very fast as the number of mode n increases. The number of mode n required is usually much less than the number of mode m required in the dynamic solution. Studies also showed that a larger number of mode n is necessary for wall-soil systems with smaller L/H ratios. Therefore a combination of n=2 and m=300 was used for L/H=5.0, and another combination of n=6 and m=100 was used for L/H=1.5.

The amplitudes of steady-state dynamic thrusts were determined using Eq. 3.28 and Eq. 3.30 for harmonic excitations at different frequencies. The amplitudes of dynamic thrusts are normalized according to Eq. (3.36). The normalized thrust ratios are plotted against the frequency ratio f_{R1} in Figure 3.6(a) for L/H=5.0 and in Figure 3.6(b) for L/H=1.5. The dynamic thrusts increase very fast as the excitation frequency approaches the fundamental frequency of the wall-soil system. At resonant conditions, the peak dynamic thrusts are $2.4\rho H^2 A_{max}$ for L/H=5.0 and $3.0\rho H^2 A_{max}$ for L/H=1.5. Because the static thrusts are $1.0\rho H^2 A_{max}$ for L/H=5.0 and $0.86\rho H^2 A_{max}$ for L/H=1.5, their corresponding dynamic amplification factors are 2.4 for L/H=5.0 and 3.5 for L/H=1.5. The results suggest that the dynamic amplification for wall-soil systems with finite backfills is larger than that for wall-soil systems with semi-infinite backfills.

The results also show that resonance occurs at a frequency ratio $f_{R1} = 1.05$ for L/H=5.0 and at $f_{R1} = 1.55$ for L/H=1.5. Hence for two identical walls with identical soil properties, the fundamental frequency of the wall-soil system with L/H=1.5 is about 1.45 times that with L/H=5.0.
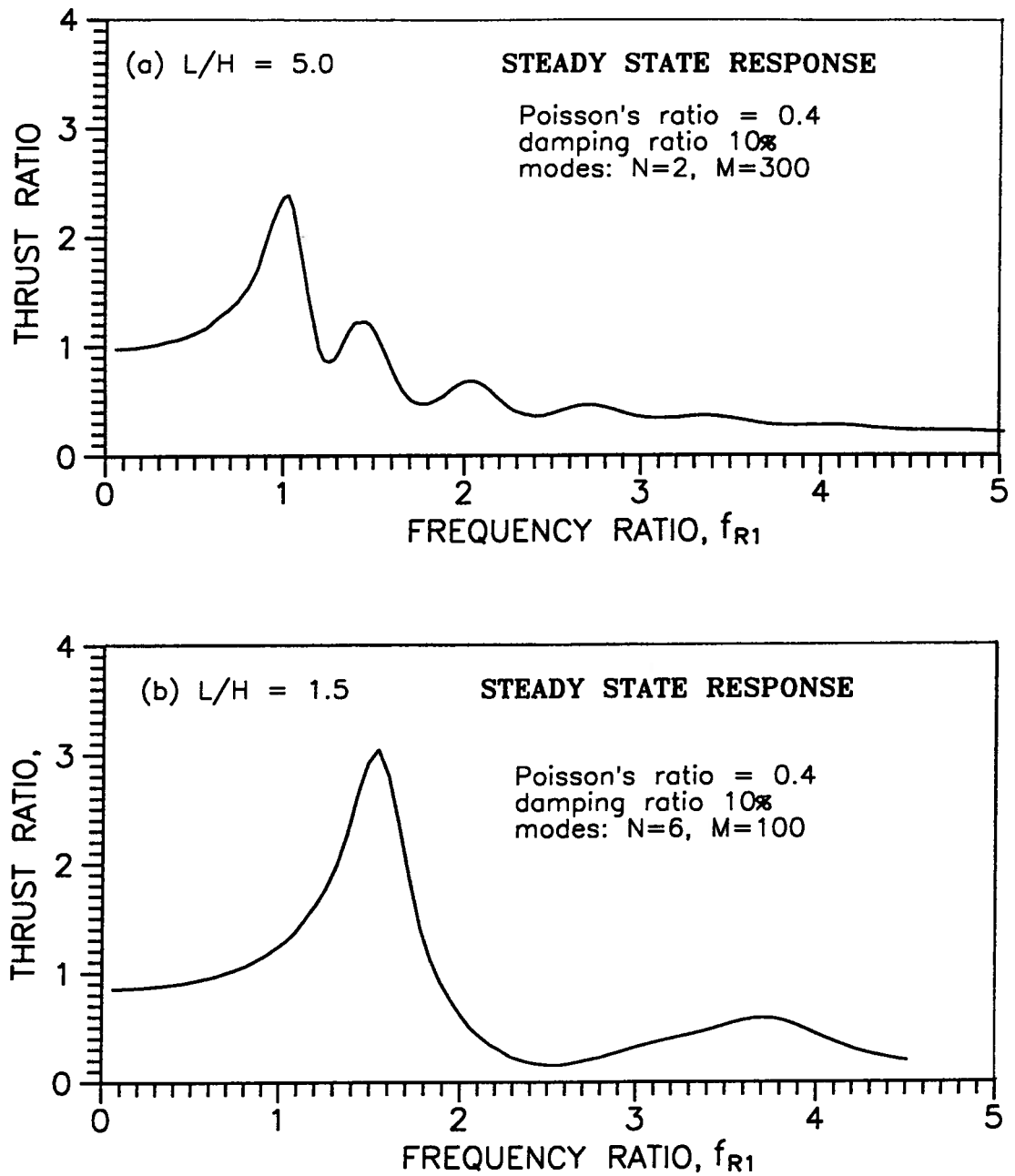
Figure 3.6: Normalized thrust ratios for sinusoidal motions (a) L/H=5.0 (b) L/H =1.5

3.5   Dynamic thrusts under earthquake motions

Dynamic thrusts are computed for wall-soil systems with L/H=5.0 and L/H=1.5. The walls have a fixed height H=10 m. The soil backfill has Poisson's ratio $\nu = 0.4$, unit weight $\gamma = 19.6 \ kN/m^3$ and a constant damping ratio λ=10%.

Two earthquake acceleration records were used in the analysis, the S00E acceleration component of the 1940 El Centro earthquake, and the S90E acceleration component of the 1989 Loma Prieta earthquake recorded at Yerba Buena island. The peak acceleration of the El Centro input is 0.348g, but it was scaled down to 0.07g to simulate the linear elastic response of the wall-soil system under a small input motion. The peak acceleration of the Loma Prieta input is 0.067g.

The time histories of dynamic thrusts were computed using Eq. (3.28) by mode superposition method. As examples, time histories of dynamic thrusts against rigid walls are shown in Figure 3.7 for the El Centro input and in Figure 3.8 for the Loma Prieta input. From Figure 3.7 (a) it is interesting to see that the high frequency content of the input motion has been filtered out when the input motion passes through a relatively soft backfill with G=9810 kPa. For this case, the computed peak dynamic thrust is about 182 kN/m.

A typical time history of the height of dynamic thrust is illustrated in Figure 3.9. The most frequently occurring height of dynamic thrust is 0.62H above the base of the wall. In the region of peak thrust a height of 0.6H would be seem a good value for design.

The impact of frequency ratios f_{R1} and f_{R2} on the dynamic thrusts against rigid walls
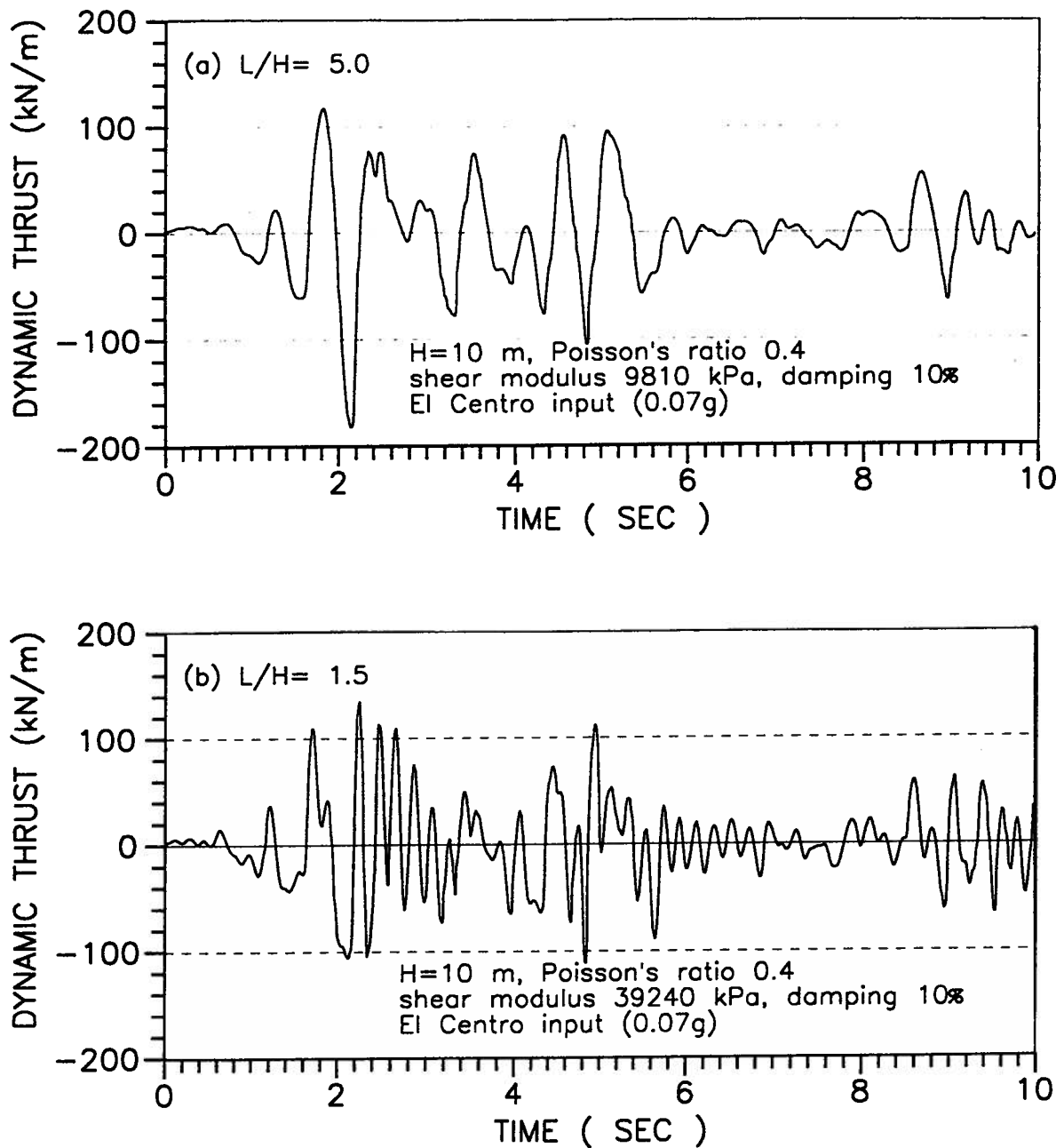
Figure 3.7: Time histories of dynamic thrusts using the El Centro input (a) L/H=5.0 (b) L/H=1.5
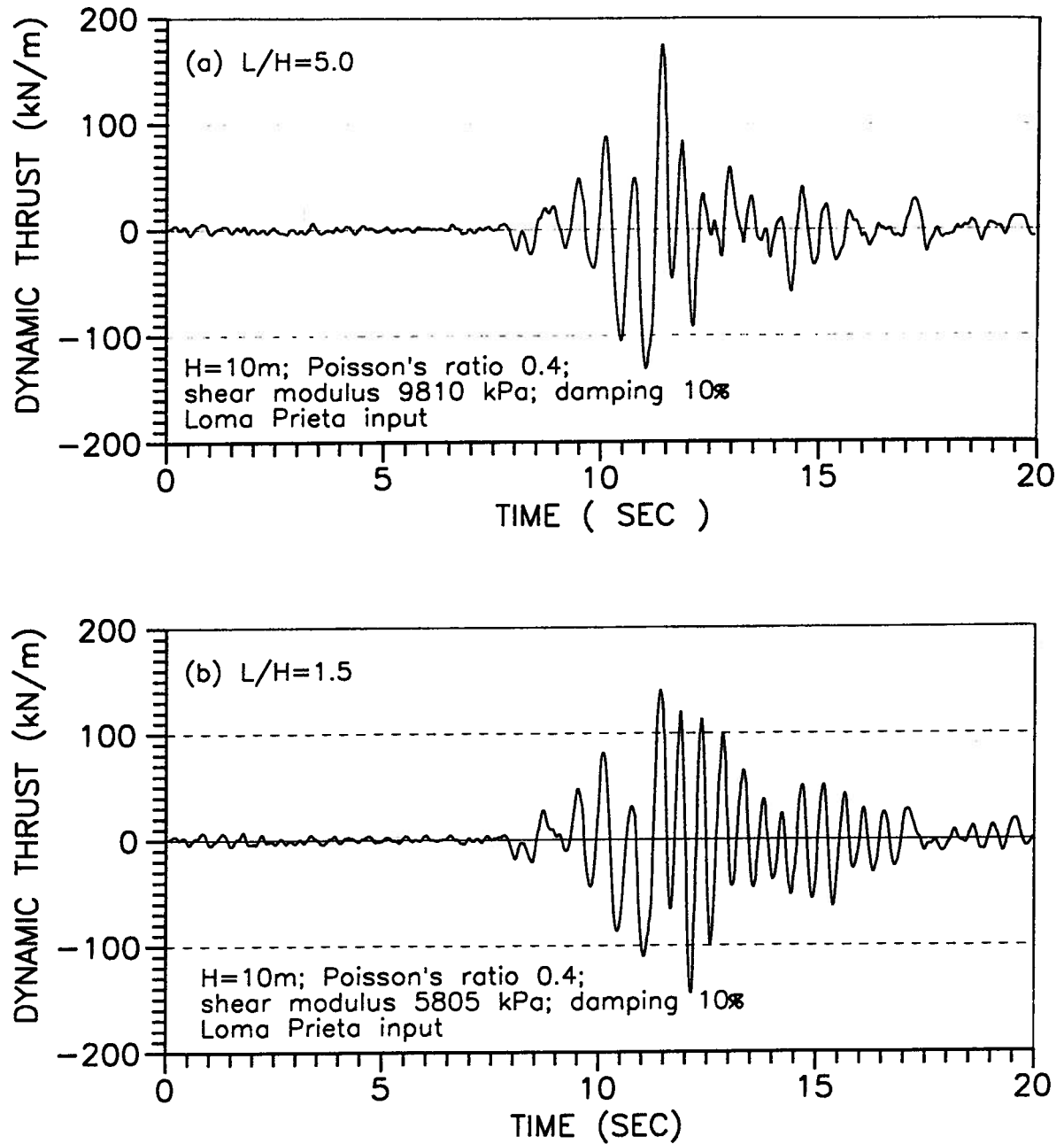
Figure 3.8: Time histories of dynamic thrusts using the Loma Prieta input (a) L/H=5.0 (b) L/H=1.5

Table 3.1: Peak dynamic thrusts for walls with L/H=5.0 and H=10 m, λ=10%

G (kPa)	ω_s rad/sec	Dynamic thrust (kN/m) (El Centro input)	Dynamic thrust (kN/m) (Loma Prieta input)
613.0	2.750	48.4	77.5
1360.0	4.096	54.2	-
2453.0	5.501	74.2	79.3
4286.0	7.272	120.1	-
6131.0	8.697	152.6	-
9810.0	11.001	182.2	174.7
20020.0	15.716	132.8	159.5
61313.0	27.503	144.5	161.4

is examined by varying the shear modulus G of the backfill. The shear moduli of the backfills vary from 613 kPa to 61313 kPa, which gives a distribution of the fundamental frequency of the backfill ω_s from 2.75 to 27.503 rad/sec. The computed peak dynamic thrusts are listed in Table 3.1 for wall-soil systems with L/H=5.0 and in Table 3.2 for L/H=1.5. The variation of shear moduli and the angular frequencies ω_s are also listed in these Tables. For the El Centro input, the maximum values among the peak dynamic thrusts are 182 kN/m for L/H=5.0 and 194.6 kN/m for L/H=1.5. For the Loma Prieta input, the maximum values among the peak dynamic thrusts are 174.7N/m for L/H=5.0 and 170.0 kN/m for L/H=1.5. These results suggest that the peak dynamic thrusts are little dependent on the L/H ratio under earthquake motions.

The frequency ratios f_{R1} and f_{R2} are determined using Eq. 3.37 and Eq. 3.38, respectively. In these equations the excitation frequency ω of the input motion is required. For earthquake motions, the excitation frequency ω is taken to be the predominant frequency of the earthquake. The predominant frequency of an earthquake motion is the frequency at which the response spectral acceleration has the maximum value in the

Table 3.2: Peak dynamic thrusts for walls with L/H=1.5 and H=10 m,λ=10%

G (kPa)	ω_s rad/sec	Dynamic thrust (kN/m) (El Centro input)	Dynamic thrust (kN/m) (Loma Prieta input)
801.5	3.144	54.8	-
1090.0	3.667	75.0	86.8
1905.0	4.848	116.0	-
2453.0	5.501	133.7	126.4
4360.0	7.334	194.6	170.0
5805.0	8.463	179.1	145.4
9810.0	11.001	130.9	151.0
39240.0	22.002	134.5	143.9
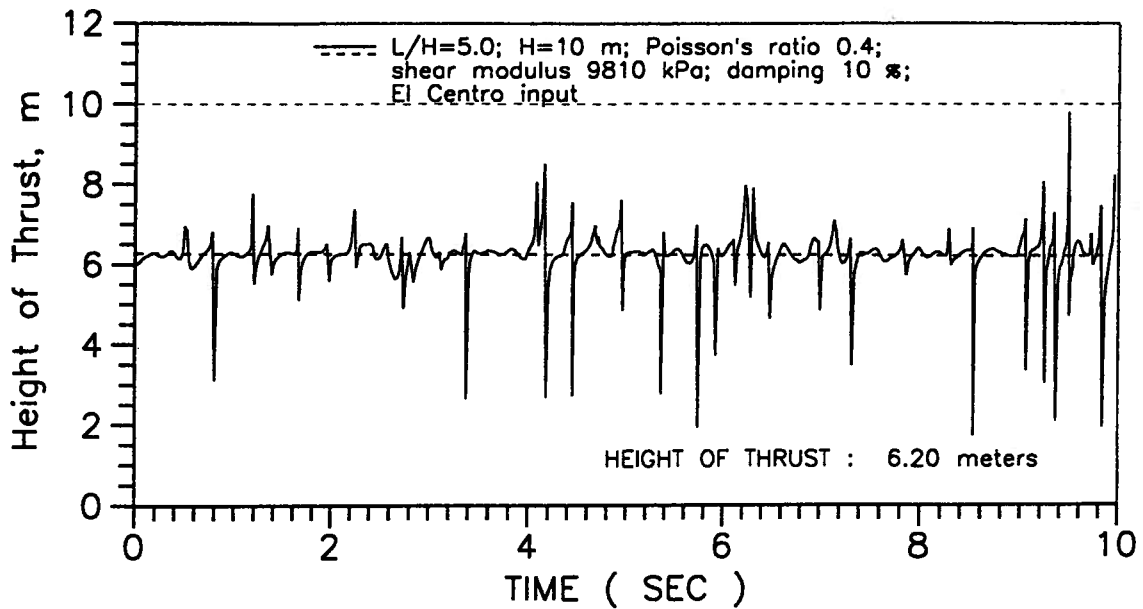
Figure 3.9: A time history of the height of dynamic thrust, L/H=5.0

acceleration spectrum. Therefore the excitation frequencies of the El Centro input and the Loma Prieta input are determined to be 11.64 rad/sec and 10.13 rad/sec, respectively.

The peak dynamic thrusts are normalized using Eq. 3.36. The normalized thrust ratios are plotted against the frequency ratio f_{R1} in Figure 3.10 and against the frequency ratio f_{R2} in Figure 3.11. Based on results from the limited number of analyses for earthquake motions, it is suggested that the peak dynamic thrusts are $1.30\rho H^2 A_{max}$ for L/H=5.0 and $1.38\rho H^2 A_{max}$ for L/H=1.5. Because the static thrusts are $1.0\rho H^2 A_{max}$ for L/H=5.0 and $0.86\rho H^2 A_{max}$ for L/H=1.5, their corresponding the dynamic amplification factors are about 1.3 for L/H=5.0 and 1.6 for L/H=1.5.

A significant observation is made that the dynamic amplification under earthquake motions due to resonance is much less than that under sinusoidal motions. Under sinusoidal motions, the dynamic amplification factors at resonance are 2.4 for L/H=5.0 and 3.5 for L/H=1.5. The dynamic amplification factors under earthquake motions are about 50% of that under sinusoidal motions.

3.6 Accuracy of the response spectrum method

The response spectrum method is commonly used to determine the responses of structures subjected to earthquake motions. The response spectrum method which adds modal values without taking the phases of the modes into account is much simpler than the direct mode superposition method. Therefore it is of interest to check on the accuracy with which the peak dynamic thrust can be determined using the response spectrum approach.
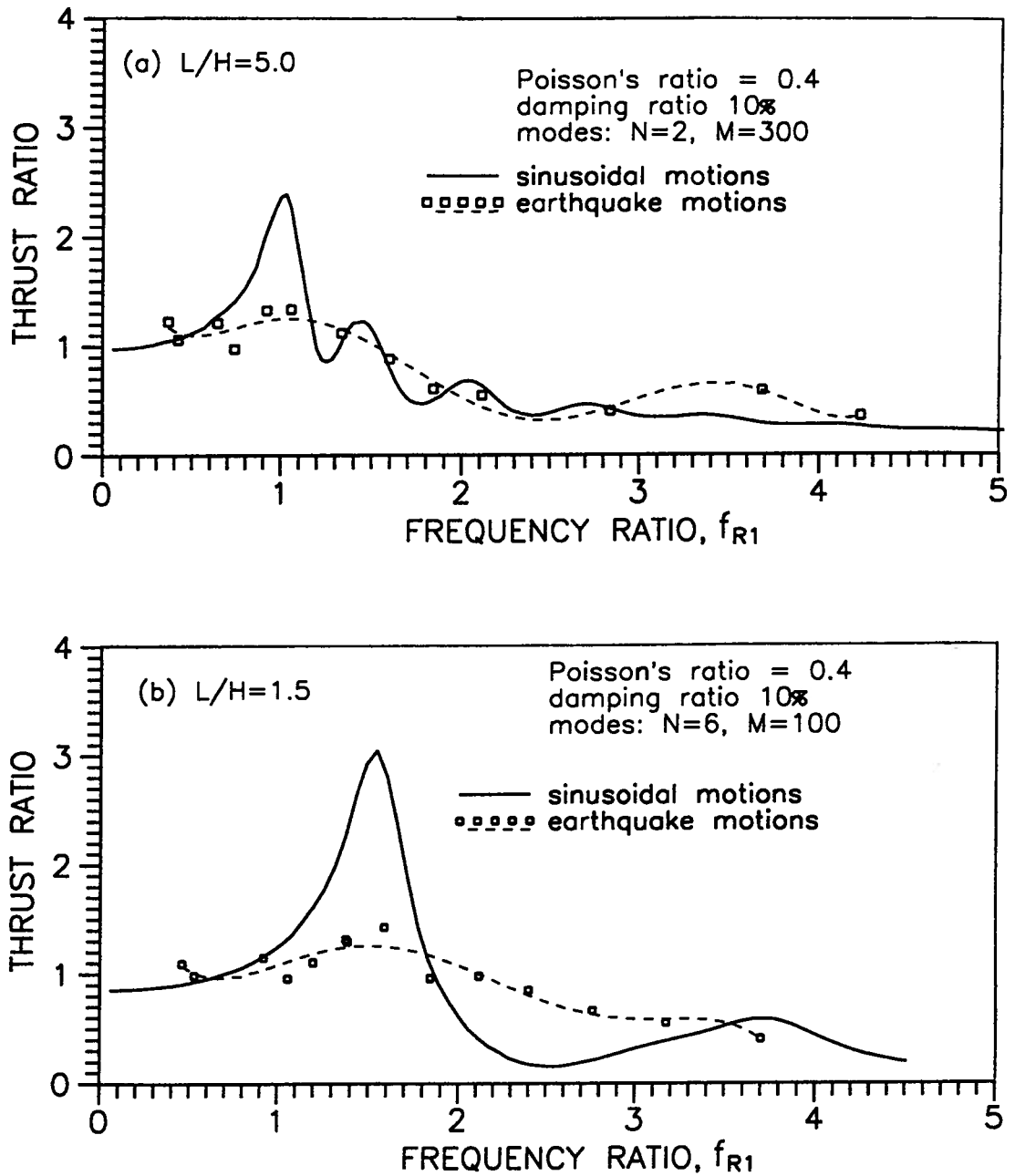
Figure 3.10: Normalized thrust ratios versus f_{R1} for earthquake motions (a) L/H=5.0 (b) L/H=1.5
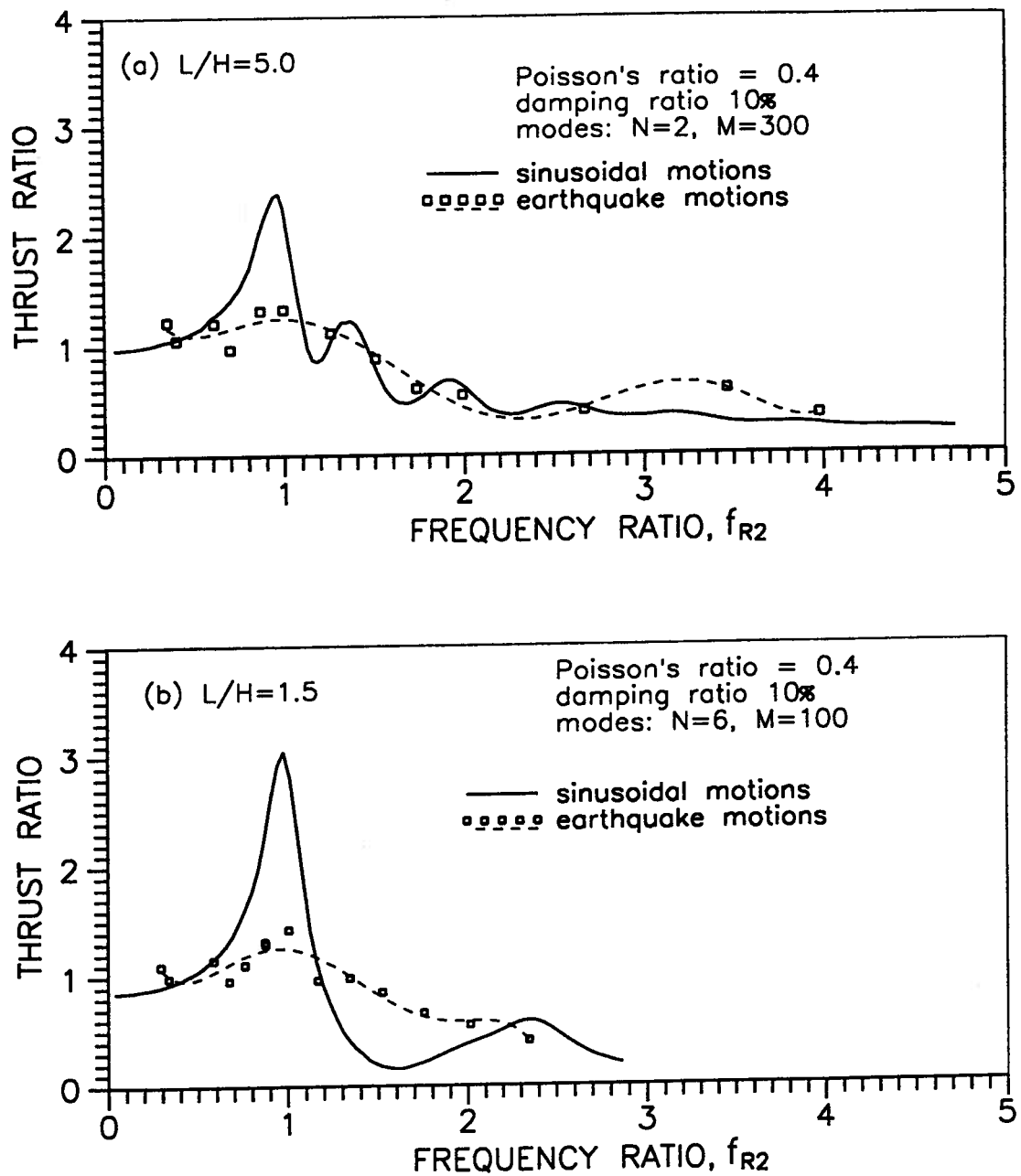
Figure 3.11: Normalized thrust ratios versus f_{R2} for earthquake motions (a) L/H=5.0 (b) L/H=1.5

The accuracy of the response spectrum method is measured by a thrust factor C_P defined as

$$C_P = \frac{P_{max}}{P_{sp}} \tag{3.39}$$

where the total spectral thrust P_{sp} is evaluated using the response spectrum method by summation of peak modal thrusts P_{mn}. P_{max} is the exact solution which is evaluated using the mode superposition method. The values of the thrust factor C_P gives a measure of the accuracy of the response spectrum method.

The peak modal thrust P_{mn} is determined from Eq. 3.32 using the pseudo-spectral velocity S_v^{mn} of the input motion corresponding the modal frequency ω_{mn}. The pseudo-spectral velocities for the two selected acceleration records, the El Centro input and the Loma Prieta input, are shown in Figure 3.12(a) and 3.12(b), respectively.

Since the peak modal thrust only represents the peak value for a particular mode, the determination of the total spectral thrust P_{sp} must be based on some form of mode summation. Summation of the absolute peak modal values (ABS) or the Square Root of the sum of the Squares of the peak modal values (RSS) are used.

When the absolute summation (ABS) is used in the response spectrum method, the total spectral thrust P_{sp} is determined by

$$P_{sp} = \Sigma\Sigma P_{mn} \tag{3.40}$$

When the root square summation (RSS) is used in the response spectrum method, the total spectral thrust P_{sp} is determined by
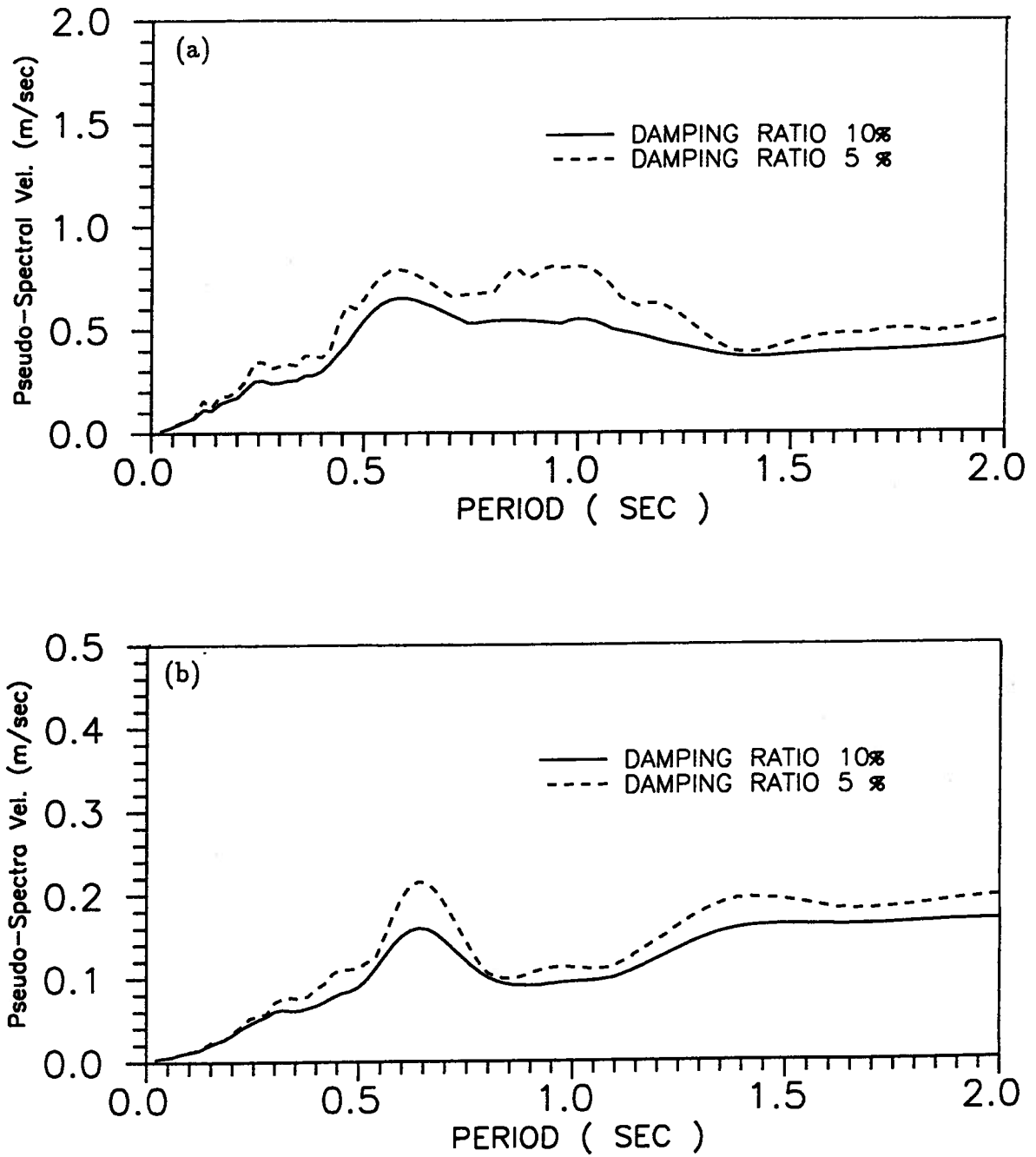
Figure 3.12: Pseudo-spectral velocities of (a) the El Centro input and (b) the Loma Prieta input

$$P_{sp} = \sqrt{\Sigma\Sigma P_{mn}^2} \tag{3.41}$$

Values of the thrust factor C_P were determined for both sinusoidal motions and earthquake motions. The earthquake motions are represented by the El Centro input and the Loma Prieta input. The studies were made for L/H=5.0 and L/H=1.5. 600 modes were used for obtaining both P_{sp} and P_{max}.

Discussion of results   When the RSS method was used, the relationship between the thrust factor C_P and the frequency ratio f_{R1} was obtained and is shown in Figure 3.13. For harmonic loading the thrust factor C_P changes very much with frequency. The response spectrum method could overestimate or underestimate the peak dynamic thrust by 80% to 100%. For earthquake loading the thrust factor C_P is usually greater than one, mostly around 1.5. The response spectrum method usually underestimates the peak dynamic thrust by as much as 50%. However the thrust factor changes for a different soil profile and a different frequency ratio. The uncertain variation of C_P makes it difficult to apply the response spectrum method for determining the actual peak dynamic thrust P_{max} in practice.

When the absolute summation (ABS method) was used, the relationship between the thrust factor C_P and the frequency ratio f_{R1} was determined and is shown in Figure 3.14. For low frequency ratios, such as $f_{R1} < 0.8$, the total spectral thrust P_{sp} obtaining from the ABS method agrees very well with the exact solution P_{max} under sinusoidal motions. However under earthquake motions, about 20% overestimate of peak dynamic thrust is expected for the same frequency ratio. For high frequency ratios, such as $f_{R1} > 1.5$, the peak dynamic thrust may be overestimated by as much as 50% when the response
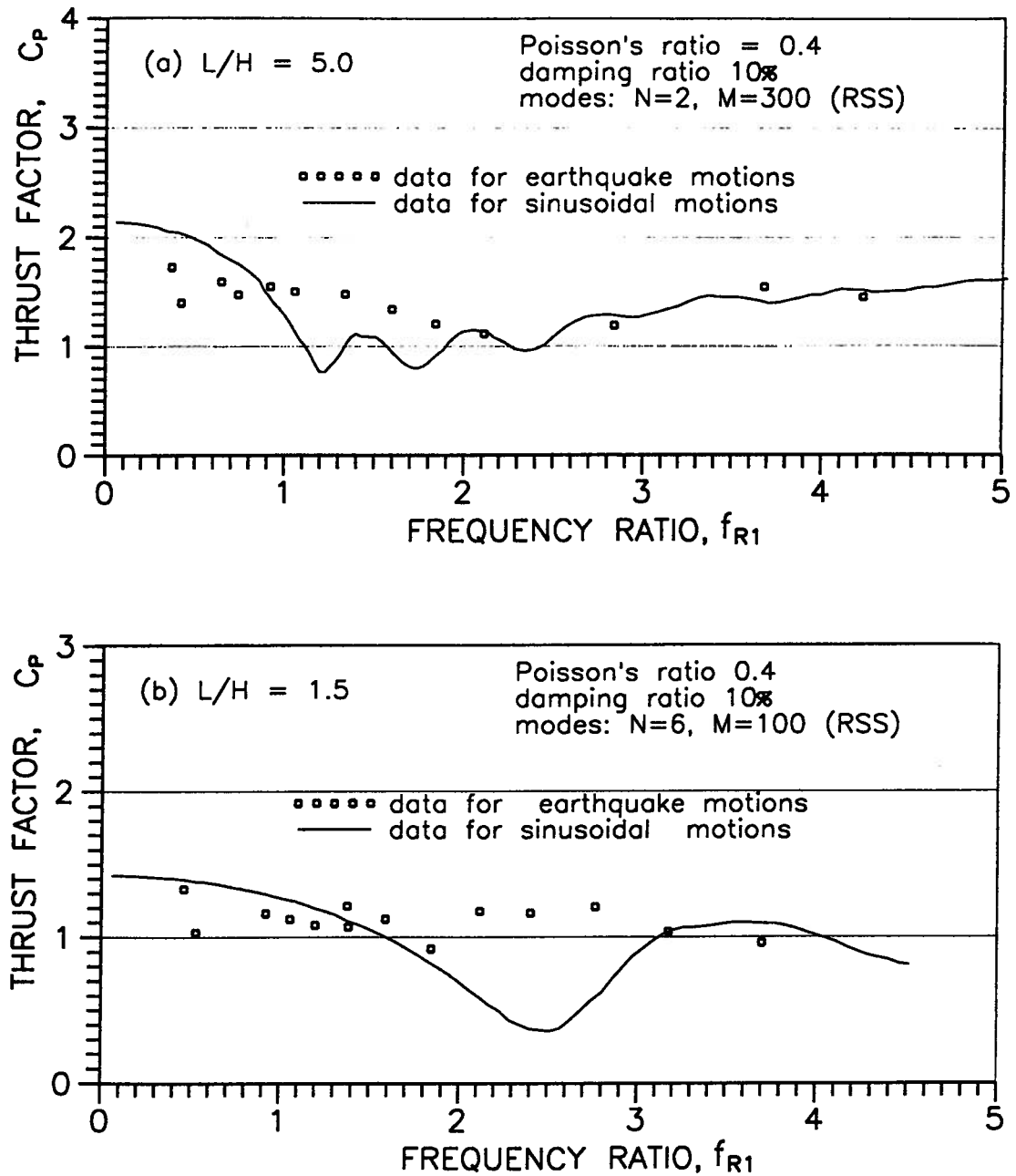
Figure 3.13: Variations of thrust factor C_P versus frequency ratio f_{R1} (RSS method) (A) L/H=5.0, (B) L/H=1.5
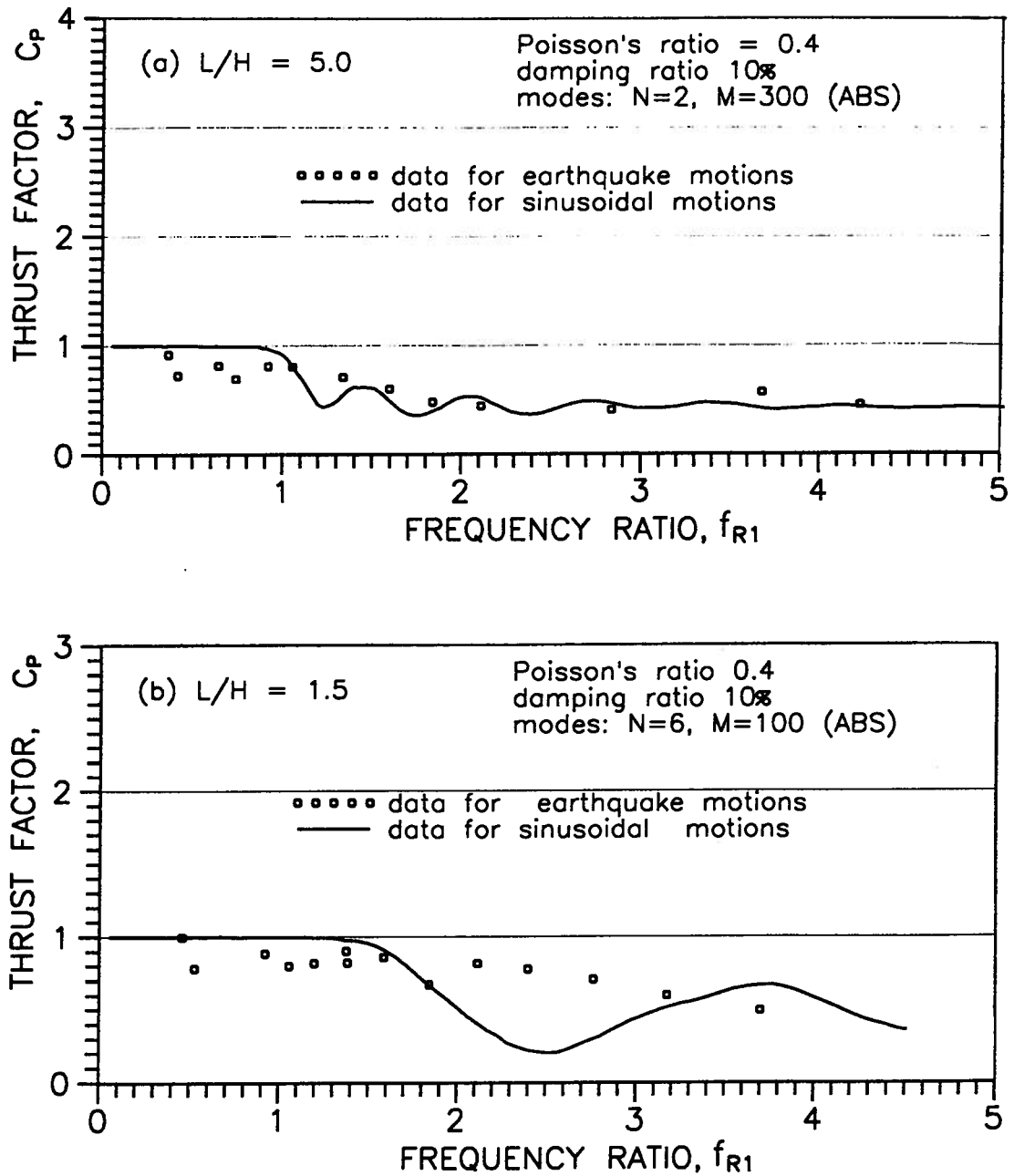
Figure 3.14: Variations of thrust factor C_P versus frequency ratio f_{R1} (ABS method) (A) L/H=5.0, (B) L/H=1.5

spectrum method is used.

Therefore it is recommended that the mode superposition method be used in order to accurately determine the peak dynamic thrusts against rigid walls. The response spectrum method may be used for approximately estimating the peak dynamic thrusts against rigid walls. The use of ABS method is suggested when the response spectrum method is selected, especially at low frequency ratios.

Chapter 4

Dynamic Thrusts on Rigid Walls with Non-homogeneous Soil Profiles

4.1 Introduction

The first objective of this chapter is to explore the effects of typical backfill non-homogeneity on the magnitude of dynamic thrusts for elastic response. Two types of soil profiles have been analyzed. They are profiles with linear and parabolic variations of shear modulus with depth.

The second objective of this chapter is to evaluate the influence of soil non-linearity on the magnitude and point of application of dynamic thrusts. The moduli and damping of soils are known to be strain dependent (Seed and Idriss, 1967). The equivalent linear elastic analysis developed by Seed and Idriss (1967) is used to simulate the soil non-linear response. Dynamic response characteristics such as magnitude of dynamic thrust, fundamental frequency of the system, and amplification factors of ground acceleration are determined for different intensities of acceleration input.

Elastic analysis. The undamped forced vibration equation of motion of the backfill is written as

$$\rho \frac{\partial^2 u}{\partial t^2} - (\theta G \frac{\partial^2 u}{\partial x^2} + G \frac{\partial^2 u}{\partial y^2}) = -\rho \ddot{u}_0(t) \qquad (4.1)$$
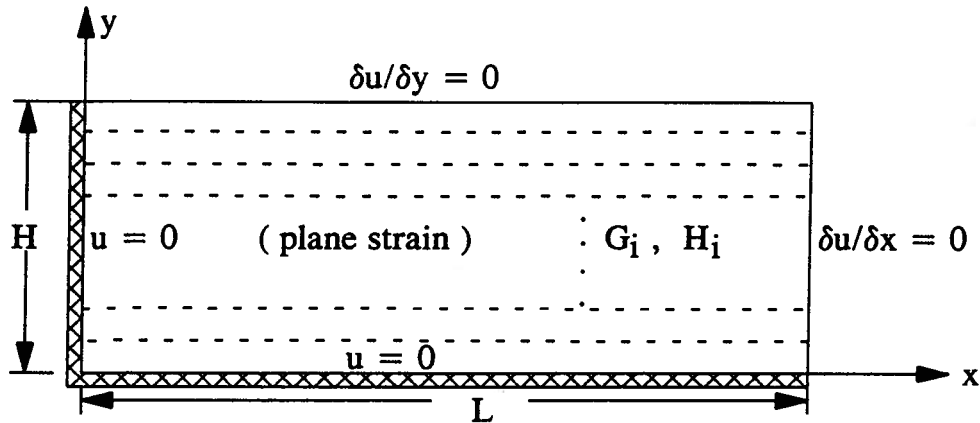
Figure 4.1: A composition of non-homogenous soil profile

where θ is equal to $2/(1-\nu)$, ν is Poisson's ratio of soil, and $\ddot{u}_0(t)$ is the base acceleration caused by the earthquake.

Figure 4.1 shows the type of non-homogeneous soil profiles that will be analyzed in this chapter. The backfill behind the wall is consisted of layered soils with different properties in each layer. The wall is considered to be rigid, and it does not move relative to the base. The boundary conditions for this system are also shown in Figure 4.1.

Analytical solutions are in general not possible for nonhomogeneous backfills. Therefore, the finite element method is employed to analyze dynamic response of the wall-soil system.

4.2 Finite element formulation and its validation

A finite element developed especially for this study is shown in Figure 4.2. The element consists of 6 nodes with 6 horizontal displacement variables. The displacement field has a
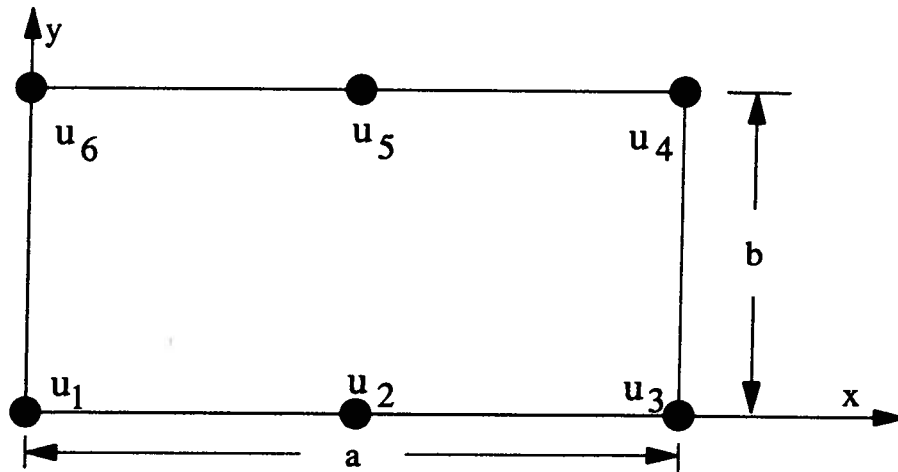
Figure 4.2: A composition of the finite element used in SPAW

linear variation along the vertical direction and a quadratic variation along the horizontal direction.

Let the displacement u be represented by

$$u = \Sigma N_i \cdot u_i \ldots\ldots i = 1, 6$$

The shape functions N_i are given by

$$N_1 = \tfrac{1}{ab}(a - x)(b - y)$$

$$N_2 = \tfrac{1}{ab}x(b - y)$$

$$N_3 = \tfrac{1}{ab}xy$$

$$N_4 = \tfrac{1}{ab}(a - x)y$$

$$N_5 = \tfrac{4}{a^2 b}x(a - x)(b - y)$$

$$N_6 = \tfrac{4}{a^2 b}xy(a - x)$$

Galerkin's general procedure of weighted residuals is used to develop the stiffness and mass matrices of the finite element shown in Figure 4.2. The stiffness matrix $[K]_e$ is given by

$$[K]_e = \int \int (\theta G \frac{\partial N_i}{\partial x} \frac{\partial N_j}{\partial x} + G \frac{\partial N_i}{\partial y} \frac{\partial N_j}{\partial y}) dx dy \qquad (4.2)$$

The diagonal mass matrix of the element is found to be

$$[M]_e = \frac{\rho a b}{12} \{1, 1, 1, 1, 4, 4, \} \qquad (4.3)$$

The stiffness and mass formulations shown in Eq. (4.2) and Eq. (4.3) are then applied to every element in the system. The global stiffness matrix [K] and the mass matrix [M] are assembled accordingly. The equations of motion in matrix form are written

$$[M]\{\ddot{u}\} + [C]\{\dot{u}\} + [K]\{u\} = -[M]\{I\}\ddot{u}_0(t) \qquad (4.4)$$

where [C] is the damping matrix, and {I} is a column vector of 1.

The natural frequencies of the system are determined by analyzing the eigen values of the system. The damping matrix of each finite element is obtained according to the desired degree of damping of the element. In this manner the damping matrix [C] is evaluated. A finite element program SPAW was developed based on these considerations.

Validation of F.E. method   To validate the reliability of the finite element analysis, it was applied first to two uniform soil profiles for which close-form solutions were obtained in the previous chapter.

The geometric mesh used in the finite element analyses is shown in Figure 4.3. This mesh consists of 3 elements in each layer with 20 layers. The horizontal dimensions of these elements are subjected to change proportionally to the L/H ratio. This mesh has
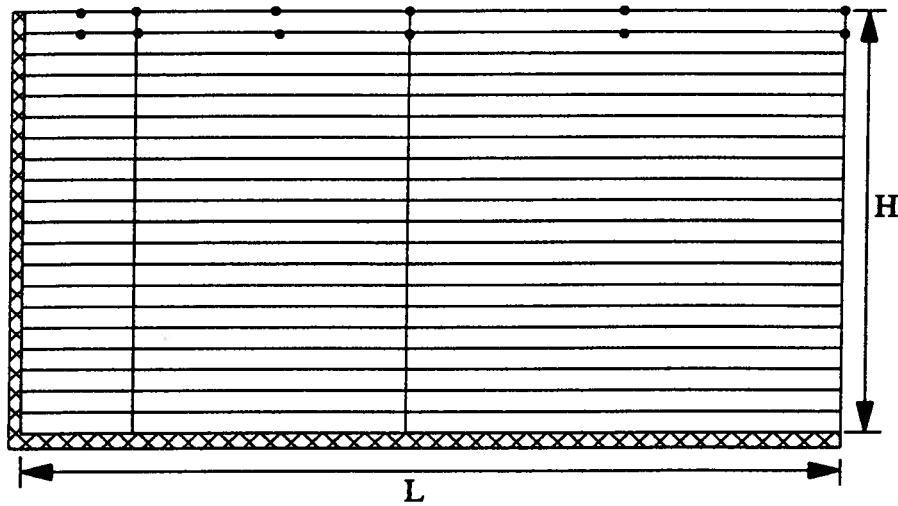
Figure 4.3: A finite element mesh used for dynamic analyses

been used for all finite element analyses presented in this chapter.

The finite element method is applied first to a uniform soil profile (L/H=5.0,H=10.0m) with G=9810 kPa and λ=10 %. The fundamental frequency of this wall-soil system is 1.75 Hz. This system is shaken by the S00E acceleration component of the 1940 El Centro earthquake scaled to 0.07g. The time history of dynamic thrust against the wall computed using the finite element method is shown by the solid line in Figure 4.4(a). The dashed line represents the closed form solution in Figure 3.7. The agreement between the two solutions is excellent over the entire time histories of dynamic thrusts.

The finite element method is next applied to a second uniform soil profile (L/H=1.5, H=10.0m) with a higher shear modulus of G=39240 kPa and λ = 10%. This wall-soil system is stiffer than the previous one. The fundamental frequency of this system is 2.54 Hz. The time histories of dynamic thrusts computed using the finite element method and the close-form solution are shown in Figure 4.4(b). Here again excellent agreement is observed between the dynamic thrusts computed by the two methods of analysis.
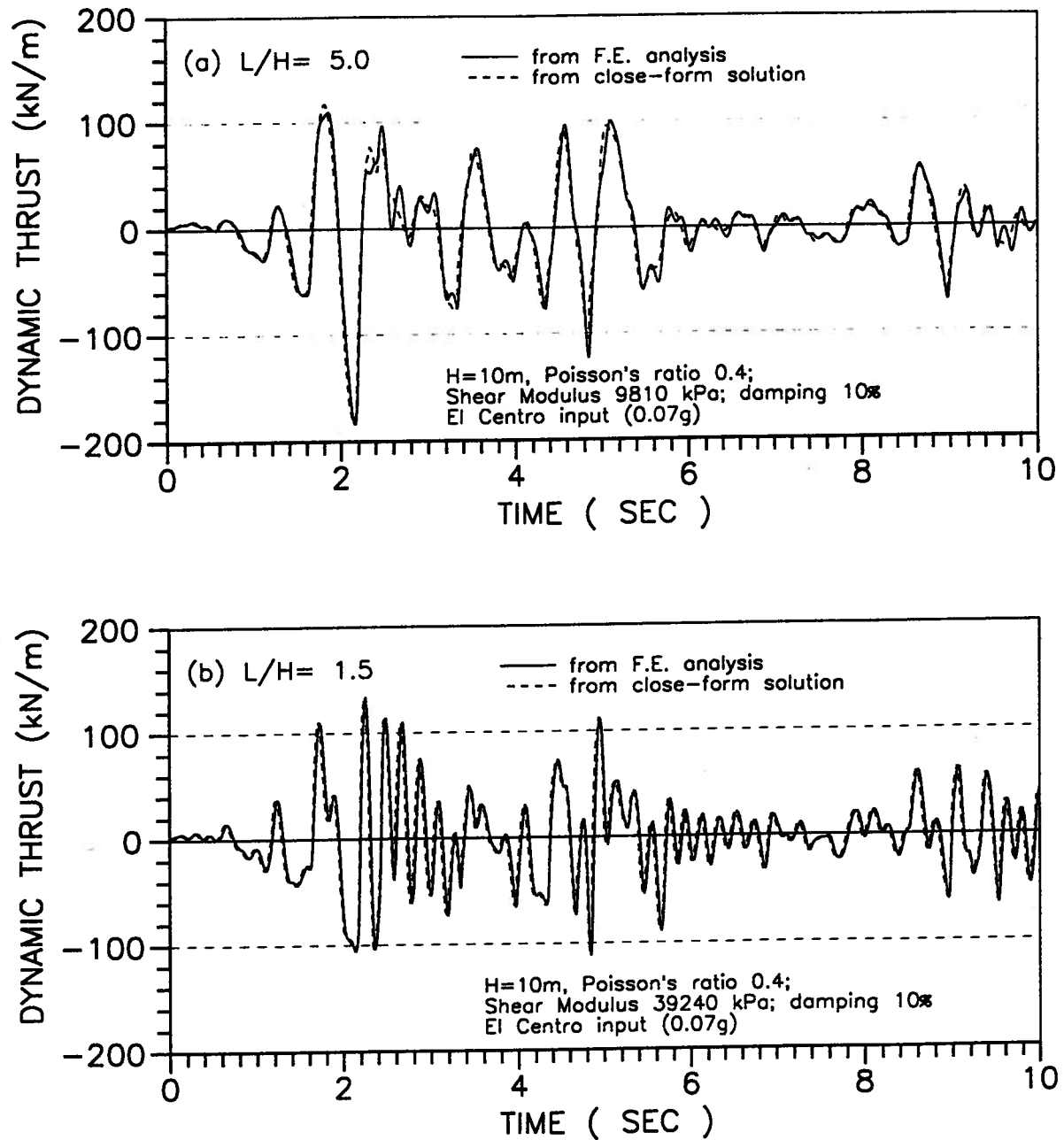
Figure 4.4: Comparisons of dynamic thrusts between the F.E. method and the close-form solution for uniform soils(a) L/H=5 (b) L/H=1.5

These comparative studies verify that the finite element formulation constructed for this problem is a reliable technique for evaluating the dynamic response of the wall-soil system and that the mesh employed is an appropriate one.

The finite element mesh used for the rigid wall analysis has been embedded in the computer program SPAW. There is no need for other users to construct the mesh. The dynamic analyses can be performed by just inputting the basic soil properties of each layer. The time history analyses only take few minutes in a PC486 33MHz computer.

4.3   Linear elastic analyses with non-homogeneous soil profiles

In this analysis the shear modulus G and damping ratio λ for a given soil profile retain constant values throughout the analysis. They are not considered to be functions of strains. $\lambda = 10\%$ and $\nu = 0.4$ are used. The horizontal length of the soil layer is constrained at L/H=5.0. Two types of soil profiles are examined, a profile with a linear variation of shear moduli with depth and a profile with a parabolic variation of shear moduli with depth.

Two types of motions, the sinusoidal motion and the earthquake motion, are applied to the two types of soil profiles. For the sinusoidal motion, the amplitudes of the steady-state dynamic thrusts are determined. For earthquake motion, the peak dynamic thrusts developed during shaking are determined. Again the El Centro input is used as the input of earthquake motion in this study.

Analyses were performed to examine the relationship between the thrust ratio and

the frequency ratio. The frequency ratio f_{R2} defined in Eq. 3.38 is used for this study. The thrust ratio has been defined in Eq. 3.36 to be $thrust/(\rho H^2 A_{max})$, where A_{max} is the peak acceleration of the input motion in m/sec^2, ft/sec^2 or other consistent unit.

Figure 4.5 shows the relationship between the thrust ratio and the frequency ratio f_{R2} for linear soil profiles. At resonance, the peak dynamic thrusts are $1.56\rho H^2 A_{max}$ under sinusoidal motions and $1.00\rho H^2 A_{max}$ under earthquake motions. Because the static thrust is about $0.71\rho H^2 A_{max}$, their corresponding dynamic amplification factors are determined to be 2.2 for sinusoidal motions and 1.4 for earthquake motions.

Figure 4.6 shows the relationship between the thrust ratio and the frequency ratio for parabolic soil profiles. In general, the thrust ratios are greater than those for linear soil profiles by 20%. At resonance, the peak dynamic thrusts are $1.87\rho H^2 A_{max}$ under sinusoidal motions and $1.18\rho H^2 A_{max}$ under earthquake motions. Because the static thrust is about $0.82\rho H^2 A_{max}$, their corresponding dynamic amplification factors are determined to be 2.3 for sinusoidal motions and 1.4 for earthquake motions.

The dynamic response of parabolic soil profiles is compared with dynamic response of uniform soil profile in Figure 4.7. For sinusoidal motions, the dynamic thrust ratios for parabolic soil profiles are less than those for uniform soil profiles in the frequency range of $f_{R2} < 2.0$.

The limited analyses conducted suggest that the dynamic thrust at resonance for sinusoidal motions are about 60% greater than that for earthquake motions with same peak acceleration. It should be noted that the earthquake motions are represented by the El Centro input only.
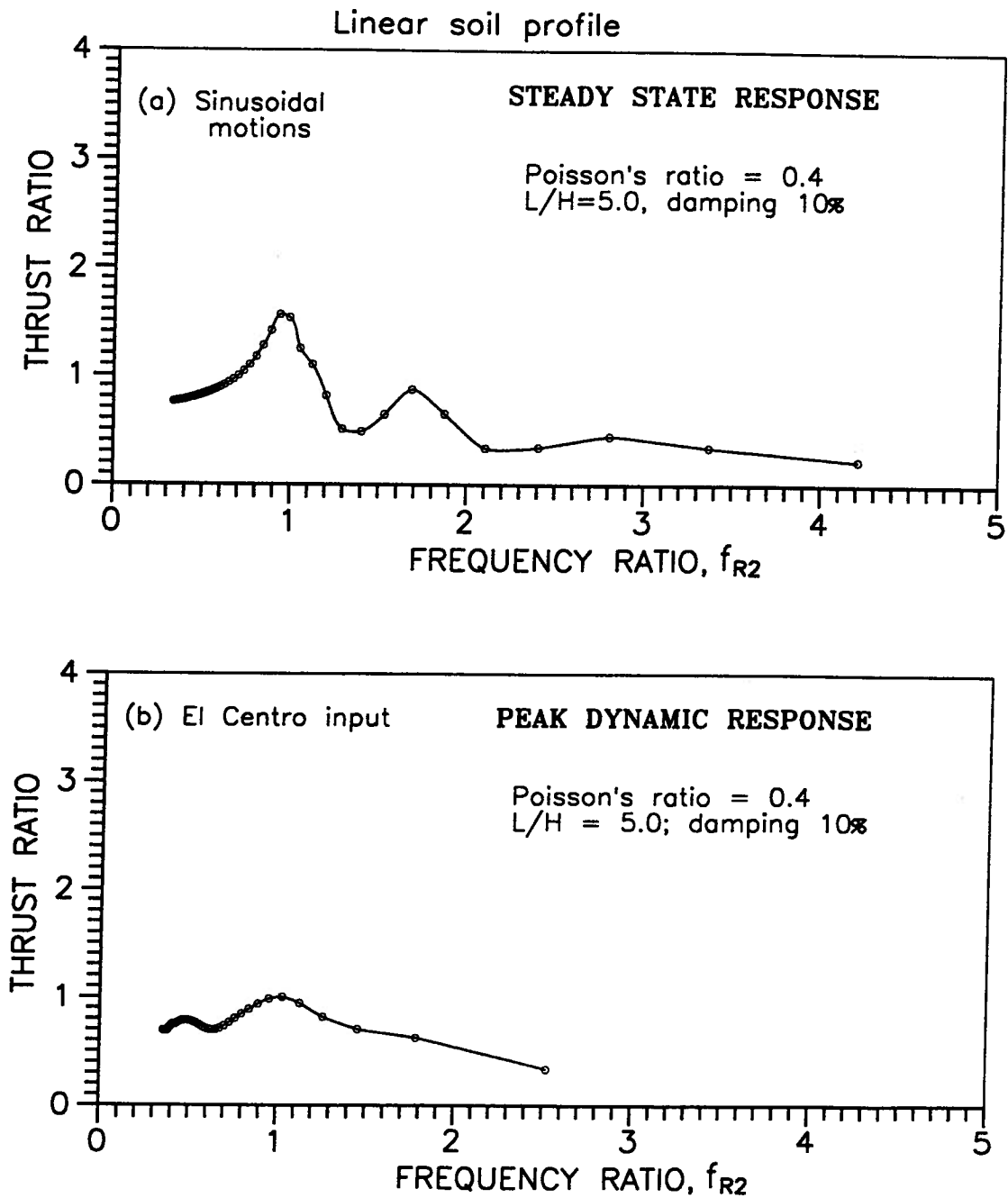
Figure 4.5: Relationships between thrust ratio and frequency ratio f_{R2} for linear soil profiles (a) sinusoidal motions (b) the El Centro input
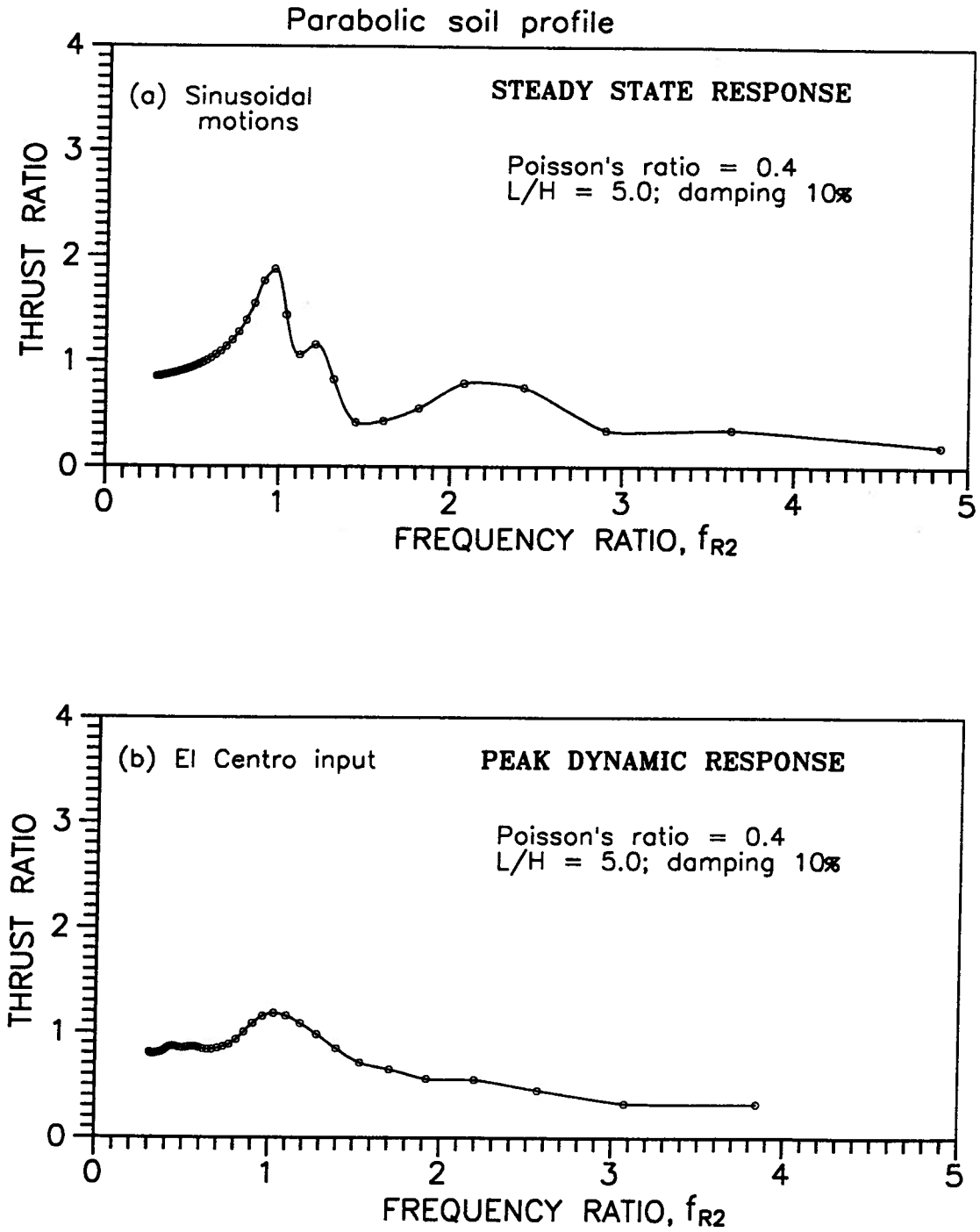
Figure 4.6: Relationships between thrust ratio and frequency ratio f_{R2} for parabolic soil profiles (a) sinusoidal motions (b) the El Centro input
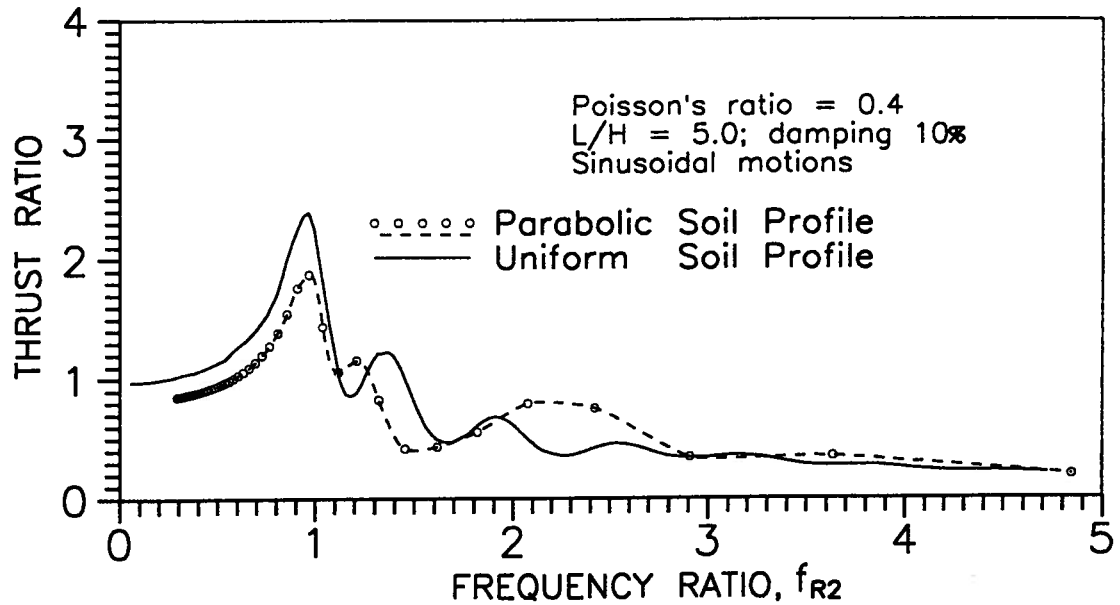
Figure 4.7: Comparison of dynamic thrust ratios for parabolic soil profiles and uniform soil profiles under sinusoidal motions (L/H=5)

The other important aspect of dynamic thrust is the location of the resultant thrust on the wall. Typical time histories of heights of dynamic thrusts for the three types of soil profiles are illustrated in Figure 4.8. The results are obtained using the El Centro input as input motion. For linear soil profiles dominant height of dynamic thrust is at 0.48H above the wall base. For parabolic soil profiles this height becomes 0.51H above the wall base. The uniform soil profile gives an average height of 0.62H above the wall base. Generally the height of dynamic thrust increases as the soil profile becomes more uniform.

Modal frequencies of wall-soil systems with different soil profiles are shown in Table 4.3. Essentially the natural frequencies of the wall-soil systems become more widely spaced as the soil becomes more uniform.
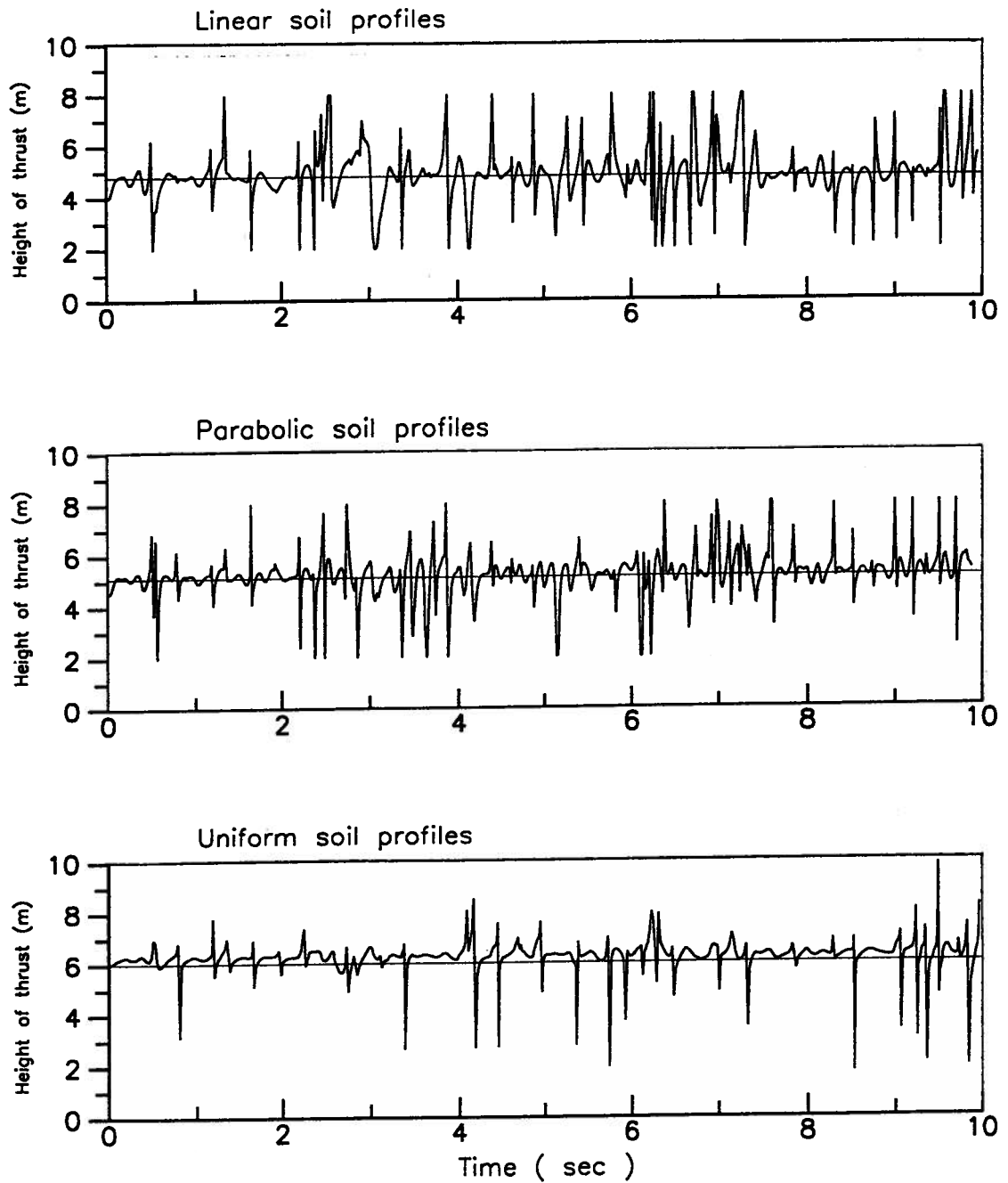
Figure 4.8: Typical time histories of heights of dynamic thrusts for three types of soil profiles (H=10m)

Table 4.3: Patterns of first 10th natural frequencies for three types of soil profiles (ω_n, rad/sec)

n^{th} freq.	frequencies (linear profile)	frequencies (parabolic profile)	frequencies (constant profile)
1	11.3	11.35	11.70
2	13.1	14.20	16.32
3	15.2	18.80	22.90
4	16.4	20.60	30.19
5	19.9	26.00	33.24
6	25.6	29.10	35.13
7	26.4	29.70	37.79
8	27.2	30.80	45.53
9	29.4	33.40	53.36
10	33.2	38.50	55.15

4.4 Equivalent linear simulation of non-linear response under earthquake loads

A method of analysis for modelling the non-linear response of soil was proposed by Seed and Idriss (Seed & Idriss, 1967), which is designated the equivalent linear method of analysis. In this method a set of elastic shear moduli and viscous damping ratios which are compatible with a measure of the effective shear strains induced by an earthquake are used to approximate the hysteretic behaviours of soils. The equivalent linear elastic method is widely used for dynamic analyses in practice.

The equivalent linear method for modelling nonlinear behaviour is used in this study. Since the level of shear strain in each element is not known at the beginning of the analysis, strain compatible moduli and damping ratios are achieved by an iterative process. The effective strain used to determine moduli and damping is chosen to be 0.65 of the

peak dynamic strain for the earthquake type of motions. The damping ratio of the wall-soil system in each iteration is estimated by using an average value of damping ratios for all soil elements in the system.

Two wall-soil systems with parabolic variation of shear modulus are analyzed using the equivalent linear technique. One wall has a stiff backfill with a shear modulus of 132,000 kPa at the base of the backfill. The other wall has a backfill with a shear modulus of 66,000 kPa at the base. The wall height in each case is H=10 m with L/H=5.0. The wall-soil systems are shaken using the El Centro acceleration record as the base motion. The effects of non-linearity on the dynamic responses of the systems are explored using increasing levels of input acceleration. The peak accelerations of input motions vary from 0.05g to 0.35g in increments of 0.05g.

The data on shear strain dependent moduli and damping presented by Seed and Idriss (Seed & Idriss, 1970) were employed. At shear strain levels of 0.0001, 0.0005, 0.001, 0.005, 0.01, 0.05, 0.1, 0.5, and 1.0 percent, the values of G/G_{max} were selected as 100, 98.3, 95.8, 84.3, 74.3, 43.0, 29.6, 10.9, 6.1 percent, respectively. The values of D/D_{max} corresponding to the above strain levels are the follows: 0.018, 0.055, 0.073, 0.158, 0.275, 0.457, 0.579, 0.891, 1.0. The maximum damping ratio D_{max} is chosen to be 30%.

Figure 4.9 shows the dynamic response of the stiff site. The intensity of shaking is measured by the peak acceleration of the input motion. The amplification of ground acceleration shows its peak at an input acceleration of 0.15g. The dynamic thrust ratio, the frequency ratio and the damping ratio increase steadily with the increase of the level of shaking. The increasing level of shaking results in reduction of shear moduli and consequently reduction in the fundamental frequency of the wall-soil system. This results
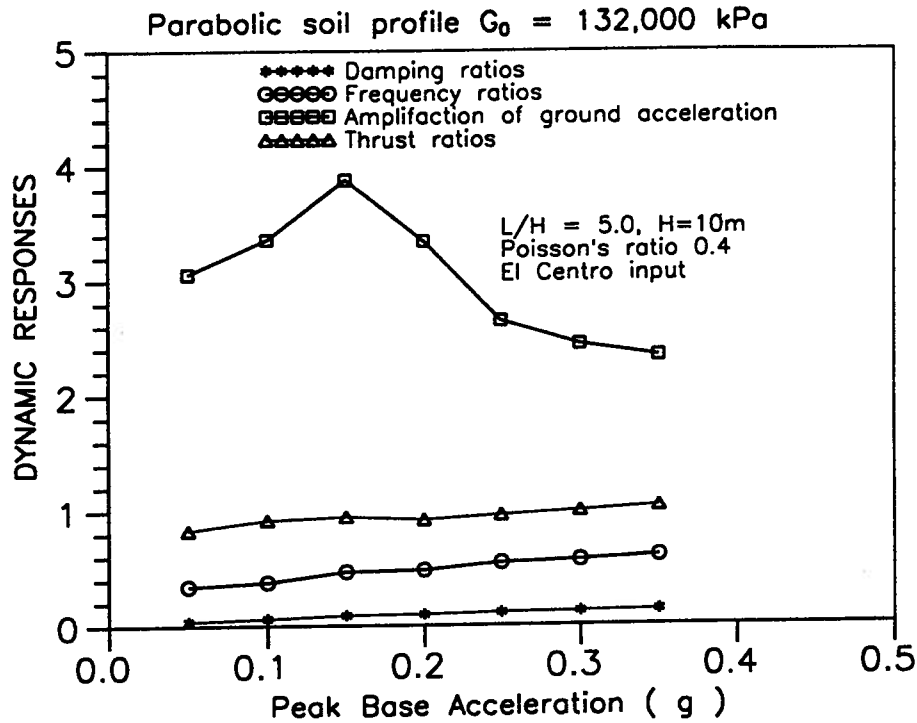
Figure 4.9: Dynamic responses of a stiff.site due to non-linear effect, G_0=132,000 kPa

in an increase in the frequency ratio f_{R2}. The dynamic thrust ratio increases from 0.83 for linear elastic response associated with low input accelerations to 1.04 for highly non-linear response at the higher levels of input acceleration. The effect of strong shaking on the dynamic thrust is clearly shown in Figure 4.10. At a base acceleration of 0.35g the dynamic thrust increases 25% due to the non-linear effect.

Figure 4.11 shows the dynamic response of the soft site. There is no clear indication of resonant response such as seen in Figure 4.9. The dynamic thrust ratio is 1.233 at a peak base acceleration of 0.2g and remains almost constant up to an input acceleration of 0.35g. The dynamic thrust increases about 23% due to the non-linear effect. The amplification factor of ground accelerations decreases from 3.0 to 2.2 with the increasing level of input acceleration.
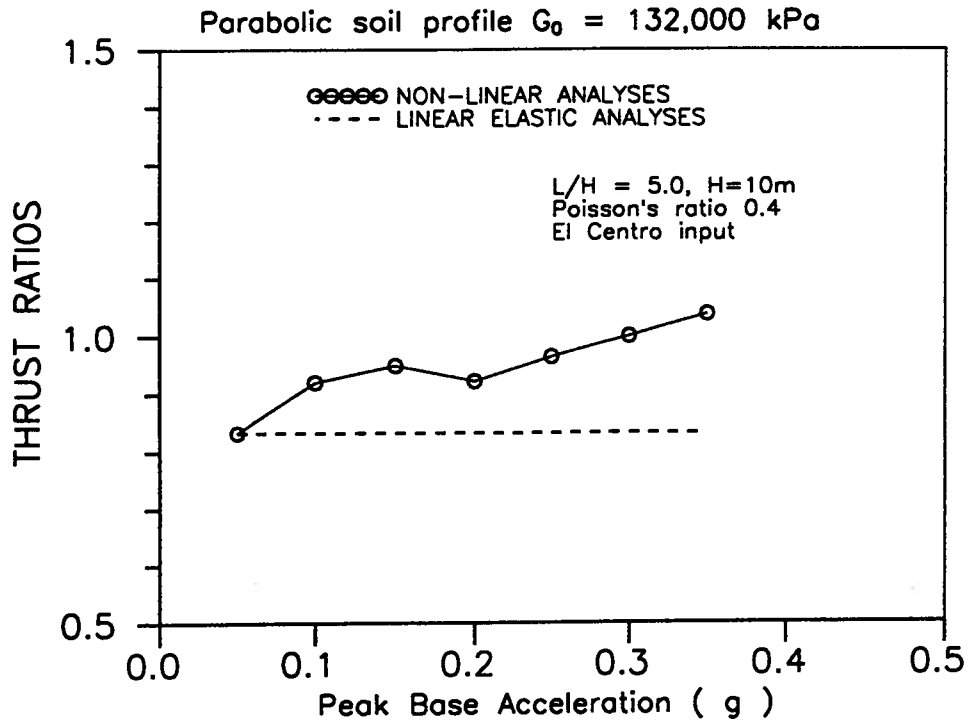
Figure 4.10: Effect of level of shaking on the dynamic thrust, G_0=132,000 kPa
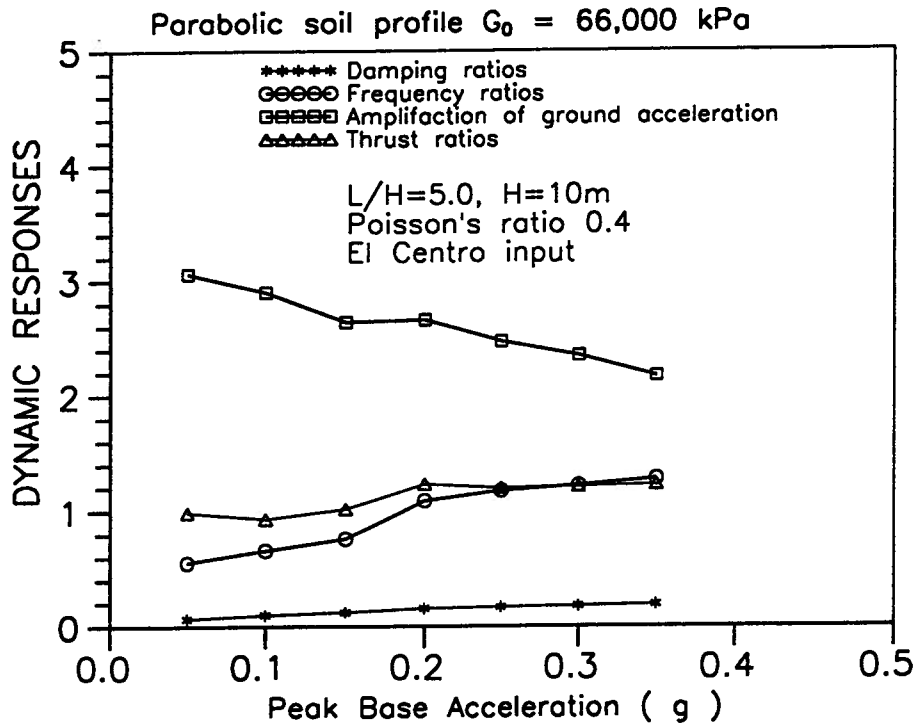
Figure 4.11: Dynamic responses of a soft site due to non-linear effects, G_0=66,000 kPa

The studies from equivalent linear analyses reveal that the dynamic thrust ratios usually increase with the levels of input accelerations. For the cases investigated, the increase of dynamic thrust due to non-linear effect is about 25% of the dynamic thrust obtained from a linear elastic analysis.

Part II

Dynamic Analyses of Pile Foundations

Chapter 5

Dynamic analyses of pile foundations

Dynamic soil-pile-structure interaction is a challenging area to geotechnical researchers and engineers. A very common example is the 3-D dynamic analysis of a pile foundation for a bridge abutment. The analysis involves modelling of soil-pile-soil interaction, the effects of the pile cap, non-linear soil response, and in many cases incorporates seismically induced pore water pressures. There are many approaches to solving the dynamic response of pile foundation.

Novak (1991) gave an extensive review of the more widely accepted methods of analysis for piles under dynamic loads. His study showed that pile group response can not be deduced from single pile response without taking pile-soil-pile interaction into account and that the dynamic characteristics of pile groups are strongly frequency dependent and may differ significantly from the characteristics of a single pile.

5.1 Dynamic analyses of single pile response

Analytical modelling of single pile response may be divided into two major categories, elastic continuum models coupling the soil and pile in a unified system and the lumped mass-spring-dashpot models. The elastic continuum models are mostly used for the analysis of pile foundation subjected to low level excitation such as problems related

to machine foundations. The lumped mass models are formulated by separating the response of piles from the soil medium. The contribution of the soil medium to the dynamic response of pile foundation is taken into account by using empirically or analytically derived Winkler type springs and viscous dashpots along the pile shaft.

Elastic continuum models The analytical approach that can model the interaction between the pile and soil using the theory of continuum mechanics is very difficult. Accurate mathematical solutions of the problem are not available even for the idealistic assumptions of linear elasticity or viscoelasticity, homogeneous soils and the pile being welded to the soil. Thus various approximate formulations have been developed. An approximate solution for the horizontal response of an endbearing pile in a homogeneous soil layer was presented by Tajimi (1966). His formulation neglected the vertical component of the motion.

The work of Novak, Nogami and their co-workers (Novak, 1974; Nogami and Novak, 1977; Novak and Aboul-Ella, 1978a,1978b; Novak et al., 1978; Novak and Sheta, 1980,1982) is particularly significant in advancing solutions to the problem of an elastic beam vibrating in a homogeneous or multi-layered elastic isotropic continuum subjected to dynamic pile head loading. In 1974, Novak formulated a simple approach based on plane strain soil reactions. His formulation may be interpreted as a plane strain complex transmitting boundary attached directly to the pile. The solution was first presented for a homogeneous soil layer without any material damping. Material damping was later included in closed form expressions for soil reactions in Novak et al. (1978). The formulation of the plane strain approach was further extended by Novak and Aboul-Ella (1978a,1978b) to include layered media. The computer program PILAY was formulated

for these types of solutions.

In using Novak's formulation much of attention is focused on the pile head impedance functions. The impedances have a great influence on the response of pile supported buildings and structures. The pile head impedances can be defined as the transfer functions describing the ratios between the complex valued displacement response at the pile head and the harmonic forces (or moments) applied at the pile head.

Pile head impedances derived using elastic theory are most appropriate for low level shaking where the dynamic pile head forces induce essentially elastic strains in the soil around the pile. The pile head impedance is usually expressed in terms of complex shear moduli, the real part of which represents the secant elastic stiffness of the soil and the imaginary part accounts for material (hysteretic) damping. Consequently the pile head impedance has both a real component and an imaginary component. The real component represents the elastic stiffness of soil while the imaginary component indicates energy losses due to wave propagation away from the pile (radiation damping) and hysteretic damping in the soil. For low level of excitation hysteretic damping is small and system damping is mostly dominated by radiation energy losses.

The real component of pile head impedance derived using Novak's plane strain approach has been found to diminish as the frequency approaches zero (Novak and Aboul-Ella, 1978a). This result is not realistic. Novak and Nogami have suggested that plane strain soil reactions can be used provided low frequency corrections are applied. In the computer program PILAY, a frequency cut-off is applied for determining pile head impedances of single piles. Nogami and Novak use static stiffness when the dimensionless frequency $a = \omega r_0/V_s$ is less than about 0.3, where ω is the excitation frequency, r_0

is the pile radius and V_s is the effective shear wave velocity of soil in the depth range where maximum pile bending occurs. Alternatively at lower frequencies, the pile head impedance can be taken as constant and equal to that calculated at a suitable dimensionless frequency, such as $a = 0.3$.

In PILAY analysis, constant damping coefficients are assumed when the dimensionless frequency a is less than 0.3. That is, the damping coefficients are assumed to be independent of frequency when $a < 0.3$. This assumption does not necessary hold especially when the frequency independent hysteretic damping is significant. Other methods for determining the damping of pile foundations are given below. It should be noted, however, the Novak's solutions were primarily intended for for machine foundations for which a is usually greater than 0.3.

The imaginary component (damping) of pile head impedance, C_{ij}, represents the energy losses along the pile. For an equivalent viscously damped system, the viscous dashpot coefficient c_{ij} (damping coefficient) is defined as the ratio of the damping and the frequency $c_{ij} = C_{ij}/\omega$. The equivalent viscous damping coefficients c_{ij} vary with depth z along the pile because the hysteretic damping varies with pile deflections and strain in the near field. Gazetas and Dobry (1984) proposed a simple formulation for computing the damping coefficients. According to them, the damping coefficients consist of the radiation and hysteretic damping components, or $c_{ij} = c_r + c_h$. The radiation damping coefficients c_r given by Gazetas and Dobry have been found in good agreement with those derived by Novak et al. (1978) and Roesset and Angelides (1980). The expressions proposed by Gazetas and Dobry are frequency and depth dependent. For depths greater than 2.5 times the pile diameter the radiation dashpot coefficient is given as

$$c_r = 4r_0\rho_s V_s \{1 + [\frac{3.4}{\pi(1-\nu)}]^{1.25}\}(\frac{\pi}{4})^{0.75} a^{-0.25} \tag{5.1}$$

in which a is the dimensionless frequency $a = \omega r_0/V_s$, ω is the frequency of excitation, r_0 is the pile radius and V_s is the free field shear wave velocity. For shallower depths, the radiation dashpot coefficient is given as

$$c_r = 8r_0\rho_s V_s (\frac{\pi}{4})^{0.75} a^{-0.25} \tag{5.2}$$

Recently Gazetas et al. (1993) proposed a simpler expression for the viscous damping coefficient along the pile. The frequency dependent radiation damping coefficient for vertical motions is expressed as

$$c_z = \rho_s V_s d\, a_0^{-0.25} \tag{5.3}$$

and for horizontal motions

$$c_x = 6\rho_s V_s d\, a_0^{-0.25} \tag{5.4}$$

in which d is the pile diameter and $a_0 = \omega d/V_s$. These formulations were used in a Beam-on-Dynamic-Winkler foundation simplified model by Gazetas et al. (1993).

The pile head impedances are often used as foundation spring and dashpot parameters in the analysis of superstructures subjected to earthquake loading. This type of analysis in which the pile foundations are replaced by springs and dashpots is usually called uncoupled analysis.

The assumption generally made in an uncoupled analysis is that one may use the free field surface accelerations as input into the base of the superstructure. The assumption

actually neglects the influence of foundation-ground may have on the motions of the pile cap. The motions of the pile cap may differ significantly from the motions of the free field surface due to kinematic interaction between the pile and soil.

The influence of kinematic interaction on pile head accelerations has been studied by Gazetas (1984) and Fan et al. (1991). In the latter publication, comprehensive studies were made on the kinematic seismic response of single piles and pile groups. The influence of kinematic interaction may become significant if the stiffness ratio between the pile and the soil is high, such as $E_p/E_s > 10,000$.

An uncoupled superstructure analysis that neglects kinematic interaction appears to be valid provided the free field surface motions are dominated by relatively low frequency waves. The neglect of kinematic interaction generally results in an overestimate of dynamic pile cap motions transmitted to the superstructure.

The other difficulty in an uncoupled analysis lies in selecting appropriate equivalent elastic moduli of soil compatible with strains occurring during a strong earthquake. The reduction of soil stiffness and the increase of damping associated with a strong shaking are sometimes modelled crudely in these analyses by making arbitrary reductions in the shear moduli and arbitrarily increasing the viscous damping. For this reason the results of these studies have not proved very useful for the response of pile foundations to earthquake loading.

The effect of soil non-linearity on pile head impedances of single piles has been investigated for dynamic pile-head loads by Angelides and Roesset (1981). A cylindrical
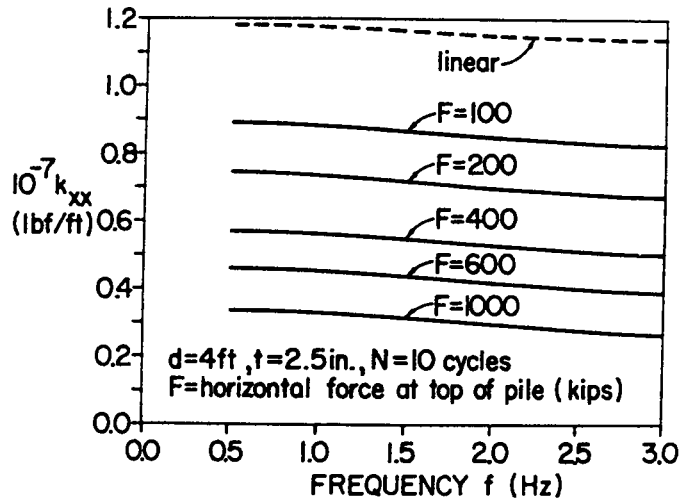
Figure 5.12: Variation of pile horizontal stiffness, k_{xx} with force and frequency due to soil non-linearity (after Angelides and Roesset, 1981)

region of soil surrounding the pile is modelled by using toroidal finite elements. A consistent boundary matrix was placed at the edge of this core region. The equivalent linear method (Seed and Idriss, 1967) was used to model the non-linear soil response. Even neglecting slippage and gapping, they demonstrated a dramatic reduction of horizontal pile head stiffness by applying harmonic horizontal force at the pile head (Figure 5.12). Similar studies using the program PILE3D described in chapter 8 confirm the finding of Angelides and Roesset (1981). The effect of soil non-linearity on pile head stiffness is significant and must be taken into account with appropriate accuracy.

Lumped mass-spring-dashpot models. A more complex analysis of the seismic response of single piles which incoporates the non-linear response of soil is based on an approach in which pile foundation and the superstructure are analyzed as a combined system. The interaction between the pile and the near field soil is modelled using a series

of non-linear Winkler springs derived from full scale test measurements or non-linear finite element solutions (Yegian and Wright, 1973; Arnold et al., 1977; Matlock et al., 1978a,1978b; Bea et al.,1984; Nogami and Chen, 1987). The stiffness of one of these springs represents the combined stiffness of the strain softened, near field soil and the exterior free field soil whose properties are governed by the intensity of the earthquake ground motions. The method of analysis relating to the use of Winkler springs is usually referred as lumped mass models.

At large displacements, the response of pile foundation is controlled by the non-linear characteristics of soil at high strain, pile separation (gapping), slippage and friction. It is difficult to incorporate these factors in a continuum model. Therefore lumped mass models, such as these employed by Penzien (1970), Matlock et al. (1978a,1980) and others, have been used to model the pile response at large displacements. For example the dynamic pile analysis program SPASM (single pile analysis with support motion) was formulated by Matlock et al. (1978a,1980) for realistic pile response analysis.

Models of this type are versatile for analysis of single piles. However difficulties exist in relating the characteristics of the discrete elements to standard geotechnical parameters of soil. Various non-linear resistance-deflection relationships known as p-y curves and t-z curves have been proposed. The soil stiffness at a particular depth is established using as input a non-linear soil resistance versus lateral pile deflection (p-y) curve where y represents the relative deflection between the pile and the moving ground during shaking and p is the net soil resistance to the pile motion.

Specification of the mathematical form of the backbone p-y curves for both static and

cyclic pile head loading of piles in sand and clay are available from several sources (American Petroleum Institute,1979; Stevens and Audibert,1986; Gazioglu and O'Neill,1984; Murchison and O'Neill, 1984). These recommendations have come from the results of full scale pile head loading tests. Extensive data on the p-y curves and non-linear pile response were obtained by Yan (1990) using the hydraulic gradient similitude method and by Gohl (1991) using the centrifuge testing. The most commonly used set of specification for constructing p-y curves is based on the recommendations of the American Petroleum Institute (1986). Mostly used in offshore structures, these p-y curves are available for clay and sand, and they make a difference between static loading and cyclic loading. However the validity of their use for earthquake analysis of piles has not been verified.

In SPASM analysis, the response of the structure relies on both the accuracy of p-y curves for representing the soil non-linearity and the accuracy of time-history input of free field displacements. Verification studies of this method by Gohl (1992) using data from centrifuge tests showed that the dynamic response of a structure is sensitive to the time-history input of free field displacements. The SPASM program underpredicts pile flexural response. A key difficulty in using SPASM is the accurate determination of free field input motions to be used along the embedded length of the pile. The damping properties are determined separately by methods such as the one proposed by Gazetas and Dobry (1984). The so-called coupled method in SPASM is actually a semi-coupled method. The method only couples the super-structure with piles, but it does not couple piles with their surrounding soils directly. Therefore the SPASM analysis is not applicable to analysis of pile groups.

5.2 Dynamic analysis of pile groups

Currently pile group stiffness and damping coefficients are widely used in dynamic sub-structuring analysis of superstructure-pile foundation. The analysis of dynamic response of pile group is limited to elastic response using uncoupled multi-step analysis. The method of analysis (Gazetas et al., 1992) involves estimation of the dynamic foundation impedance and effective input motions applied to the base of the superstructure. Dynamic sub-structuring analysis is generally carried out using modal analysis incorporating equivalent elastic pile group stiffness and damping coefficients. The pile group stiffness and damping coefficients necessary for the analysis are evaluated using one of the following methods or a combination.

A useful solution to the three-dimensional dynamic boundary-value problem has been developed by Kaynia and Kausel (1982). Results from Kaynia and Kausel (1982) show that dynamic stiffness and damping of pile group are highly frequency dependent and may significantly differ from that of a single pile. Both stiffness and damping of a pile group can be either reduced or increased due to pile-soil-pile interaction. They may exhibit very sharp peaks or be affected even for very large pile spacings. The dynamic characteristics of a pile group may be explained by pile-soil interaction which depends on the ratio of the wave length to pile spacing. At higher frequencies the waves propagating from a loaded pile in the group may be moving out of phase at the location of an adjacent pile. The occurrence of this phase shift may result in negative interaction coefficients which suggests that the stiffness of a dynamically loaded pile group may in fact be higher than the combined stiffness of a single pile multiplied by the number of piles in the group. However these analytical results are limited to linear elastic response. The sharp peaks in dynamic stiffness and damping of the elastic solution may be suppressed

due to soil non-linearity.

The concept of the dynamic interaction factor has been proposed by Kaynia and Kausel (1982) as an extension of the widely used static interaction factor approach (Poulos, 1971, 1975, 1979). The dynamic interaction factor approach is an approximation of the more rigorous pile group analysis. The use of dynamic interaction factors avoids the heavy computing effort involved in a rigorous pile group analysis. A set of interaction factors is available for floating piles, homogeneous soil and a limited selection of parameters in Kaynia and Kausel (1982) and for vertical vibration in linearly nonhomogeneous soil in Banerjee (1987). El-Marsafawi et al. (1992a, 1992b) presented approximate procedures for estimating dynamic interaction factors based on boundary element analysis, the work of Kaynia (1982), Kaynia and Kausel (1982), Davies et al. (1985) and Gazetas (1991a, 1991b). These dynamic interaction factors are limited to elastic response, and mostly for homogeneous soil.

A procedure for estimating dynamic stiffness and damping of a pile group in nonhomogeneous soil was developed and incorporated in a computer program DYNA3 (Novak et al.,1990). In DYNA3 analysis the Novak plane strain pile soil interaction approach is used to determine stiffness and damping of each single pile, which is similar to that employed in PILAY analysis. The dynamic impedance of pile group is then determined by considering the soil pile interaction (or group effect) based on the concept of dynamic interaction factors. The dynamic interaction factors used in DYNA3 are the combination of the static interaction factor by Poulos and Davies (1980) for vertical loading and El Sharnouby and Novak (1986) for horizontal loading and the dynamic interaction factors by Kaynia and Kausel (1982). Although DYNA3 analysis can deal with nonhomogeneous soil, the analysis is limited to linear elastic response and to the use of elastic dynamic

interaction factors.

The methods for direct group analysis of pile foundations based on a continuum model are limited to linear elastic behaviour using either boundary element or finite element techniques. The linear elastic assumption severely limits the applicability of these models in describing response of pile groups to moderate to strong shaking where significant soil non-linearity develops and changes the extent of interaction between piles. While non-linear 3-D finite element analyses have been carried out for research purposes to examine pile to pile interaction under static lateral loading (Brown and Shie, 1991), these methods are rarely used in practice. Dynamic 3-D finite element analyses of pile group response incorporating non-linear soil response have not been carried out to date.

5.3 Objectives of this research

In following chapters a continuum theory for analyzing dynamic response of single piles and pile groups is presented. The proposed method of analysis models the dynamic pile-soil-pile interaction as a fully coupled system and also possesses ability of modelling soil non-linear response under strong earthquake loading.

A simplified quasi-3D wave equation is proposed to describe the dynamic motion of soil under horizontal shaking. The coupled equations of motions between the pile and soil are solved using the finite element method. A finite element program PILIMP is developed to compute pile head impedances of single pile and pile group by applying harmonic forces or moments at pile head. Analyses are carried out in the frequency domain.

Studies are carried out to validate the applicability of the proposed quasi-3D model for simulating the elastic response of pile foundations. Calibration of the proposed model is made first against the elastic solutions by Kaynia and Kausel (1982). Verification of the proposed model is next conducted using data from full-scale vibration tests on an expanded base concrete pile and on a 6-pile group supporting a large transformer.

Attention is then focused on extending the proposed model to incorporate non-linear soil response under strong shaking. Dynamic analysis of pile foundation is carried out in the time domain and the procedure of this analysis is incorporated in a computer program PILE3D. The non-linear characteristics of soil is modelled by using a modified equivalent linear method of analysis. Also effective routines are incorporated in PILE3D to model the yielding of the soil and the gapping that may occur in the area near the pile head.

The capability of the quasi-3D model for simulating the non-linear dynamic response of pile foundation subjected to earthquake loading is validated using data from the centrifuge tests on a single pile and a 2x2 pile group. Under strong shaking soil non-linearity is significant and changes with time. The level of soil non-linearity also varies in space at a certain time during shaking. Therefore the dynamic stiffness and damping of pile foundation change with time. The variations of dynamic stiffness and damping of pile foundations during shaking are demonstrated for the model pile foundations used in the centrifuge tests.

Chapter 6

Elastic Response of Single Piles: Theory and Verification

6.1 Introduction

In this chapter, a quasi-3D finite element method of analysis is proposed to determine the dynamic response of pile foundations subjected to horizontal loading. The proposed model is based on a simplified 3-D wave equation. The 3-dimensional dynamic response of soil is simulated by displacements in the horizontal shaking direction. Displacements in the vertical direction and in the horizontal cross-shaking direction are neglected. Therefore a quasi-3D wave equation is established.

The finite element method is employed to solve the quasi-3D wave equation in the 3-D half-space domain. Elastic analyses are conducted in the frequency domain.

Since the elastic solutions developed by Kaynia and Kausel (1982) are the benchmark solutions for the dynamic response of pile foundations, they solutions are used to calibrate the proposed model for elastic response. Dynamic impedances of single piles are computed and compared with those obtained by Kaynia and Kausel (1982). Kinematic response of single piles is analyzed; and results are compared with those obtained by Fan et al. (1991) who used solutions by Kaynia and Kausel. Data from full-scale forced vibration testing on a single pile are also used to validate the proposed model.

6.2 Dynamic analyses of pile foundations: formulation

Under vertically propagating shear waves (Figure 6.1) the soils mainly undergo shear deformations in XOY plane except in the area near the pile where extensive compression deformations in the direction of shaking develop. The compression deformations also generate shear deformations in YOZ plane, seeing Figure 6.1. Under the light of these observations assumptions are made that dynamic motions of soils are governed by the shear waves in XOY plane and YOZ plane, and the compression waves in the shaking direction, Y. Deformations in the vertical direction and normal to the direction of shaking are neglected. Comparisons with full 3-D elastic solutions confirm that these deformations are relatively unimportant for horizontal shaking.

Let v represent the displacement of soil in the shaking direction, Y. The compression force is $\theta G^* \frac{\partial^2 v}{\partial y^2}$. The shear force in XOY plane is $G^* \frac{\partial^2 v}{\partial z^2}$, and the shear force in YOZ plane is $G^* \frac{\partial^2 v}{\partial x^2}$. The two shear waves propagate in Z direction and X direction, respectively. The inertial force is $\rho_s \frac{\partial^2 v}{\partial t^2}$; Applying dynamic force equilibrium in Y-direction, the dynamic governing equation under free vibration of the soil continuum is written as

$$G^* \frac{\partial^2 v}{\partial x^2} + \theta G^* \frac{\partial^2 v}{\partial y^2} + G^* \frac{\partial^2 v}{\partial z^2} = \rho_s \frac{\partial^2 v}{\partial t^2} \tag{6.1}$$

where G^* is the complex shear modulus, ρ_s is the mass density, and $\theta = 2/(1 - \nu)$ for a Poisson's ratio ν. Since soil is a hysteretic material, the complex shear modulus G^* is expressed as $G^* = G(1 + i \cdot 2\lambda)$, in which G is the shear modulus of soil, and λ is the hysteretic damping ratio of soil. The radiation damping will be included later.

The displacement field at any point in each element is modelled by the nodal displacements and appropriate shape functions. A linear displacement field is assumed in
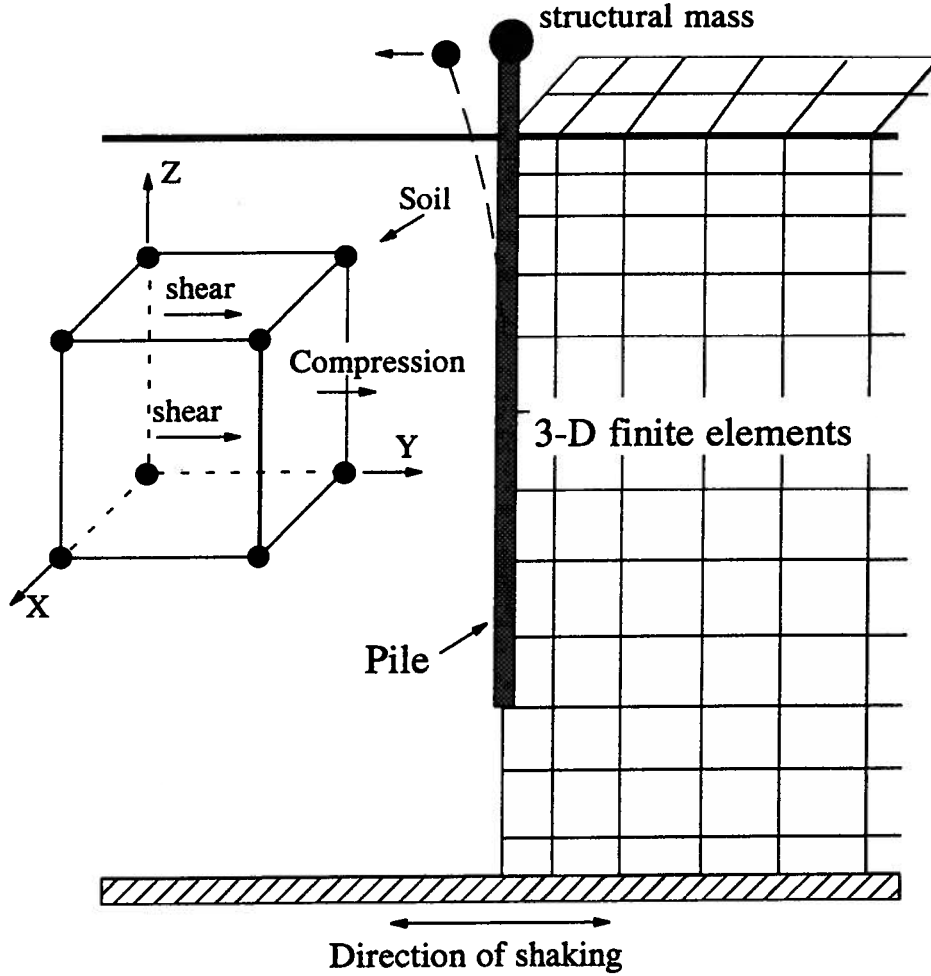
Figure 6.1: The principle of quasi-3D dynamic pile-soil interaction in the horizontal direction

$$[M^*]_{pile} = \frac{\rho_p A l}{420} \begin{bmatrix} 156 & 22l & 54 & -13l \\ 22l & 4l^2 & 13l & -3l^2 \\ 54 & 13l & 156 & -22l \\ -13l & -3l^2 & -22l & 4l^2 \end{bmatrix} \tag{6.6}$$

The radiation damping is modelled using velocity proportional damping. The damping force F_d per unit length along the pile is given by

$$F_d = c_x \cdot \frac{\partial v}{\partial t} \tag{6.7}$$

where c_x is the radiation dashpot coefficient for horizontal motion.

A simple expression for the radiation dashpot coefficients c_x, which was proposed by Gazetas et al. (1993) and is given in Eq. 5.4, is used in the analysis. Applying the same procedure as that used to obtain mass matrix, the radiation damping matrix $[C^*]$ for a pile element is

$$[C^*]_{pile} = \frac{c_x l}{420} \begin{bmatrix} 156 & 22l & 54 & -13l \\ 22l & 4l^2 & 13l & -3l^2 \\ 54 & 13l & 156 & -22l \\ -13l & -3l^2 & -22l & 4l^2 \end{bmatrix} \tag{6.8}$$

The global dynamic equilibrium equation in matrix form is written as

$$[M^*]\{\ddot{v}\} + [C^*]\{\dot{v}\} + [K^*]\{v\} = \{P(t)\} \tag{6.9}$$

in which $\{\ddot{v}\}, \{\dot{v}\}$ and $\{v\}$ are the nodal acceleration, velocity and displacement, respectively, and P(t) is the external dynamic loads applied.
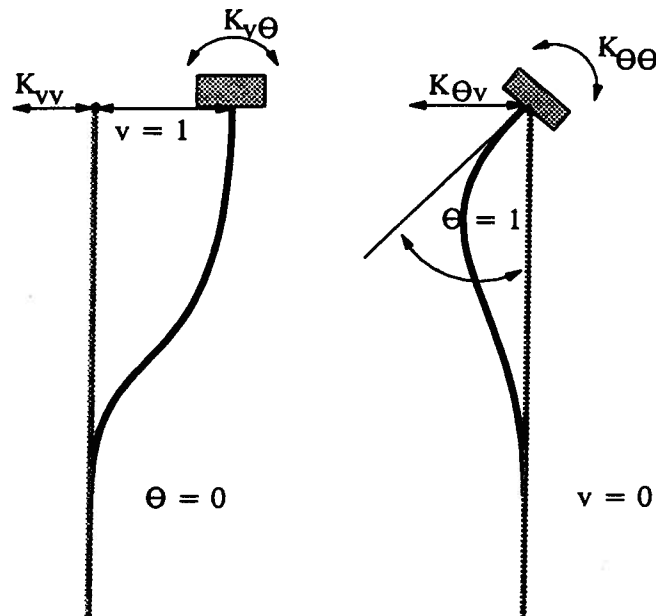
Figure 6.3: Pile head impedances

6.3 Pile head impedances

The impedances K_{ij} are defined as the complex amplitudes of harmonic forces (or moments) that have to be applied at the pile head in order to generate a harmonic motion with a unit amplitude in the specified direction (Novak,1991).

The concept of translational and rotational impedances is illustrated in Figure 6.3. The translational, the cross-coupling, and the rotational impedances of pile foundations used in this analysis are defined as

- K_{vv}: the complex-valued pile head shear force required to generate unit lateral displacement (v=1.0) at the pile head while the pile head rotation is fixed ($\theta = 0$).

- $K_{v\theta}$: the complex-valued pile head moment generated by the unit lateral displacement (v=1.0) at the pile head while the pile head rotation is fixed ($\theta = 0$)

- $K_{\theta\theta}$: the complex-valued pile head moment required to generate the unit pile head rotation ($\theta = 1.0$) while pile head lateral displacement is fixed ($v=0$)

Since the pile head impedances $K_{vv}, K_{v\theta}, K_{\theta\theta}$ are complex valued, they are usually expressed by their real and imaginary parts as

$$K_{ij} = k_{ij} + i \cdot C_{ij} \tag{6.10}$$

$$= k_{ij} + i \cdot \omega \, c_{ij} \tag{6.11}$$

in which k_{ij} and C_{ij} are the real and imaginary parts of the complex impedances, respectively, and $i = \sqrt[2]{-1}$; $c_{ij} = C_{ij}/\omega$ = coefficient of equivalent viscous damping; and ω is the circular frequency of the applied load. k_{ij} and C_{ij} are usually referred as the stiffness and damping at the pile head. All the parameters in Eq. 6.10 are dependent on frequency ω.

Determination of impedances K_{vv}, $K_{v\theta}$ and $K_{\theta\theta}$ Pile head impedances will be evaluated as functions of frequency by subjecting the system to a series of harmonic loads. Under harmonic loading $P(t) = P_0 e^{i\omega t}$, the displacement vector is of the form $v = v_0 e^{i\omega t}$, and Eq.6.9 is rewritten as

$$\{[K^*] + i \cdot \omega [C^*] - \omega^2 [M^*]\}\{v_0\} = \{P_0\} \tag{6.12}$$

or

$$[K]_{global}\{v_0\} = \{P_0\} \tag{6.13}$$

where

$$[K]_{global} = [K^*] + i \cdot \omega [C^*] - \omega^2 [M^*] \tag{6.14}$$

According to the definition, impedances K_{vv} and $K_{v\theta}$ can be found by applying a unit horizontal displacement at the pile head under the condition of a fixed pile head rotation. Eq.6.13 becomes

$$[K]_{global} \left\{ \begin{array}{c} v_0^A \\ 1.0 \\ 0.0 \end{array} \right\} = \left\{ \begin{array}{c} 0 \\ K_{vv} \\ K_{v\theta} \end{array} \right\} \tag{6.15}$$

where v_0^A are the displacements of the nodes other than pile head.

Dividing Eq. 6.15 by K_{vv} and eliminating the row of zero rotation, one obtains

$$[K]_{global} \left\{ \begin{array}{c} v_0^A / K_{vv} \\ v_0^p \end{array} \right\} = \left\{ \begin{array}{c} 0 \\ 1.0 \end{array} \right\} \tag{6.16}$$

where $v_0^p = 1/K_{vv}$. The moment at pile head M_0^p corresponding to v_0^p is also computed.

This suggests that an easy alternative for determining pile head impedances is to apply a unit horizontal force at the pile head and calculate the complex displacement at the pile head v_0^p. Therefore the pile head impedances K_{vv} and $K_{v\theta}$ are determined

$$K_{vv} = \frac{1.0}{v_0^p} \tag{6.17}$$

$$K_{v\theta} = \frac{M_0^p}{v_0^p} \tag{6.18}$$

Using the same principle, the rotational impedance $K_{\theta\theta}$ can be determined by applying a unit moment at the pile head under the condition of a fixed pile head horizontal displacement. The rotational impedance $K_{\theta\theta}$ is determined as

$$K_{\theta\theta} = \frac{1.0}{\theta_0^p} \qquad (6.19)$$

where θ_0^p is the rotation at the pile head caused by the unit moment at the pile head. Because of reciprocity principle, the cross-coupling impedance $K_{v\theta}$ and $K_{\theta v}$ are identical.

6.4 Verification of the proposed model: pile head impedances

In order to assess the accuracy of the proposed quasi-3D finite element approach, the impedance functions for single piles are determined and compared with the analytical results by Kaynia and Kausel (1982). Analyses were performed in the frequency domain for elastic conditions. Impedances $K_{vv}, K_{v\theta}, K_{\theta\theta}$ will be presented as functions of the dimensionless frequency a_0, where a_0 is defined

$$a_0 = \frac{\omega d}{V_s} \qquad (6.20)$$

in which ω is the angular frequency of the exciting loads (force and moment) at the pile head, d is the diameter of the pile, and V_s is the shear wave velocity of the soil medium. For a uniform soil profile with a shear modulus G and a mass density ρ, V_s is computed by $V_s = \sqrt{G/\rho}$.

It is found that for given values of E_p/E_s and a_0, the ratios $K_{vv}/(E_s d)$, $K_{v\theta}/(E_s d^2)$, and $K_{\theta\theta}/(E_s d^3)$ hold unchanged for any soil modulus E_s of a uniform soil profile. Therefore the normalized impedances $K_{vv}/(E_s d)$, $K_{v\theta}/(E_s d^2)$, and $K_{\theta\theta}/(E_s d^3)$, are presented

single piles:

Ep/Es = 1,000

L/d > 15 (floating pile)

soil damping 5%

poisson's ratio 0.4
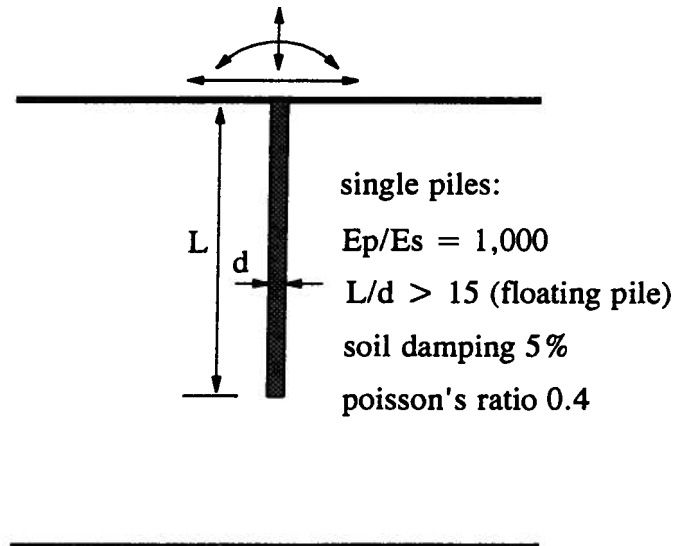
Figure 6.4: A pile-soil system used for computing impedances of single piles as a function of the dimensionless frequency a_0 when other parameters are given.

Figure 6.4 shows a pile-soil system and its relative parameters. A ratio of $E_p/E_s = 1,000$, which was used by Kaynia and Kausel, is adopted for the analysis, where E_p and E_s are the Young's moduli of the pile and the soil, respectively. The soil medium has a Poisson's ratio $\nu = 0.4$ and a hysteretic damping ratio $\lambda = 5\%$. A mass density ratio $\rho_p/\rho_s = 1.4$ is used here.

Due to symmetry, only half of the full mesh is required to model the response of pile-soil interaction. The half mesh, shown in Figure 6.5, consists of 1463 nodes and 1089 elements. The use of half mesh reduces the size of the global matrix by a factor of 4.0 with a corresponding large reduction in computational time. It took about 300 seconds to determine the dynamic impedances for each frequency using a 486 PC computer.
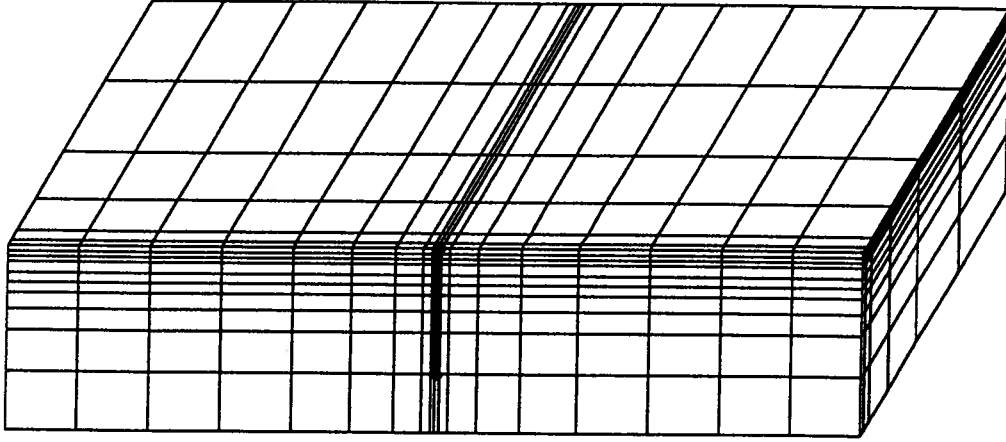
Figure 6.5: Finite element modelling of single pile for computing impedances

When the symmetric condition is applied, the Young's modulus E_p and the mass density ρ_p of the pile should be reduced by a factor of two in the case of a single pile which is bisected the axis of symmetry. This reduction is due to the fact that the central pile has been shared evenly by the other half of the full mesh. For the same reason, the applied loads (force and moment) at the pile head should be reduced by a factor of 2.0. These adjustments are automatically included in the program PILIMP.

Discussion of results The normalized quantities $K_{vv}/(E_s d)$, $K_{v\theta}/(E_s d^2)$, $K_{\theta\theta}/(E_s d^3)$ are presented as functions of dimensionless frequency a_0. Since the impedances are complex quantities, their values are expressed in term of their real parts k_{ij}(stiffness) and imaginary parts C_{ij}(damping) according to Eq.6.10. Hence the normalized stiffness and damping are compared with those obtained by Kaynia and Kausel (1982), and they are shown in Figure 6.6, 6.7, and 6.8, respectively.
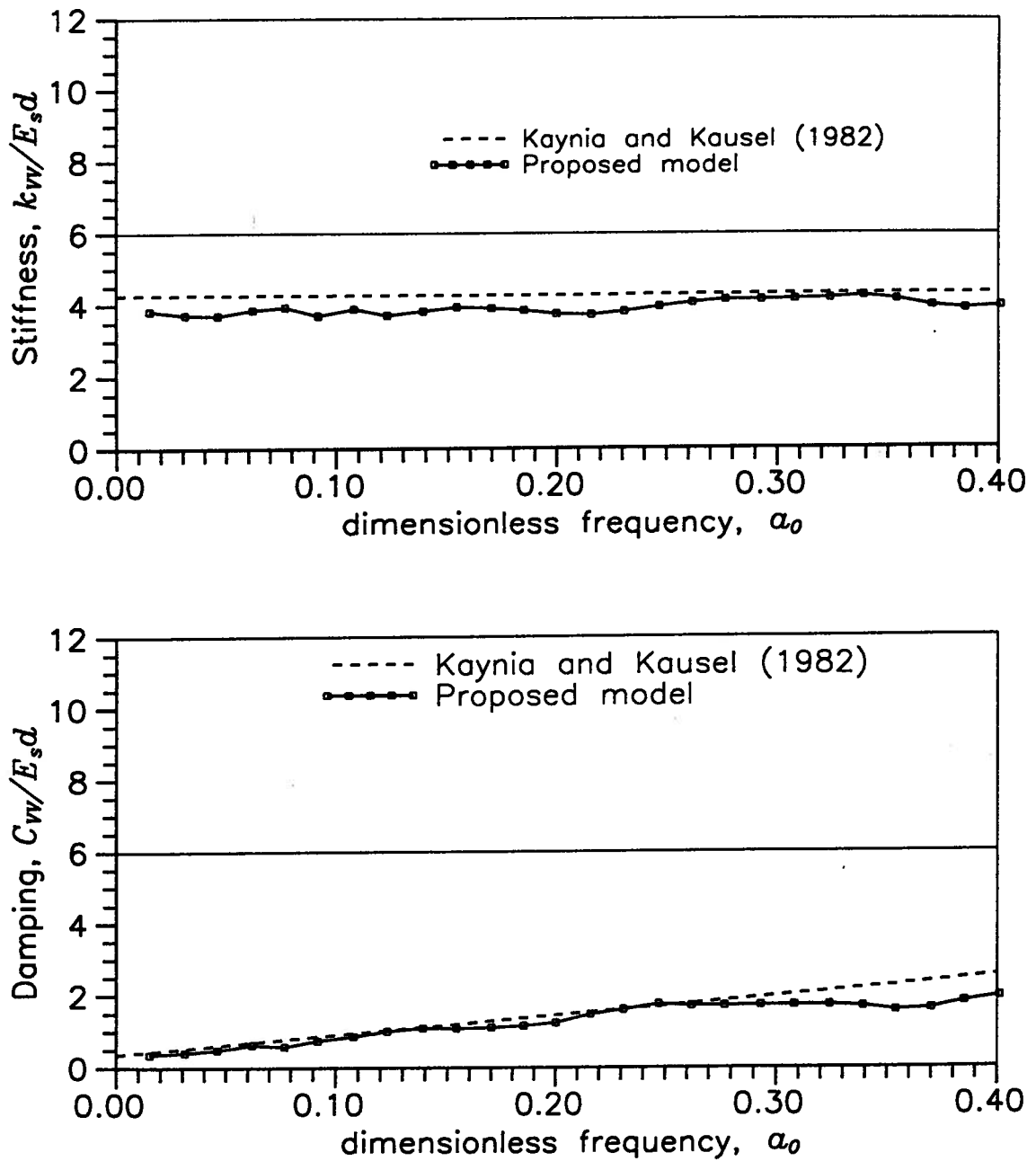
Figure 6.6: Normalized stiffness k_{vv} and damping C_{vv} versus a_0 for single piles ($E_p/E_s = 1000$, $\nu = 0.4$, $\lambda = 5\%$)
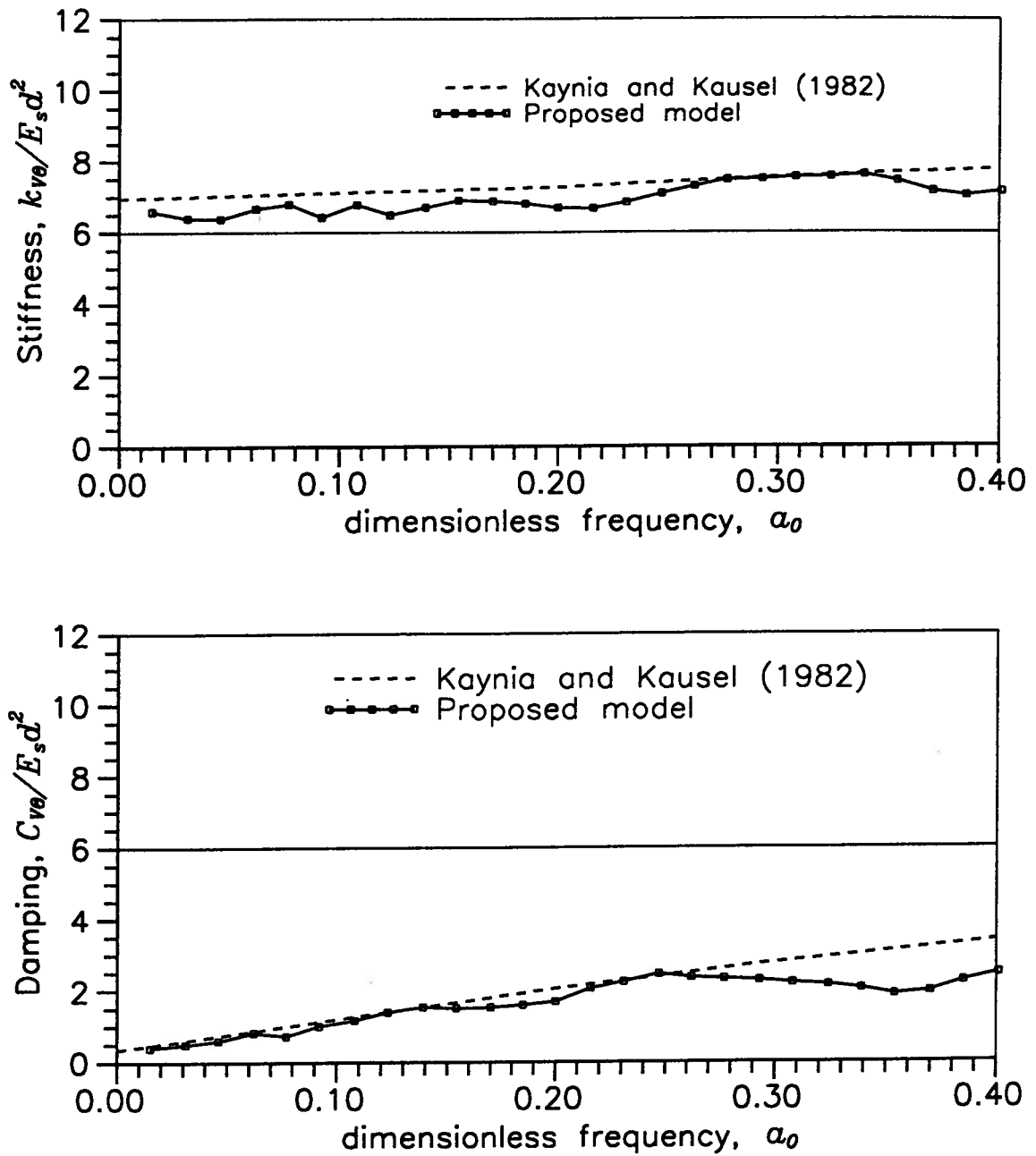
Figure 6.7: Normalized stiffness $k_{v\theta}$ and damping $C_{v\theta}$ versus a_0 for single piles ($E_p/E_s = 1000$, $\nu = 0.4$, $\lambda = 5\%$)
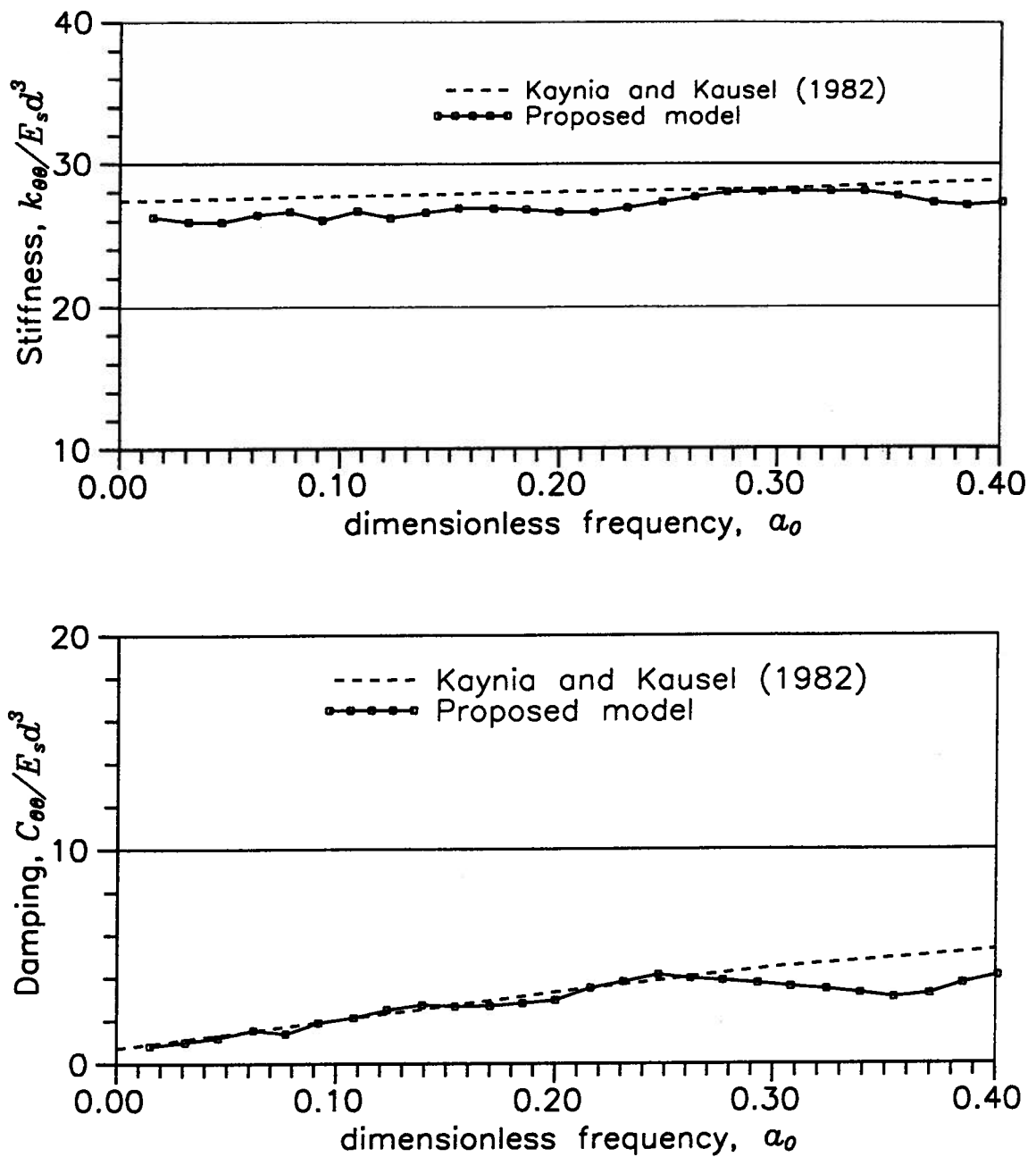
Figure 6.8: Normalized stiffness $k_{\theta\theta}$ and damping $C_{\theta\theta}$ versus a_0 for single piles ($E_p/E_s = 1000$, $\nu = 0.4$, $\lambda = 5\%$)

The computed impedances $K_{vv}, K_{v\theta}$, and $K_{\theta\theta}$ agree well with those obtained by Kaynia and Kausel. Both solutions show that dynamic stiffnesses increase slightly as the dimensionless frequency a_0 increases. The computed quantities are slightly smaller than those by Kaynia and Kausel, which implies their modelling of the pile-soil systems results in stiffer response. The translational stiffness k_{vv} computed by Kaynia and Kausel are about 10% larger than those from current study. The other two stiffnesses $k_{v\theta}$ and $k_{\theta\theta}$ show less sensitivity to the method of computation. The differences of $k_{v\theta}$ and $k_{\theta\theta}$ from the more exact solutions are about 5%.

However, the difference of impedance between the two solutions is insignificant in practice when soil non-linearity is an important factor. In many cases reduction of soil shear moduli with the increase of shear strain is significant. Quantitatively modelling of reduction of shear moduli, especially in the near field of the pile, is important for the determination of pile head impedances. It will be shown later that the proposed method has the ability to determine the non-linear dynamic impedances as the soil moduli decrease with the increase of shear strain under strong shaking.

Comparison with solutions by Novak et al. Using the mesh shown in Figure 6.5, stiffness k_{vv}, and damping C_{vv} were computed for a E_p/E_s ratio of 295. The results are then compared to solutions presented by Novak and Nogami (1977), and Novak's approximate (Novak,1974). Figure 6.9(a) and 6.9(b) show comparisons on stiffness and damping, respectively. The values of dynamic stiffness computed by Novak and Nogami are about 25% larger than those computed by author. For $a_0 > 0.3$, values of dynamic stiffness from Novak's approximate solution are about 10% larger than those computed by author. For dimensionless frequency a_0 less than 0.3, dynamic stiffness computed by
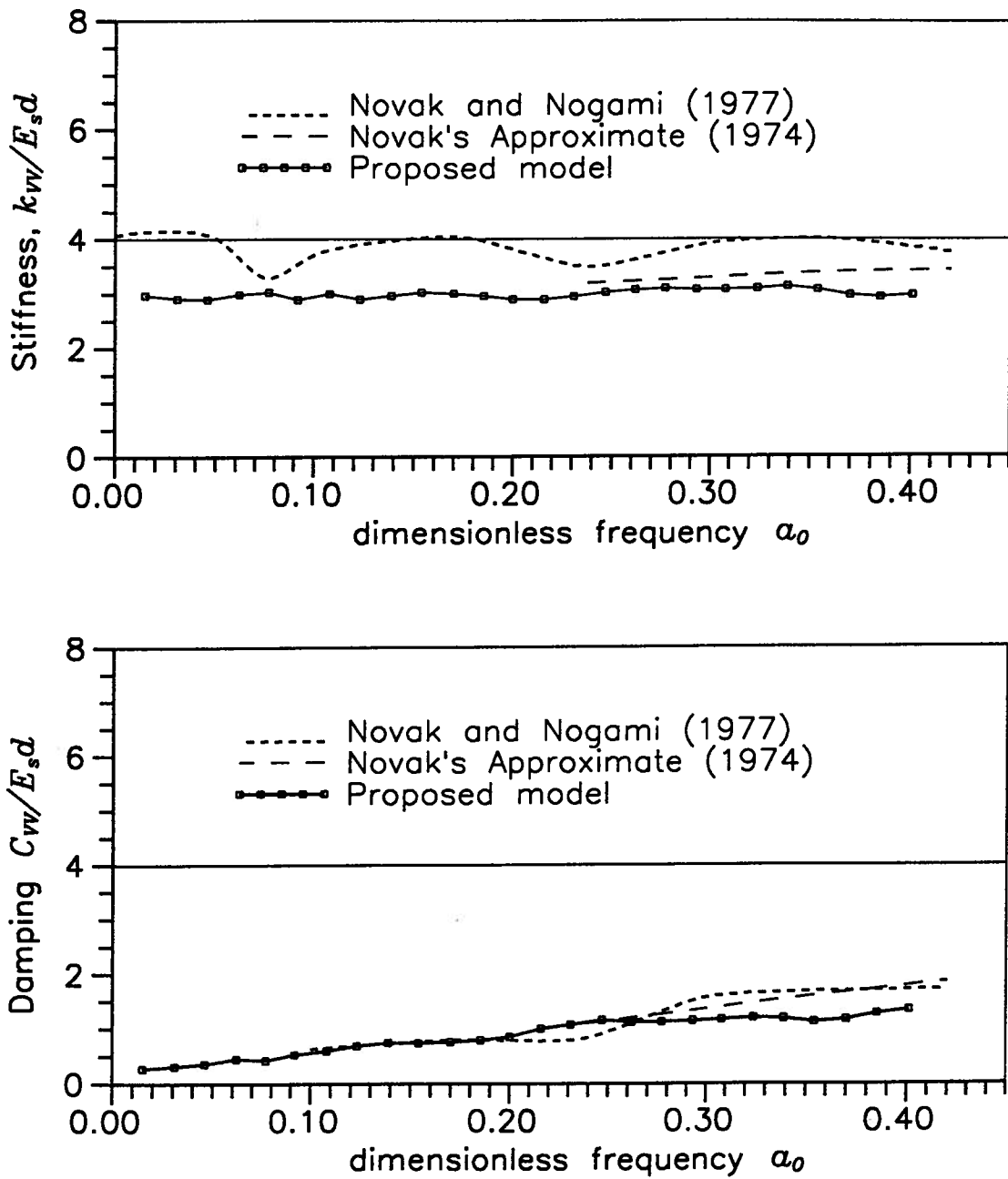
Figure 6.9: Comparison of stiffness k_{vv} and damping C_{vv} with solutions by Novak and Nogami (1977), Novak (1974)
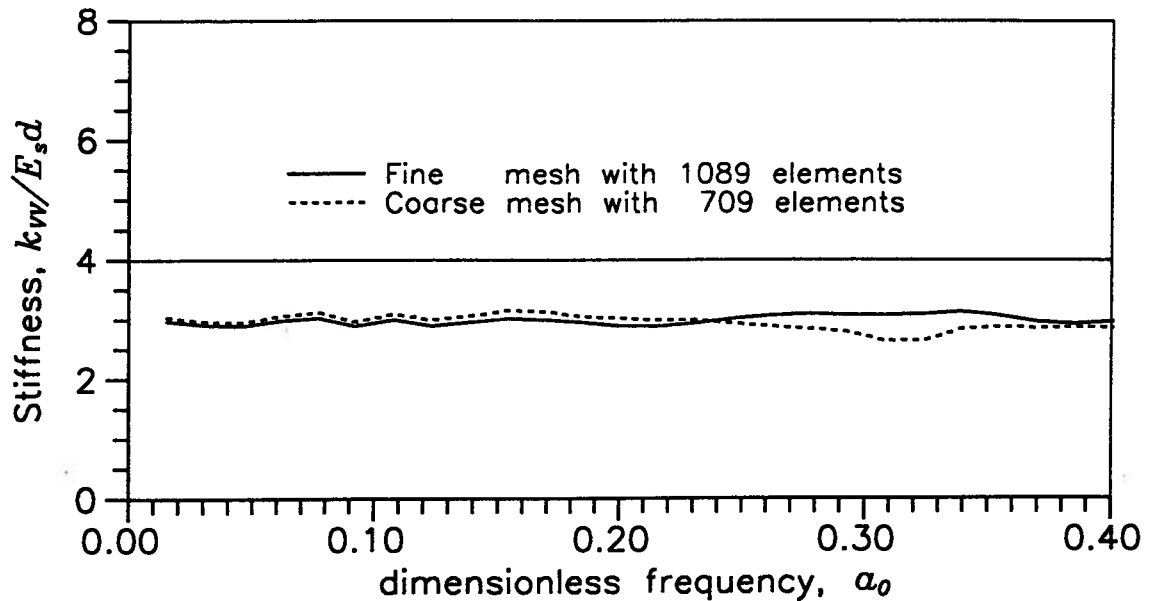
Figure 6.10: Comparison of stiffness k_{vv} for different mesh size

Novak's approximate method diminishes with the decrease of frequency. The damping from Novak and Nogami or Novak's approximate method is normally larger than damping computed in the present study (Figure 6.9(b)).

Effect of the number of finite elements The number of finite elements used in the analysis has some influence on the impedances computed using the proposed method. Theoretically accuracy of the results increases with the number of finite elements. Especially at a high frequency (such as $a_0 > 0.3$), the number of finite elements needs to be very large to capture the possible number of modes that are significant to the response of pile foundations at that frequency.

Figure 6.10 shows a comparison of the dynamic stiffness computed by two different meshes. It is clear that some differences exist between results from the two meshes around

pile head motion   free field motion

single free-head piles:

Ep/Es = 1,000 or 10,000

L/d = 20

soil damping 5%

poisson's ratio 0.4

base motion
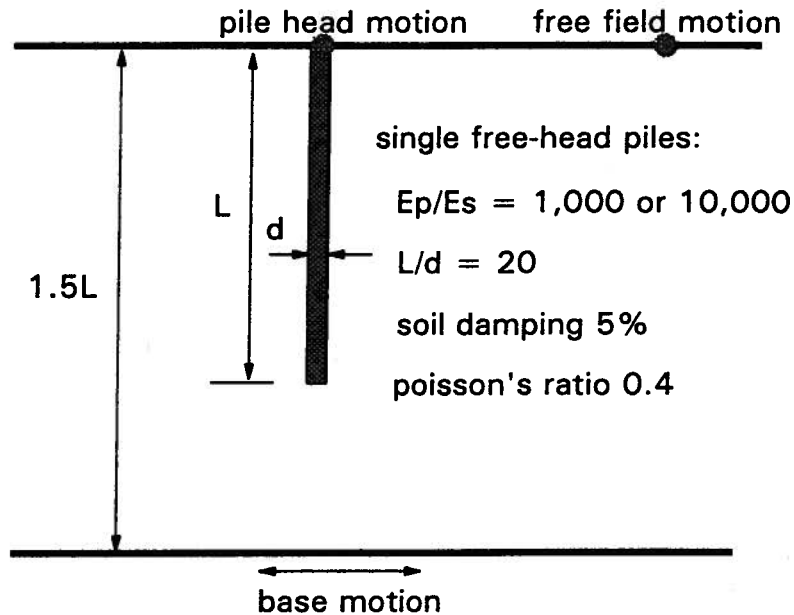
Figure 6.11: Pile foundation for analysis of kinematic response

a_0=0.3. A finer mesh with more finite elements is better to represent the dynamic response accurately.

6.5 Verification of the proposed model: kinematic interaction

A pile-soil system shown in Figure 6.11 is subjected to a harmonic displacement $v_b e^{i\omega t}$ at its rigid base. The dynamic response at the pile head may be same as or very close to the dynamic response at the free field surface if the pile is very flexible. However in many cases the dynamic response at the pile head differs significantly from the response at the free field surface because piles are generally much stiffer than soil and thus modify soil deformations. This type of interaction between piles and soils is called kinematic interaction .

6.5.1 Kinematic interaction factors

The dynamic motions at the free field surface and at the pile head are different due to the kinematic interaction between the pile and the soil. Let the harmonic displacements at the free field surface be represented by $v_{ff}e^{i\omega t}$, and at the pile head by $v_p e^{i\omega t}$ and $\theta_p e^{i\omega t}$, in which v_p and θ_p are the complex amplitudes of the translational displacement and the rotational displacement, respectively.

Absolute values of complex amplitudes of harmonic displacements are used for determining the kinematic interaction factors. The kinematic interaction factors I_u and I_ϕ are defined after Gazetas (1984) as

$$I_u = \frac{U_p}{U_{ff}} \tag{6.21}$$

$$I_\phi = \frac{\Phi_p d}{U_{ff}} \tag{6.22}$$

in which U_p, U_{ff} and Φ_p are the absolute values of the complex amplitudes v_p, v_{ff} and θ_p, respectively; and d is the diameter of the pile.

6.5.2 Computed kinematic interaction factors

The kinematic interaction factors are obtained for pile-soil systems with a flexible pile $(E_p/E_s = 1,000)$, and with a stiff pile $(E_p/E_s = 10,000)$. The other parameters of the systems are shown in Figure 6.11.

The accuracy of the quasi-3D finite element method is checked against the boundary-integral method developed by Kaynia and Kausel (1982) and used by Fan et al. (1991).

The computed kinematic interaction factors I_u and I_ϕ as functions of the dimension-less frequency a_0 are plotted in Figure 6.12 for $E_p/E_s=1,000$ and in Figure 6.13 for $E_p/E_s=10,000$ together with the interaction factors obtained by Fan et al. (1991). A comparison of the two sets of factors shows that there is very good agreement between the quasi-3D solutions and the boundary element solutions.

The kinematic interaction becomes more significant when the stiff pile is placed in the soil. For $E_p/E_s=10,000$, the response of the pile head is significantly reduced when the dimensionless frequency a_0 is greater than 0.25. At $a_0 = 0.35$, the amplitude of the translational displacement at the pile head is only 45% of the amplitude of the displacement at the free field surface.

6.6 Verification of the proposed model: forced vibration testing

Dynamic vibration testing of an expanded base concrete pile was conducted and reported by Sy and Siu (1992). The vibration test was carried out by applying very low harmonic loads at the structural mass, which generated elastic response in the system. This pro-vides an opportunity to validate the quasi-3D model for elastic response.

6.6.1 Description of site condition and test results

The testing site is located in the Fraser river delta south of Vancouver. The soil profile at the testing site consists of 4 m of sand and gravel fill overlying a 1 m thick silt layer over fine grained sand to 40 m depth. A seismic cone penetration test (SCPT 88-6) was conducted 0.9 m from the test pile location. In addition a mud-rotary drill hole (
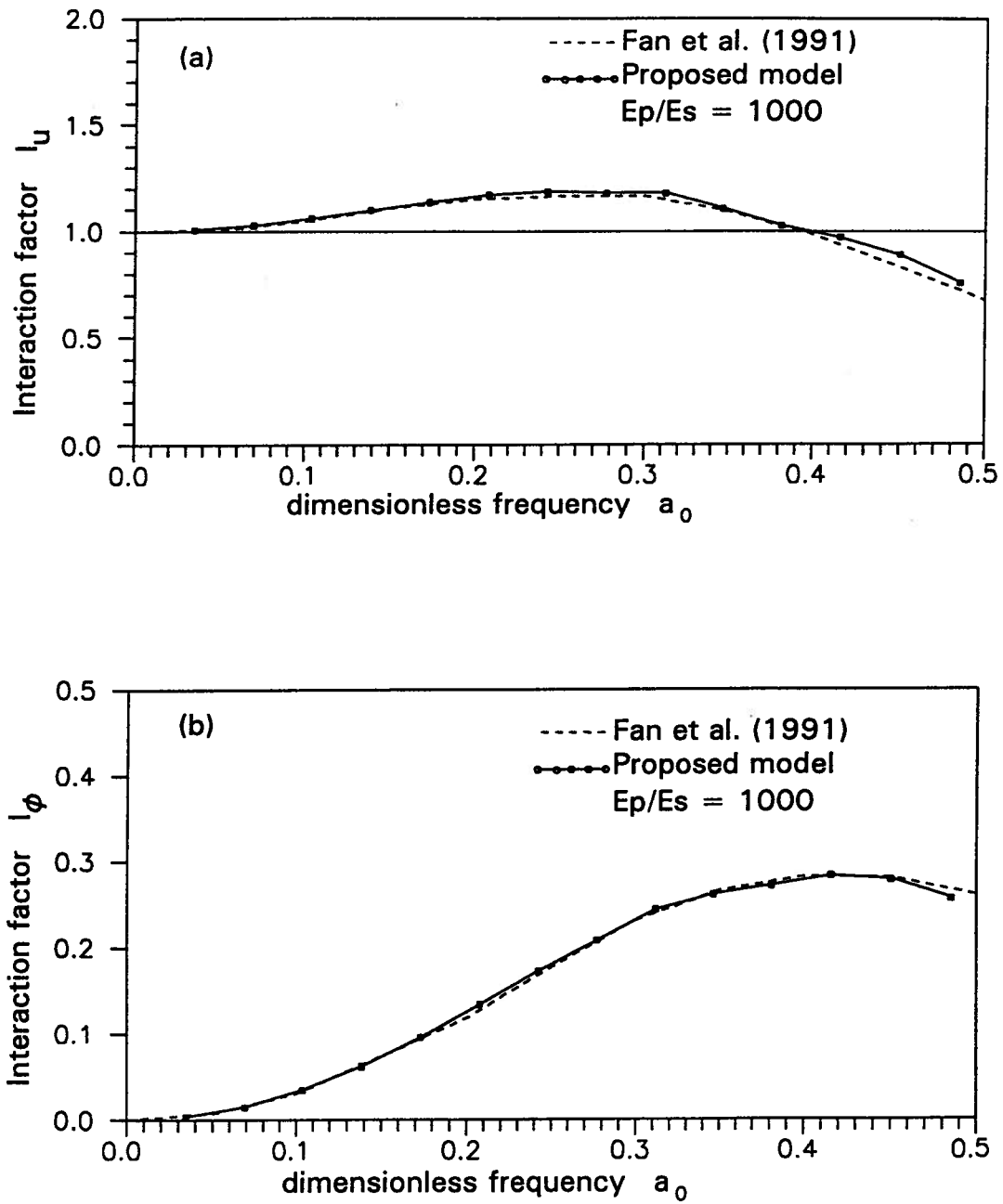
Figure 6.12: Kinematic interaction factors versus a_0 for $E_p/E_s = 1,000$
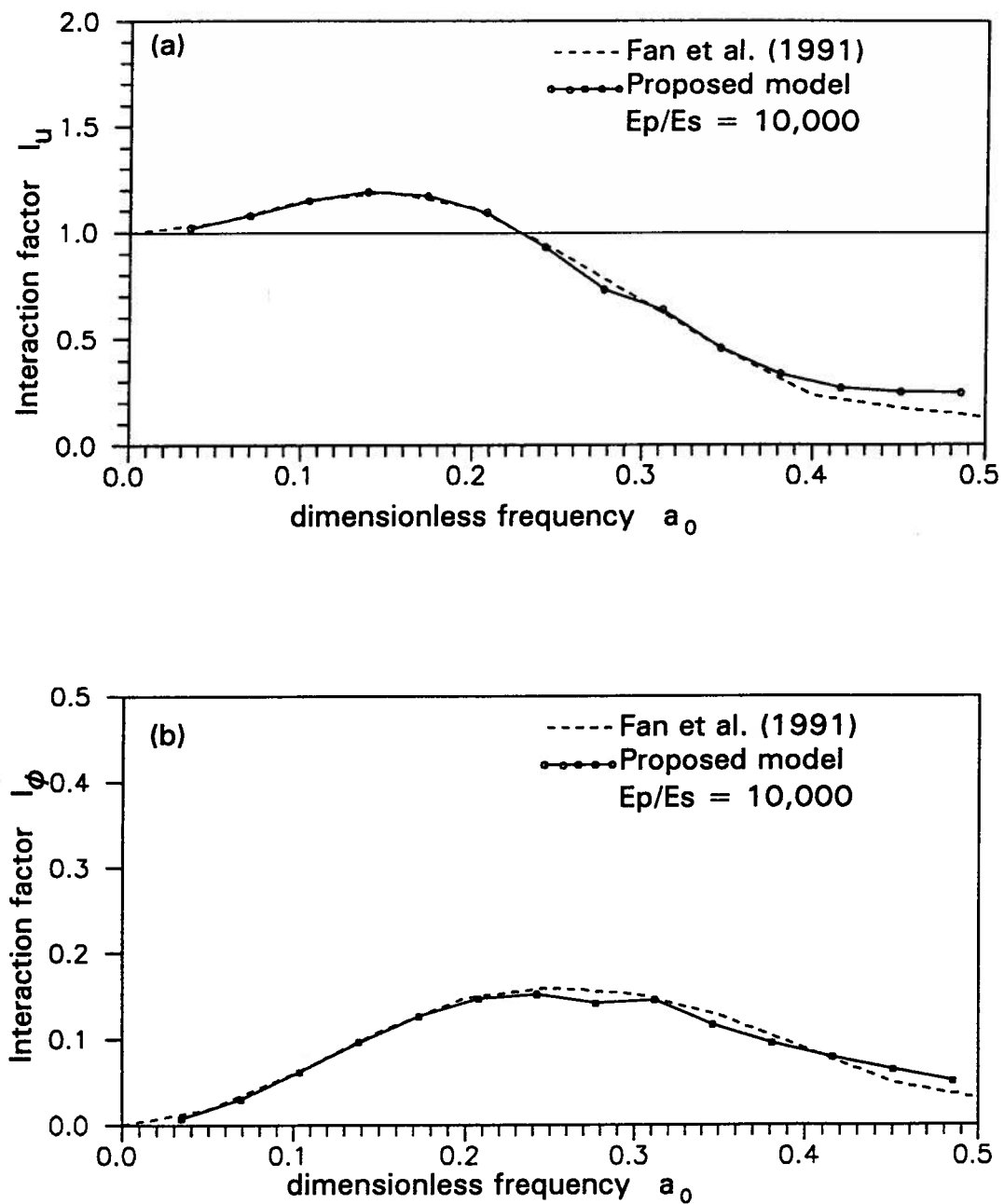
Figure 6.13: Kinematic interaction factors versus a_0 for $E_p/E_s = 10,000$
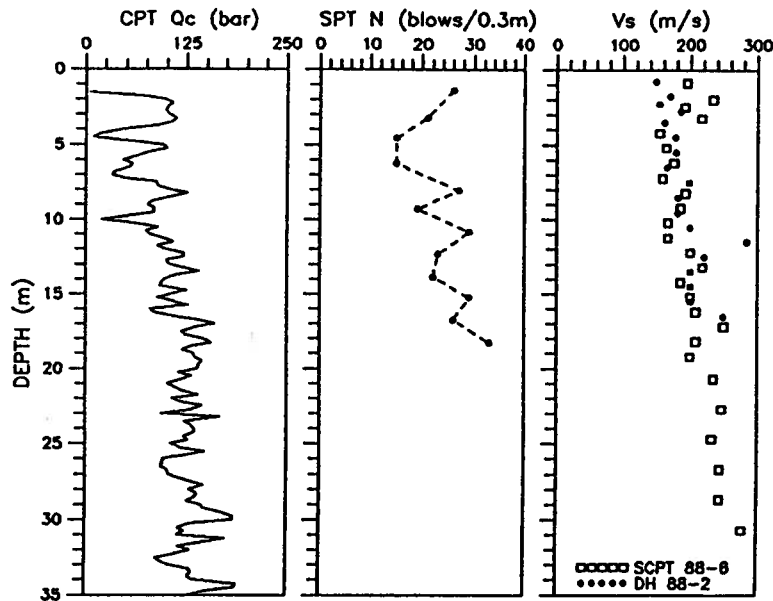
Figure 6.14: The in-situ measured geotechnical data (after Sy and Siu, 1992)

DH88-2) was carried out 2.4 m from the test pile location. The measured in-situ shear wave velocity data are presented in Figure 6.14, together with the cone penetration test (CPT) data and the Standard Penetration Test (SPT) data.

The layout of the pile test is shown in Figure 6.15. The pile is an expanded base concrete pile (Franki-type), which had a nominal 510 mm diameter shaft down to 7.6 m depth with an estimated 0.93 m diameter spherical base. In order to perform the vibration test, the top of the cast-in-situ concrete shaft was extended above the ground surface, and a structural mass consisting of 1.6 m cube of reinforced concrete was then formed on top of the pile. The final length of the additional pile shaft was 1.37 m with 150 mm above the ground surface.

Sinusoidal sweep testing was carried out for determining the fundamental frequency
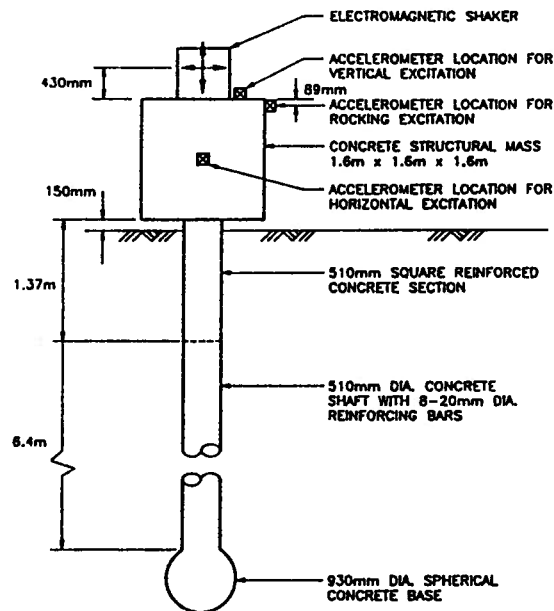
Figure 6.15: The layout of the full-scale vibration test on a single pile (after Sy and Siu, 1992)

and damping ratio of the system. Harmonic loads with an amplitude of 165 N was applied horizontally at the center of the shaker (Figure 6.15). The shaker is located at 2.03 m above the pile head. The measured fundamental frequency of the structure-pile-soil system was 6.5 Hz. The damping ratio was determined to be 4%. The damping ratio was calculated from the measured response curve using the bandwidth method (Clough and Penzien, 1975).

6.6.2 Computed results using the quasi-3D model

The structural properties of the pile cap and the test pile used in the analysis are presented in Table 6.4. The shear wave velocity (V_s), unit weight and damping ratio (D_s) used in the analysis are shown in Figure 6.16. According to Sy and Siu (1992), except for the top 1.2 m depth, an upper bound of the measured V_s values was used to account for the effect of soil densification caused by pile installation. However V_s values at the

Table 6.4: Structural properties of pile cap and test pile (after Sy and Siu, 1992)

Parameter	Unit	Value
PILE CAP AND SHAKER		
Mass	Mg	10.118
Mass moment of inertia	Mg m^2	4.317
Height to center of gravity	m	0.8
TEST PILE		
Top 1.37m : axial rigidity (EA)	MN	6350
Top 1.37m : flexural rigidity (EI)	MN m^2	141
1.37-7.77m : axial rigidity (EA)	MN	5150
1.37-7.77m : flexural rigidity (EI)	MN m^2	92
Base : axial rigidity (EA)	MN	14,720
Base : flexural rigidity (EI)	MN m^2	800
Material damping ratio		0.01
Poisson's ratio		0.25

upper 1.2 m were reduced since the original soil around the extended pile shaft section was replaced by the loose backfill. Poisson's ratio $\nu = 0.3$ was assumed for all soil layers.

Figure 6.17 shows the 3-D finite element model used for obtaining the pile head impedances. The finite element model consists of 1225 nodes and 889 elements with one beam element above the ground surface representing the pile segment above the ground. The expanded concrete base was modelled by a solid element rather than a beam element in the finite element analysis. The dynamic impedances $K_{vv}, K_{v\theta}$, and $K_{\theta\theta}$ were obtained at the pile head.

After the dynamic impedances of the pile foundation have been determined, the dynamic response of the pile cap can be obtained by performing a structural analysis. The translational and rotational response of the pile cap are obtained by using the dynamic
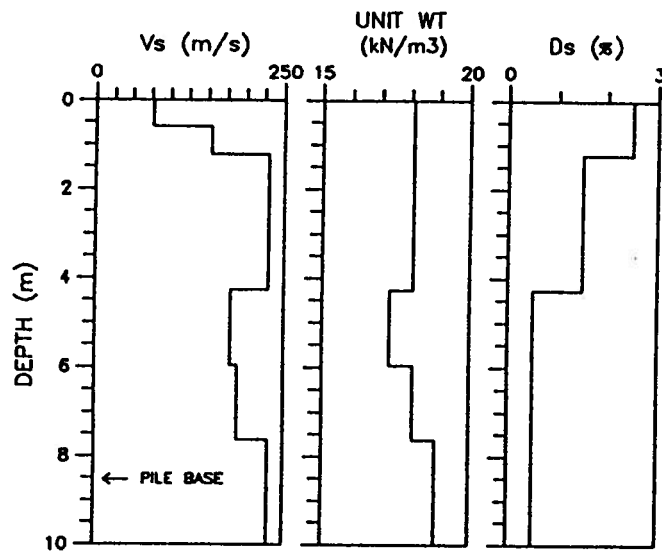
Figure 6.16: The soil parameters used in the analysis (after Sy and Siu, 1992)
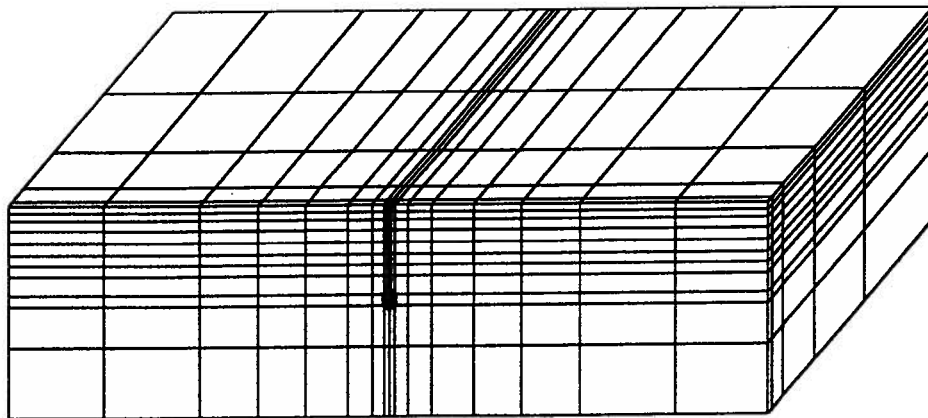
Figure 6.17: Finite element modelling of the expanded base pile

2DF system
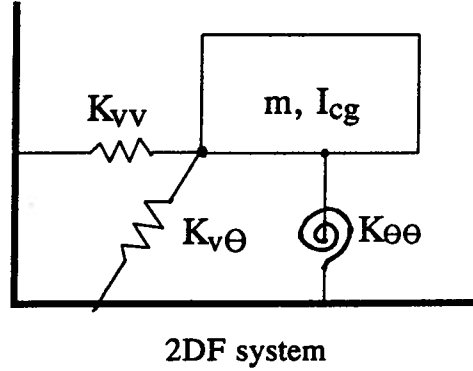
Figure 6.18: An uncoupled system modelling the horizontal motions of structure-pile cap system

solution of a two-degree of freedom system (Figure 6.18). Under harmonic loads, the translational displacement amplitude v_p and the rotational displacement amplitude θ_p at the pile head are computed according to the following equation

$$-\omega^2 \begin{bmatrix} m & m \cdot h_{cg} \\ m \cdot h_{cg} & I_{cg} \end{bmatrix} \begin{Bmatrix} v_p \\ \theta_p \end{Bmatrix} + \begin{bmatrix} k_{vv} + iC_{vv} & k_{v\theta} + iC_{v\theta} \\ k_{v\theta} + iC_{v\theta} & k_{\theta\theta} + iC_{\theta\theta} \end{bmatrix} \begin{Bmatrix} v_p \\ \theta_p \end{Bmatrix} = \begin{Bmatrix} P_0 \\ M_0 \end{Bmatrix}$$

(6.23)

where m is the mass of the pile cap and shaker, h_{cg} is the height of the centre of gravity to the pile head, and I_{cg} is the mass moment of inertia at the centre of gravity; k_{ij}, C_{ij} are the stiffnesses and dampings at the pile head; P_0 and M_0 are amplitudes of the harmonic external force and moment, respectively, applied at the pile head.

The quantities v_p and θ_p are determined using the testing loads. During the test harmonic horizontal loads with amplitude of 165 N was applied at the shaker, which caused
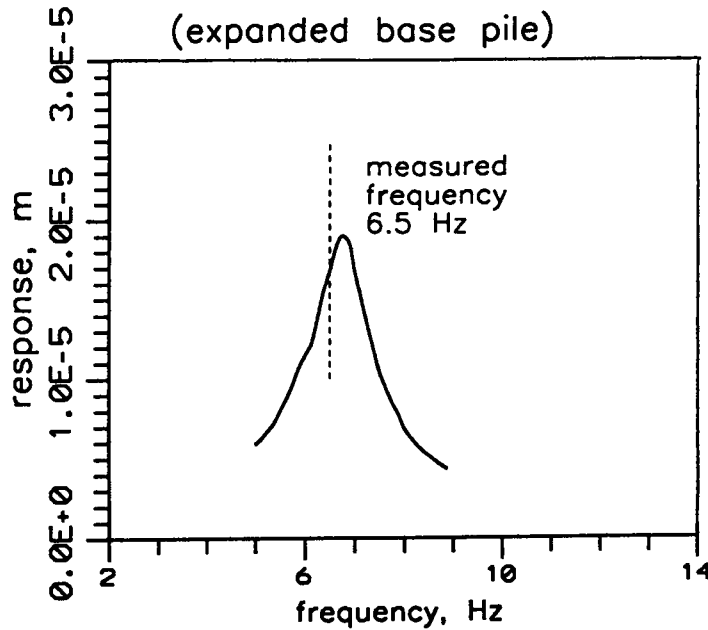
Figure 6.19: Amplitudes of horizontal displacement at the centre of gravity of the pile cap versus the excitation frequency

a moment of 335 N.m at the pile head. Therefore P_0=165 N and M_0 =335 N.m were used in Eq. 6.23 for obtaining v_p and θ_p. The horizontal displacement amplitude at the centre of gravity of the mass can now be calculated by

$$v_{cg} = v_p + \theta_p \cdot h_{cg} \tag{6.24}$$

The analyses were carried out at different frequencies ω. The computed horizontal displacement amplitude at the center of gravity of the mass versus frequency ω is shown in Figure 6.19.

Discussion of results Very clear and pronounced peak response is observed for the horizontal motion. Maximum horizontal displacement at the center of gravity of the pile cap occurs at an excitation frequency around 6.67 Hz compared to a measured resonant frequency of 6.5 Hz. The damping ratio is evaluated from the response curve in Figure

6.19 using the bandwidth method. The computed damping ratio is 6% compared to a measured damping ratio of 4%. This analysis demonstrates that the proposed model has the capability of modelling the dynamic response of single piles.

Chapter 7

Elastic Response of Pile Groups: Theory and Verification

7.1 Introduction

The quasi-3D model applied in the previous chapter to single piles is also applicable to the analysis of elastic response of pile groups under horizontal excitation. However, the horizontal displacement is coupled with rocking of the group. The rocking impedance of pile group is the measure of the resistance to rotation of the pile cap provided by the resistance of each pile in the group to vertical displacements.

In this chapter, the determination of the rocking impedance of a pile group is formulated first by applying the quasi-3D model in the vertical direction. For the verification of the proposed model, dynamic impedances of a 2x2 pile group are computed and compared with those by Kaynia and Kausel (1982). Finally, results of a full-scale vibration test on a 6-pile group are used to verify the proposed model.

7.2 Rocking impedance of pile group

The rocking impedance of a pile group reflects the resistance of the pile group to the rotation of the pile cap when piles are attached to a pile cap. If the piles can be considered pinned to the pile cap the rotation of the pile cap does not cause moments at pile heads, but it does induce vertical axial forces at pile heads as shown in Figure 7.1. The
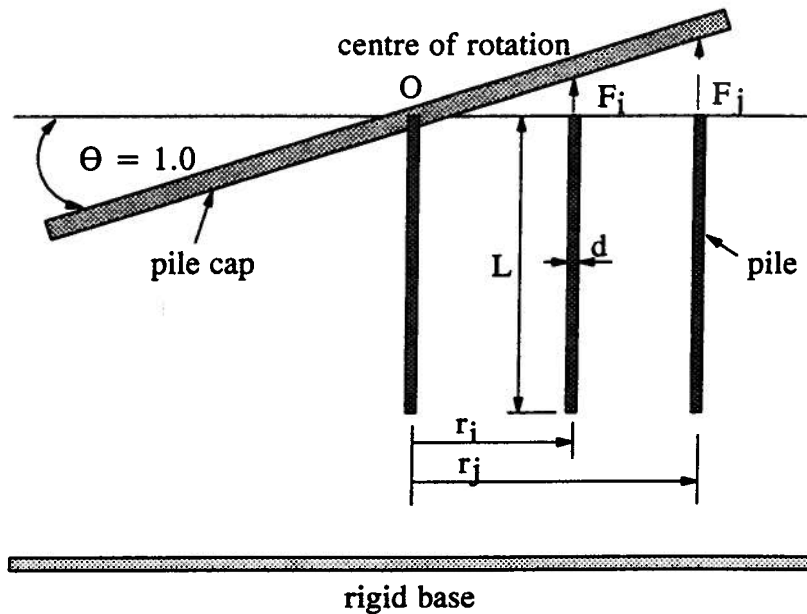
Figure 7.1: The mechanism of rocking in a pile group

rocking impedance K_{rr} of a pile group is defined as the summation of moments around the centre of rotation of the pile cap. These moments are caused by the axial forces at all pile heads required to generate a harmonic rotation with unit amplitude at the pile cap. This definition is quantitatively expressed as

$$K_{rr} = \sum r_i \cdot F_i......when...\theta_{cap} = 1.0 \qquad (7.1)$$

where r_i are distances between the centre of rotation and the pile head centres, and F_i are the amplitudes of axial forces at the pile heads.

In the analysis, the pile cap is assumed to be rigid. For a unit rotation of the pile cap, the vertical displacements w_i^p at all pile heads can be easily determined according to their distances from the center of rotation r_i. Now the task is to determine the axial forces F_i at the pile heads which are required to generate these vertical displacements w_i^p. The quasi-3D model is applied in the vertical direction to accomplish this task.

7.3 Dynamic equation of motions in the vertical direction

Under a vertically propagating compression wave, the soil medium mainly undergoes compression deformations in the vertical direction. In the two horizontal directions, shearing deformations are generated due to the internal friction of the soil. Although compressions occur in the two horizontal directions, assumptions are made that the normal stresses in the two horizontal directions are small and can be ignored. Therefore the dynamic motions of the soil are governed by the compression wave in the vertical direction and the shear waves propagating in the two horizontal direction X and Y as shown in Figure 7.2.

By analogy to the principle used in the previous chapter, the quasi-3D wave equation of soil in the vertical direction is given by

$$G^* \frac{\partial^2 w}{\partial x^2} + G^* \frac{\partial^2 w}{\partial y^2} + \theta_z G^* \frac{\partial^2 w}{\partial z^2} = \rho_s \frac{\partial^2 w}{\partial t^2} \qquad (7.2)$$

where G^* is the complex shear modulus, ρ_s is the mass density of soil, and θ_z is a function of Poisson's ratio ν. Based on assumptions that normal stresses in the two horizontal directions X and Y are zero, it is determined $\theta_z = 2(1 + \nu)$.

The stiffness matrix $[K]_{soil}$ and mass matrix $[M]_{soil}$ are evaluated from Eq. 7.2 for each soil element as described earlier.

Under a vertical propagating compression wave, the undamped free vibration equation of motion for a pile element is given by
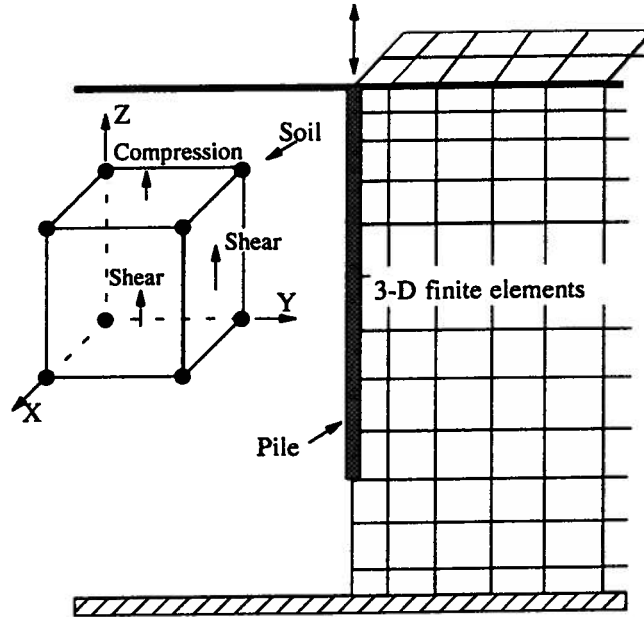
Figure 7.2: The quasi-3D model in the vertical direction, Z

$$E_p A \frac{\partial^2 w}{\partial z^2} = \rho_p A \frac{\partial^2 w}{\partial t^2} \qquad (7.3)$$

where $E_p A$ is the compression rigidity of the pile, and ρ_p is the mass density of the pile.

The stiffness matrix $[K]_{pile}$ and the mass matrix $[M]_{pile}$ of the pile element are given by

$$[K]_{pile} = \frac{E_p A}{l} \begin{bmatrix} 1 & -1 \\ -1 & 1 \end{bmatrix} \qquad (7.4)$$

and

$$[M]_{pile} = \frac{\rho_p l A}{6} \begin{bmatrix} 2 & 1 \\ 1 & 2 \end{bmatrix} \qquad (7.5)$$

The radiation damping under vertical motion is also modelled using velocity proportional damping. The radiation dashpot coefficient c_z, which was proposed by Gazetas et al. (1993) and is given in Eq. 5.3, is used in the analysis. The radiation damping matrix

for a pile element is given by

$$[C]_{pile} = \frac{c_z l}{6} \begin{bmatrix} 2 & 1 \\ 1 & 2 \end{bmatrix} \tag{7.6}$$

The global dynamic equilibrium equation in matrix form is given by

$$[M]\{\ddot{w}\} + [C]\{\dot{w}\} + [K]\{w\} = \{P(t)\} \tag{7.7}$$

in which $\{\ddot{w}\}, \{\dot{w}\}$ and $\{w\}$ are the nodal acceleration, velocity and displacement, respectively, and P(t) is the external dynamic loads applied.

7.4 Determination of rocking impedance

In order to evaluate the rocking impedance of pile group, harmonic forces $P(t) = P_0 e^{i\omega t}$ are applied, which generate harmonic displacements $w = w_0 e^{i\omega t}$. Therefore, Eq.7.7 is rewritten as

$$[K]_{global}\{w_0\} = \{P_0\} \tag{7.8}$$

where

$$[K]_{global} = [K] + i \cdot \omega[C] - \omega^2[M] \tag{7.9}$$

Since the vertical displacements at the pile heads $\{w_1^p, w_2^p, \cdot, \cdot, w_m^p\}^T$ are known, the axial forces $\{F_1, F_2, \cdot, \cdot, F_m\}^T$ at the pile heads are determined by

$$
\begin{bmatrix} K_{nn} & K_{nm} \\ K_{mn} & K_{mm} \end{bmatrix}
\begin{Bmatrix} w_1 \\ w_2 \\ \cdot \\ w_n \\ w_1^p \\ \cdot \\ w_m^p \end{Bmatrix}
=
\begin{Bmatrix} 0 \\ 0 \\ \cdot \\ 0 \\ F_1 \\ \cdot \\ F_m \end{Bmatrix}
\tag{7.10}
$$

Where K_{nn}, K_{nm}, K_{mn}, and K_{mm} are sub-matrices of the global matrix K_{global}, and $\{w_1, w_2, \cdot, \cdot, w_n\}^T$ are vertical displacements at nodes other than the pile heads. The pile head axial forces $\{F_1, F_2, \cdot, \cdot, F_m\}^T$ can be determined if the displacements $\{w_1, w_2, \cdot, \cdot, w_n\}^T$ are known. Applying the matrix separation technique to Eq. 7.10 yields

$$
[K_{nn}] \begin{Bmatrix} w_1 \\ w_1 \\ \cdot \\ w_n \end{Bmatrix}
+ [K_{nm}] \begin{Bmatrix} w_1^p \\ \cdot \\ w_m^p \end{Bmatrix}
= \begin{Bmatrix} 0 \end{Bmatrix}
\tag{7.11}
$$

and

$$
\begin{Bmatrix} F_1 \\ \cdot \\ F_m \end{Bmatrix}
= [K_{mn}] \begin{Bmatrix} w_1 \\ w_1 \\ \cdot \\ w_n \end{Bmatrix}
+ [K_{mm}] \begin{Bmatrix} w_1^p \\ \cdot \\ w_m^p \end{Bmatrix}
\tag{7.12}
$$

After the displacement vector $\{w_1, w_2, \cdot, \cdot, w_n\}^T$ is computed from Eq.7.11, the pile head axial force vector $\{F_1, \cdot, F_m\}$ is then determined using Eq. 7.12 . Now the rocking impedances of the pile group are evaluated using Eq. 7.1. The procedure for computing rocking impedances of pile group is incorporated in the computer program PILIMP.

2x2 pile group:

Ep/Es = 1,000

s/d = 5.0

L/d > 15 (floating pile)

soil damping 5%

poisson's ratio 0.4
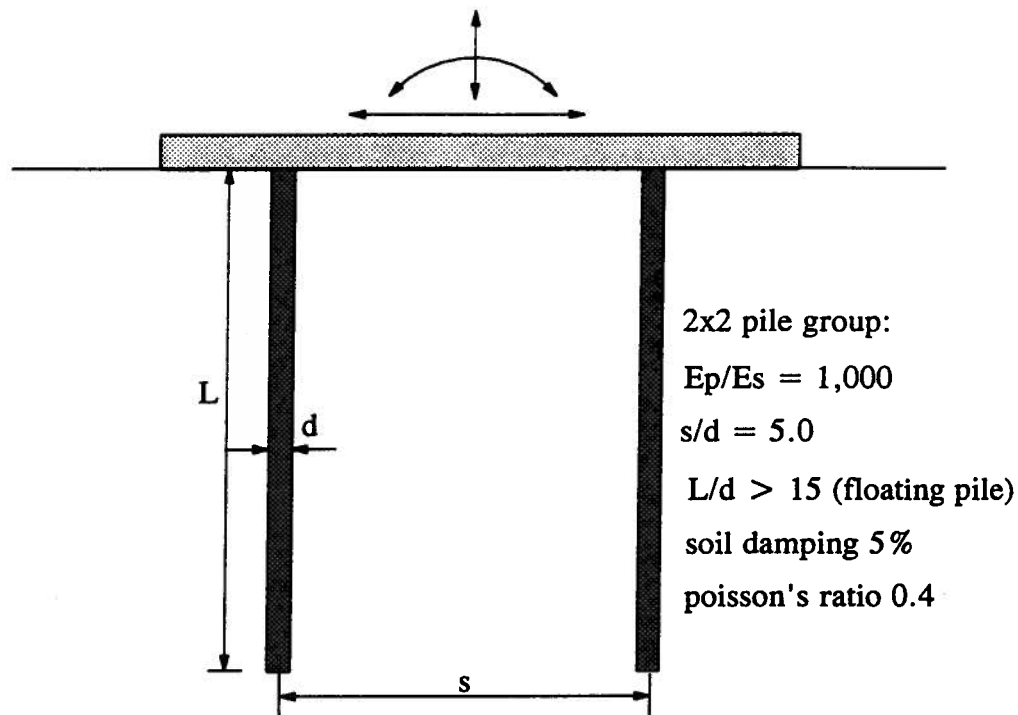
Figure 7.3: A pile-soil system used for computing impedances of pile groups

7.5 Elastic response of pile group: results and comparisons

The dynamic impedances of a 4-pile (2x2) group with s/d=5.0 are presented, in which s is the centre to centre distance of two adjacent piles and d is the pile diameter. A rigid pile cap is rigidly connected to the four pile heads as shown in Figure 7.3. A stiffness ratio of the pile and soil $E_p/E_s = 1000$ is used, and a mass density ratio $\rho_s/\rho_p =0.7$ is applied.

The dynamic impedances of pile groups were obtained by Kaynia and Kausel (1982) for a half-space soil medium. In approximating the half-space soil medium using the finite elements, a rigid base is assumed at a depth of 5L (L=length of pile) beyond the tip of the pile. The dynamic impedances are evaluated at the bottom of the pile cap.

Discussion of results In order to show the pile group effect, dynamic impedances of the pile group are normalized to the static stiffness of the pile group expressed as the stiffness of a single pile times the number of piles in the group. The normalized dynamic impedances of the pile group, which are called the dynamic interaction factors, are therefore defined as

$$\alpha_{vv} = \frac{K_{vv}}{N \cdot k_{vv}^0} \tag{7.13}$$

$$\alpha_{v\theta} = \frac{K_{v\theta}}{N \cdot k_{v\theta}^0} \tag{7.14}$$

$$\alpha_{\theta\theta} = \frac{K_{\theta\theta}}{N \cdot k_{\theta\theta}^0} \tag{7.15}$$

in which $k_{vv}^0, k_{v\theta}^0, k_{\theta\theta}^0$ are static stiffnesses of a single pile identical to those in the pile group that is placed in the same soil medium, and N is the number of piles in the pile group ($N=4$ for a 4-pile group). $K_{\theta\theta}$ in Eq. 7.15 is the individual rotational impedance at the head of each pile due to the geometrical and material properties of the pile.

In order to present the results graphically, the complex-valued dynamic interaction factors α_{ij} are separated by their real parts α_{ij}(stiffness) and imaginary parts α_{ij}(damping). The computed dynamic interaction factor α_{vv}(stiffness) is compared in Figure 7.4(a) with that by Kaynia and Kausel (1982). Very good agreement is observed between the two solutions for dimensionless frequency $a_0 < 0.28$. For $a_0 > 0.28$, the computed values are about 25% higher than those by Kaynia and Kausel. The computed interaction factors $\alpha_{vv}(damping)$ are in good agreement with those by Kaynia and Kausel (Figure 7.4(b)).

The dynamic interaction factors $\alpha_{vv}, \alpha_{v\theta}$, and $\alpha_{\theta\theta}$ of the pile group are shown in Figure 7.5(a) for stiffness component and in Figure 7.5(b) for damping component. The

results show that the translational stiffness k_{vv} (or α_{vv}) shows the greatest effect of group pile-soil interaction; whereas the rotational stiffness $k_{\theta\theta}$ (or $\alpha_{\theta\theta}$) shows the least effect (Figure 7.5(a)). However their corresponding damping components show the reverse trend (Figure 7.5(b)). For $a_0 < 0.3$ the stiffness interaction factors $\alpha_{vv}, \alpha_{v\theta}$, and $\alpha_{\theta\theta}$ are in the range of 0.6, 0.7 and 0.9, respectively.

Because the piles are rigidly connected to the pile cap at the pile heads, the total rotational impedance of the pile group $K_{\theta\theta}^{cap}$ consists of both the rocking impedance K_{rr} of the pile group and the rotational impedance $K_{\theta\theta}$ at the head of each pile

$$K_{\theta\theta}^{cap} = K_{rr} + K_{\theta\theta} \qquad (7.16)$$

Following the notation used by Kaynia and Kausel, the total rotational impedance of the pile group $K_{\theta\theta}^{cap}$ is normalized as $K_{\theta\theta}^{cap}/(N \cdot \sum r_i^2 k_{zz}^0)$, in which k_{zz}^0 is the static vertical stiffness of a single pile placed in the same soil medium.

The normalized quantity $K_{\theta\theta}^{cap}/(N \cdot \sum r_i^2 k_{zz}^0)$ is compared in Figure 7.6 with that by Kaynia and Kausel. Very good agreement between the two solutions is seen for the stiffness component (Figure 7.6(a)). Good agreement between the two solutions for the damping components also exists for $a_0 < 0.3$ (Figure 7.6(b)). For $a_0 > 0.3$, the computed damping component is about 25% less than that by Kaynia and Kausel.

It has been shown that the proposed model can well simulate the dynamic characteristics of pile groups. The conclusion is drawn from comparisons with analytical results by Kaynia and Kausel. To further verify the applicability of the proposed model for simulating the elastic response of pile group, field vibration tests of a 6-pile group are
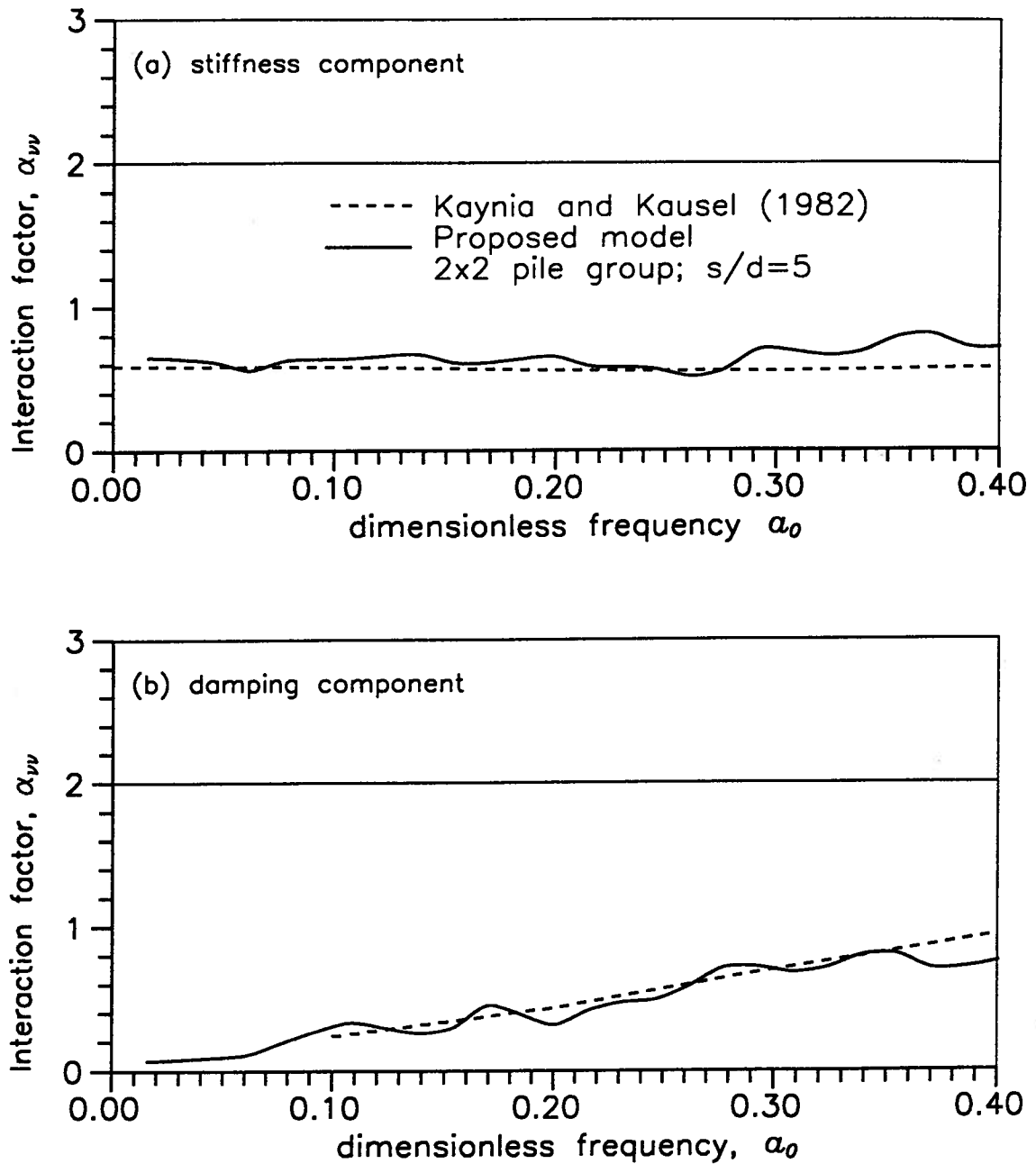
Figure 7.4: Comparison of dynamic interaction factor α_{vv} with solution by Kaynia and Kausel for 2x2 pile groups ($E_p/E_s = 1000, s/d = 5.0$)
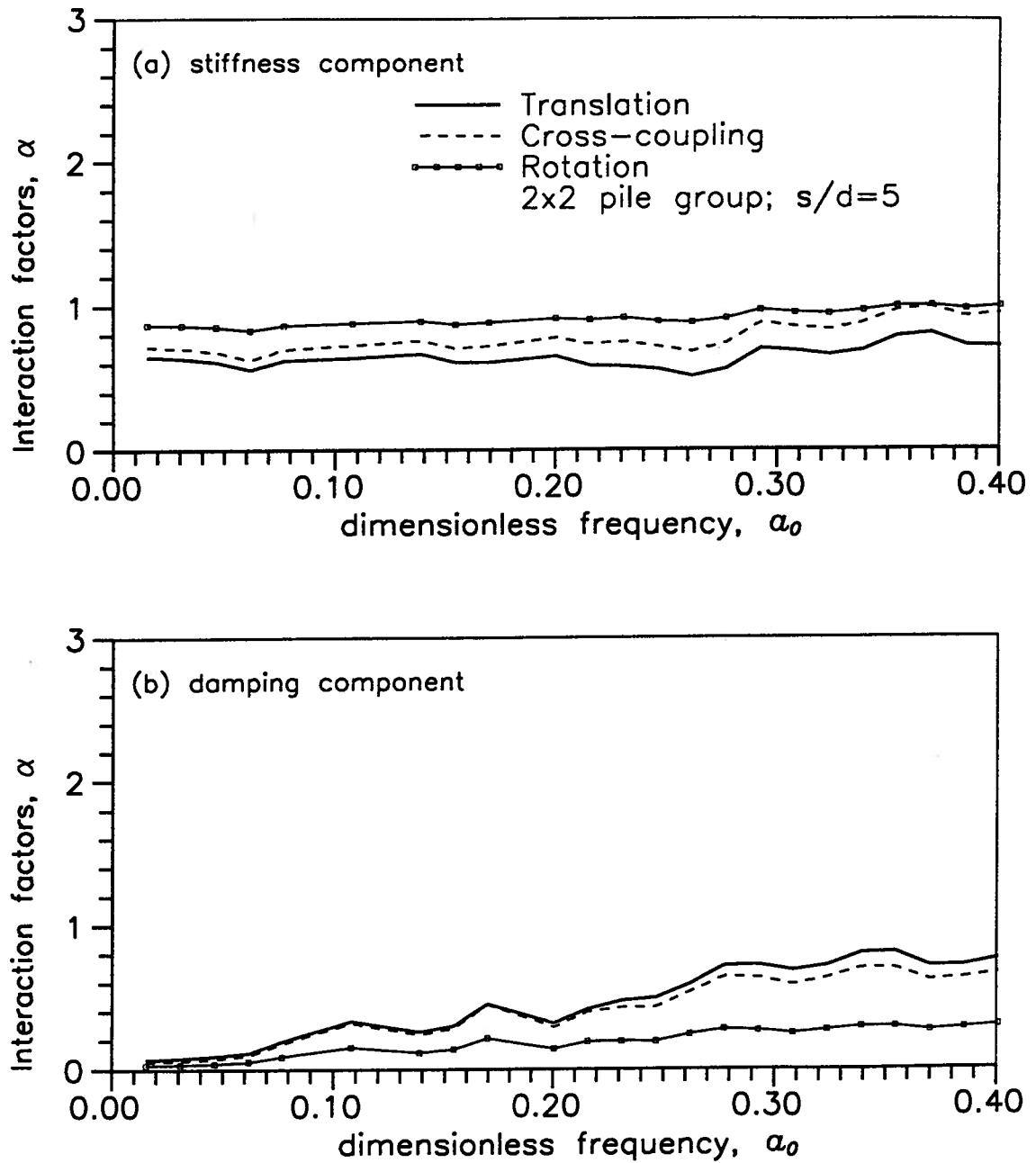
Figure 7.5: Dynamic interaction factors $\alpha_{vv}, \alpha_{v\theta}, \alpha_{\theta\theta}$ versus a_0 for 2x2 pile groups $(E_p/E_s = 1000, s/d = 5.0)$
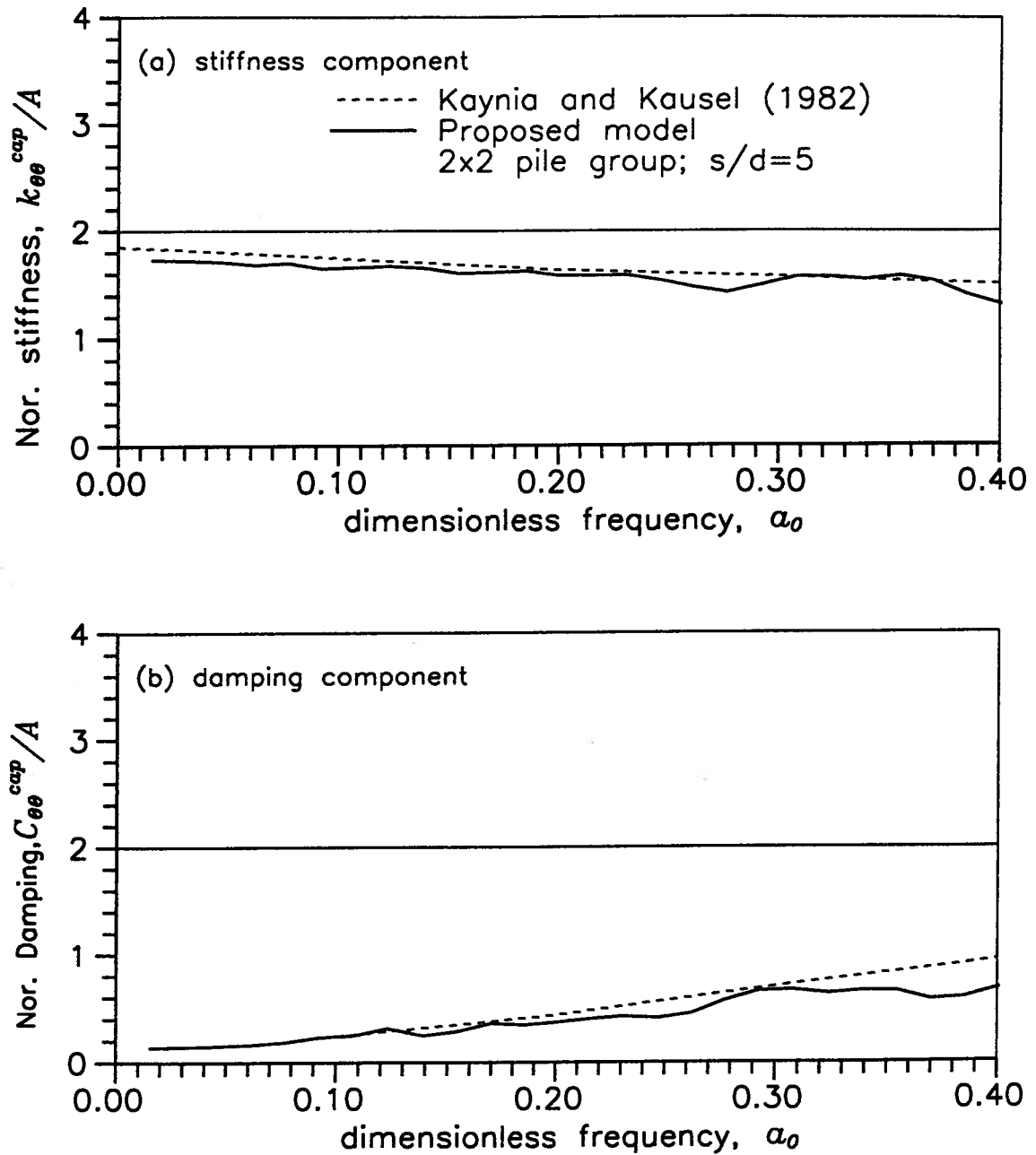
Figure 7.6: Comparison of normalized total rotational impedance $K_{\theta\theta}^{cap}/A$ with solution by Kaynia and Kausel for 2x2 pile groups ($E_p/E_s = 1000$, s/d=5, $A = N * \Sigma r_i^2 k_{zz}^0$)

analyzed in the next section.

7.6 Full-scale vibration test on a 6-pile group

A quick release horizontal vibration test was performed on a full-scale pile group foundation of a large transformer bank (Bank 79) located at the Duwamish substation, Seattle, Washington. Test data and analytical results were reported by Crouse and Cheang (1987). The foundation of the transformer consists of a pile cap with 6 vertical piles embedded in 40 ft of loose saturated, sandy soils overlying stiff soil.

The transformer-pile cap system is analyzed using the proposed quasi-3D finite element method of analysis. Results of this analysis are used to verify the applicability of the proposed model for pile group.

7.6.1 Description of vibration and its testing results

The transformer and foundation system has been described in detail in Crouse and Cheang (1987) and are briefly summarized below. The soil profile at the location of transformer bank consists of mostly loose to medium dense sand to silty sand, with some dense sand or gravelly sand layers, overlying very dense gravelly sand glacial till at 12.2 m depth. The ground water table was at a depth of 3.7 m. The in-situ shear wave velocities (V_s) measured from a downhole seismic survey in the sand to silty sand deposits are 125 m/sec in the upper 3.7 m and 165 m/sec below 3.7 m depth. Figure 7.7 shows the idealized soil profile at Duwamish Station according to Crouse and Cheang (1987).

LAYER THICKNESS	DEPTH (ft)	σ'_v (psf)	τ_{max} (psf)	G_{max} (10^5 psf)	γ_t (pcf)	ϕ (°)
4'	2	220	79.2	6	110	30
4'	6	660	237.6	6		
4'	10	1110	399.6	6		
2'	13	1368	492.5	10		
2'	15	1463	526.7			
4'	18	1606	578.2			
5'	22.5	1820	655.2			
3'	26.5	2010	723.6		129	40
4'	30	2177	783.7		119	30
4'	34	2367	852.1		119	30
6'	39	2605	937.8		119	30

SAND TO SILTY SAND

GRAVELLY SAND

SAND TO SILTY SAND

GRAVELLY SAND (GLACIAL TILL)

SYMBOLS

σ'_v = VERTICAL CONFINING STRESS

τ_{max} = SHEAR STRENGTH

G_{max} = LOW-STRAIN SHEAR MODULUS

γ_t = TOTAL DENSITY

ϕ = INTERNAL FRICTION ANGLE

Figure 7.7: Idealized soil profile at Duwamish Substation (after Crouse and Cheang, 1987)

Figure 7.8 shows the transformer bank and the pile foundation. The transformer, weighing 326 kip is anchored to concrete pedestals which is a continuous part of the pile cap. The pile cap has a dimension of 13.4 ft by 8.00 ft. The pile cap is embedded beneath the ground surface as shown in Figure 7.8. The pile foundation consists of 6 vertical, 12 inches O.D. by 0.172 inch wall thickness, concrete filled steel pipe piles. These piles are spaced at 4.67 ft and 5.00 ft centre to centre in the X and Y directions, respectively. All the piles are extended into the very dense glacial till layer at 40 ft depth. The composite compressional rigidity (EA) and the flexural rigidity (EI) of the each concrete filled pipe pile are $5.1 \times 10^8 lb$ and $4.24 \times 10^7 lb.ft^2$, respectively, where E= Young's modulus, A= cross section area, and I= bending moment of inertia.

The quick-release free vibration test was conducted by Crouse and Cheang (1987).
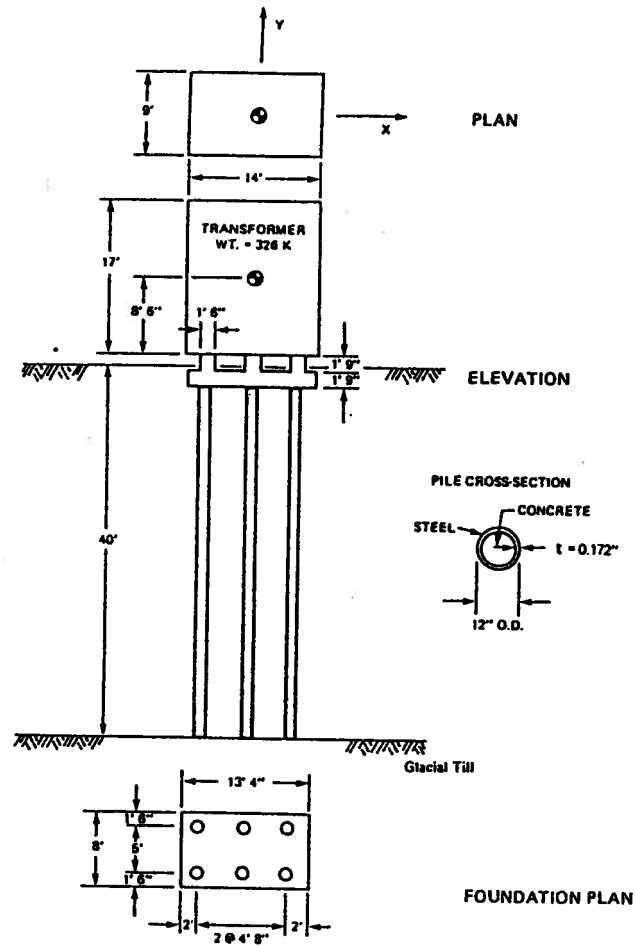
Figure 7.8: Setup of a full-scale free vibration test on a 6-pile group (after Crouse and Cheang, 1987)

A sling was attached to the transformer, and then pulled and quickly released to let the structure vibrate freely. The motions were recorded at various locations on the foundation. Tests were performed in both principal horizontal directions, NS or Y-axis and EW or X-axis, of the transformer foundation.

The resonant frequencies and damping ratios of the transformer foundation system were determined from the recorded time histories of transient vibrations by Crouse and Cheang (1987). The measured fundamental frequencies in NS and EW directions are 3.8 Hz and 4.6 Hz, respectively. The measured damping ratios in the NS and EW directions are 6% and 5%, respectively.

7.6.2 Computed results using the proposed model

In present analysis the soil profile shown in Figure 7.7 is used except the shear modulus distribution modified by Sy (1992) is adopted. According to Sy (1992), a correction on measured shear wave velocity was made to account for the soil densification due to pile installation. An increase of 4% in low strain shear modulus G_{max} values was applied to the measured free field values for this correction. Poisson's ratio $\nu = 0.3$ and material damping ratio $\lambda = 5\%$ are used for all soil layers in present analysis.

Figure 7.9(a) and 7.9(b) show the finite element models used in the analysis for obtaining dynamic impedances in NS direction and EW direction, respectively. Dynamic impedances of the pile foundation are computed covering an excitation frequency range from 0 Hz to 6 Hz. At this stage of the analysis, the effect of pile cap embedment is not taken into account. The computed impedances of the pile group corresponding to the excitation frequencies at 3.74 Hz in NS direction and at 4.63 Hz in EW direction are

listed in Table 7.6. The stiffness and damping values shown in this Table are referenced to the bottom of the pile cap.

In order to determine the resonant frequencies of the transformer-pile cap system, dynamic response of the system is computed by subjecting the system to horizontal harmonic forced excitation at different frequencies. Figure 6.18 shows the structural mass and its supporting dynamic impedances (springs and dashpots). Eq. 6.23 is used again for obtaining dynamic response of the structural mass at a particular excitation frequency. Harmonic force and moment were applied at the centre of gravity of the transformer-pile cap system. According to Crouse and Cheang, the transformer and pile cap have a total mass of 1.13×10^4 slugs. The height of centre of gravity of the system is 10.9 ft above the pile head. The moments of inertia are $4.38 \times 10^5 slug.ft^2$ and $5.46 \times 10^5 slug.ft^2$ about axes in the NS direction and in the EW direction, respectively.

The response curves of the transformer-pile cap system are shown in Figure 7.10 in dashed lines. The resonant frequency of the system is the excitation frequency at which the peak dynamic response of the system occurs. The damping ratios are determined using the the bandwidth method from the response curves. The computed resonant frequencies and damping ratios are shown in Table 7.5. Results are presented together with the measured values.

Effect of pile cap embedment   In the previous analysis the effect of pile cap-soil interaction was not included. According to Crouse and Cheang, gaps between the pile cap and the soil underneath it may exist due to settlement of soil. Also conventionally the effect of pile cap-soil interaction has been included by considering the soil reaction acting

(a)

(b)
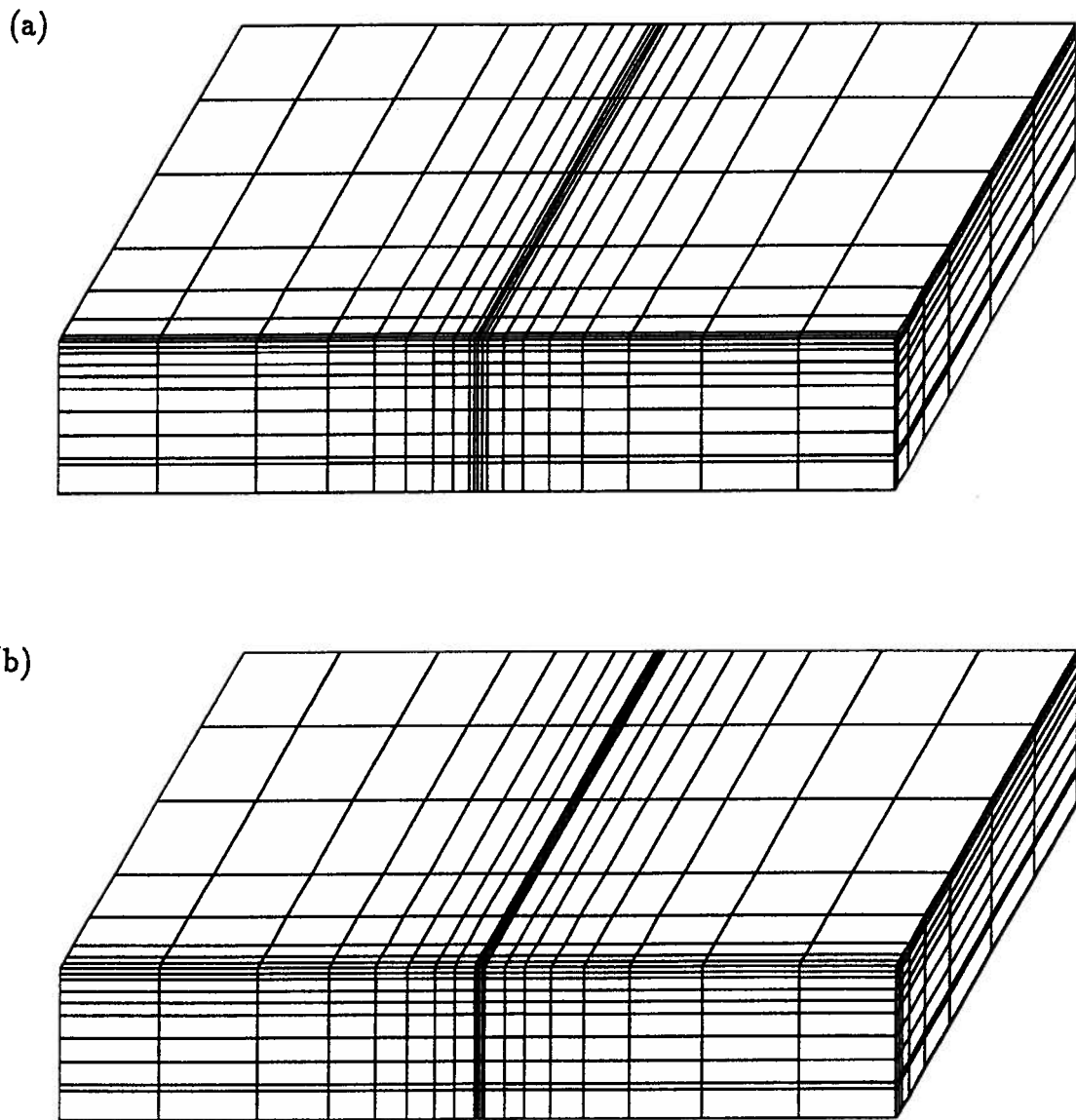
Figure 7.9: 3-D finite element models of the 6-pile foundation (a) NS direction, (b) EW direction

Table 7.5: Computed resonant frequencies and damping ratios without the effect of pile cap embedment

Resonant frequencies (Hz)				Damping ratios			
Computed		Measured		Computed		Measured	
NS	EW	NS	EW	NS	EW	NS	EW
3.50	4.37	3.8	4.60	0.08	0.06	0.06	0.05

on the vertical sides of the pile cap (Prakash and Sharma, 1990 & Novak et al.,1990).

Therefore in this analysis only the soil reactions acting on the vertical sides of the pile cap are included and the soil reactions acting on the base of the pile cap are not considered. The side reaction due to pile cap embedment usually result in increased foundation stiffness and damping. According to Beredugo and Novak (1972), the foundation stiffness and damping due to pile cap embedment can be determined using the plain strain soil model.

The rectangular pile cap had an area of 106.67 ft^2, an equivalent radius of 5.83 ft. The embedment depth of the pile cap was 1.75 ft, and the shear modulus of soil at that depth was 6.0×10^5 psf. Based on these data, using Beredugo and Novak's solution, the stiffness and damping due to pile cap embedment are determined at the bottom of the pile cap as

Translation

$$k_{vv}^* = 4.20 \times 10^6 \text{ lb/ft}$$

$$C_{vv}^* = 1.33 \times 10^5 \cdot \omega \text{ lb/ft}$$

Cross-coupling

Table 7.6: Computed stiffness and damping of the transformer pile foundation

	N-S (f=3.74 Hz)		*E-W (f=4.63 Hz)*	
	with embed. effect	without embed. effect	with embed. effect	without embed. effect
$k_{vv}(lb/ft)$	2.46e+7	2.04e+7	2.55e+7	2.13e+7
$k_{v\theta}(lb/rad)$	-2.21e+7	-2.57e+7	-2.43e+7	-2.79e+7
$k_{\theta\theta}^{cap}(lb.ft/rad)$	1.34e+9	1.25e+9	2.59e+9	2.50e+9
$C_{vv}(lb/ft)$	10.0e+6	7.05e+6	8.81e+6	5.05e+6
$C_{v\theta}(lb/rad)$	-5.10e+6	-7.62e+6	-1.97e+6	-5.25e+6
$C_{\theta\theta}^{cap}(lb.ft/rad)$	9.20e+7	6.91e+7	1.74e+8	1.44e+8

$$k_{v\theta}^* = 3.68 \times 10^6 \text{ lb/rad}$$

$$C_{v\theta}^* = 1.16 \times 10^5 \cdot \omega \text{ lb/rad}$$

Rotation

$$k_{\theta\theta}^* = 9.34 \times 10^7 \text{ lb.ft/rad}$$

$$C_{\theta\theta}^* = 1.03 \times 10^6 \cdot \omega \text{ lb.ft/rad}$$

After adding the stiffness and damping due to pile cap embedment to these of the pile group, the combined stiffness and damping of the transformer foundation are determined and they are shown in Table 7.6 at the resonant frequencies.

The dynamic response of the transformer-pile cap system is obtained including the effect of pile cap embedment. Figure 7.10 shows the response curves of the transformer-pile cap system when the effect of pile cap embedment is included. They are compared with those when the embedment effect is not included. It can be seen that the pile cap embedment results in increased stiffness and damping of the transformer foundation.
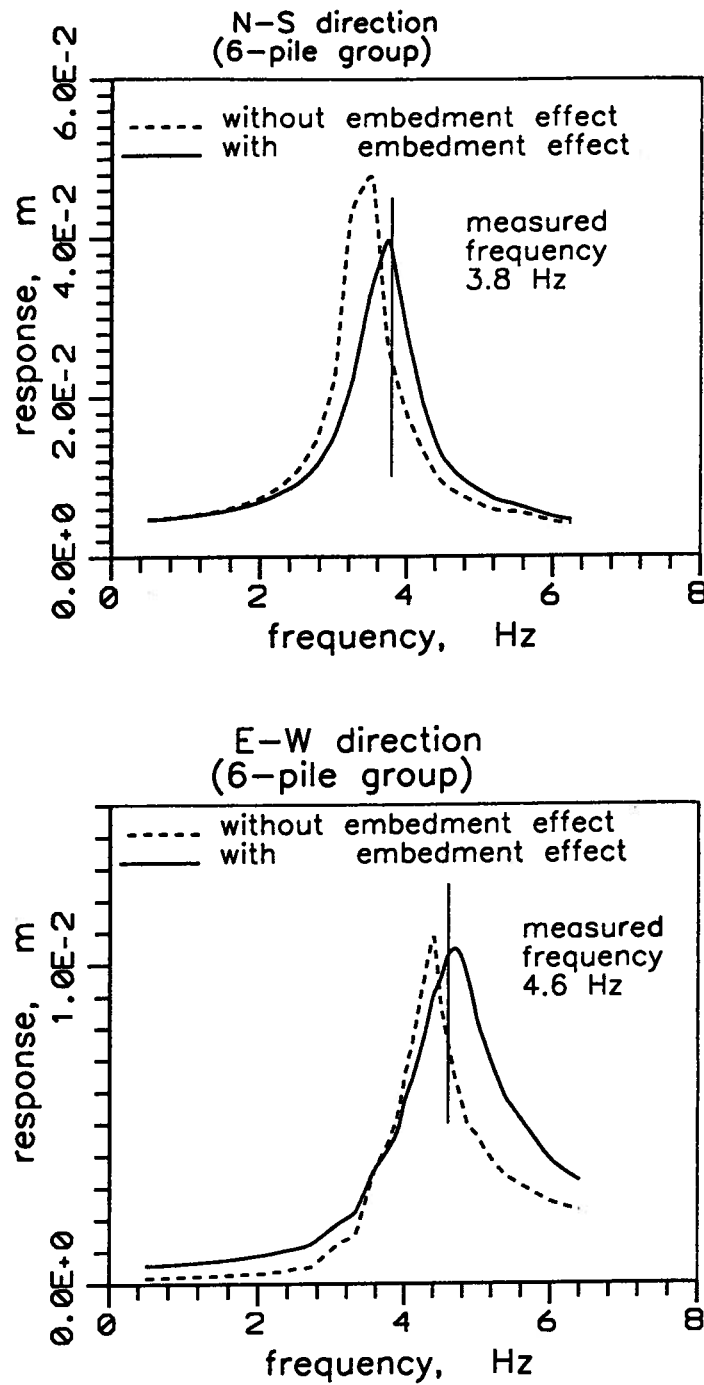
Figure 7.10: Response curves of the of transformer-pile cap system (a) NS direction (b) EW direction

Table 7.7: Measured and computed resonant frequencies and damping ratios including the effect of pile cap embedment

Natural frequencies (Hz)				*Damping ratios*			
Computed		*Measured*		*Computed*		*Measured*	
NS	EW	NS	EW	NS	EW	NS	EW
3.74	4.63	3.8	4.60	0.09	0.09	0.06	0.05

The computed and measured resonant frequencies and damping ratios of the transformer-pile cap system are given in Table 7.7. The computed resonant frequencies including the effect of pile cap embedment are 3.74 Hz and 4.63 Hz in the NS direction and in the EW direction, respectively. The corresponding measured resonant frequencies are 3.8 Hz and 4.6 Hz. The computed resonant frequencies match very well with the measured frequencies in both principal directions. However, the computed damping ratios are about 50% to 80% higher than the measured damping ratios.

Chapter 8

Non-Linear Analysis of Seismic Soil-Pile-Structure Interaction

8.1 Introduction

In this chapter the quasi-3D finite element method of analysis described in chapter 6 and 7 is used to model dynamic response of pile foundations subjected to earthquake loading. Since earthquake excitation is a random process, the non-linear finite element analysis is conducted in the time domain. The use of time-domain analysis makes it possible to model the variations of soil properties with time under earthquake loading. Therefore, adjustments in the proposed model are made first to accommodate the time-domain analysis. Then studies are focused on modelling non-linear response of the soil under earthquake loading.

A finite element program PILE3D has been developed for dynamic analysis of pile foundation under earthquake loading. In PILE3D, the shear stress-strain relationship of soil is simulated to be either linear elastic or non-linear incrementally elastic. When the non-linear option is used, the shear modulus and the hysteretic damping are determined using a modified equivalent linear approach based on the levels of dynamic shear strains. Features such as shear yielding and tension cut-off are incorporated in PILE3D also. The dynamic response of pile groups can be effectively modelled using PILE3D.

8.2   Quasi-3D finite element analysis in the time domain

The basis of the quasi-3D finite element method of analysis for pile foundations has been given in Chapter 6 and Chapter 7. In these chapters, dynamic analyses were performed in the frequency domain. To accommodate the time-domain analysis presented herein, some adjustments are required in the formulation of the global dynamic equilibrium equation given in Eq. 6.9.

The adjustment is made first to the formulation of the mass matrix. For dynamic analyses in the time domain, the use of a diagonal mass matrix can save both computational time and space. Thus the diagonal mass matrix formulations are used in PILE3D to construct $[M]_{elem}$ for both the soil element and the beam element. The diagonal mass matrices for the soil element and the beam element are given by

$$[M]_{soil} = \frac{\rho_s \cdot vol}{8}\{1.0, 1.0, 1.0, 1.0, 1.0, 1.0, 1.0, 1.0\} \tag{8.1}$$

$$[M]_{beam} = \rho_p A\, l\{1/2,\ 1/78,\ 1/2,\ 1/78\} \tag{8.2}$$

The adjustment is made next to the formulation of stiffness matrix and damping matrix. In Eq. 6.9, the stiffness matrix $[K^*]$ is formulated using the complex shear modulus $G^* = G(1 + i \cdot 2\lambda)$. In the time-domain analysis, the stiffness matrix $[K]$ is formulated using the real shear modulus G. The hysteretic damping ratio λ of soil is included using equivalent viscous damping and its formulation is given below.

A procedure for estimating damping coefficients for each individual element proposed by Idriss et al. (1974) is employed in PILE3D. The main advantage of this procedure is that a different degree of damping can be applied in each finite element according its shear strain level. The damping is essentially a Rayleigh-type damping, assuming the

damping is contributed one half by mass and the other half by stiffness. In each time period ΔT_i the global stiffness matrix $[K]$ is computed based on the individual shear modulus in each element, and the global mass matrix $[M]$ is always constant through the time domain. The fundamental natural frequency ω_1 of the pile-soil system is obtained by solving the corresponding eigenvalue problem.

The fundamental frequency of the pile-soil system ω_1 is then applied to every soil element in the system. The damping matrix for a soil element is given by

$$[C]_{elem} = \alpha \cdot [M]_{elem} + \beta \cdot [K]_{elem} \tag{8.3}$$

in which

$$\alpha = \lambda_{elem} \cdot \omega_1$$

$$\beta = \lambda_{elem}/\omega_1$$

and λ_{elem} is the hysteretic damping ratio of soil in the element and is determined based on the level of shear strain in the element.

The global mass matrix $[M]$, the global stiffness matrix $[K]$ and the global damping matrix $[C]$ are assembled from each individual finite element. Therefore under earthquake loading, the global dynamic force equilibrium equation in matrix form is given by

$$[M]\{\ddot{v}\} + [C]\{\dot{v}\} + [K]\{v\} = -[M]\{I\} \cdot \ddot{v}_b(t) \tag{8.4}$$

in which $\ddot{v}_b(t)$ is the base acceleration, and $\{I\}$ is a column vector of 1. $\{\ddot{v}\}, \{\dot{v}\}$ and $\{v\}$ are the relative nodal acceleration, velocity and displacement, respectively.

8.3   Solution scheme for dynamic equation

There are two methods for solving a dynamic equation, the mode-superposition method and the direct step-by-step integration method (Clough and Penzien,1975; Newmark,1959; Wilson et al.,1973).

The mode-superposition method is very useful when a linear system is to be analyzed. This method requires the evaluation of the vibration modal frequencies and their corresponding modal vectors. It basically uncouples the response of the system, and evaluates the response of each mode independently of others. The main advantage of this approach is that the dynamic response of a system can be evaluated by considering only some vibration modes even in systems that may have many degrees of freedom; thus the computational efforts may be significantly reduced. However the mode-superposition approach is not applicable to non-linear systems.

The direct step-by-step integration method is applicable to both linear and non-linear systems. The non-linear analysis is approximated by analyses of a succession of different linear systems. In other words, the responses of the system are computed for a short time interval assuming a linear system having the same properties determined at the start of the interval. Before proceeding to the next time interval, the properties are determined so that they are consistent with the state of displacement and stress at that time.

The direct step-by-step integration procedure developed by Wilson et al. (1973) was employed in PILE3D to solve the dynamic equation Eq.8.4.

The equation Eq.8.4 is solved by an incremental form

$$[M]\{\Delta\ddot{v}\} + [C]\{\Delta\dot{v}\} + [K]\{\Delta v\} = -[M]\{I\} \cdot \Delta\ddot{v}_b(t) \tag{8.5}$$

Since Eq. 8.5 is used for solving the incremental values of dynamic response, the dynamic equilibrium should be ensured by checking equation Eq. 8.4 after each step of integration. During the dynamic analysis unbalanced force $\{\Delta P\}_{unbal}$ is computed after each integration step

$$\{\Delta P\}_{unbal} = -[M]\{\ddot{v}\} - [C]\{\dot{v}\} - [K]\{v\} - [M]\{I\} \cdot \ddot{v}_b(t) \tag{8.6}$$

This unbalanced force is then added to the right hand side of equation Eq. 8.5 in the next step of integration to satisfy dynamic equilibrium.

8.4 Non-linear analysis

Typical relationships between shear stress and strain at different strain amplitudes under dynamic cyclic loading is shown in Figure 8.1. Firstly the shear stress increases with the shear strain non-linearly. Secondly the loading-unloading curve forms a hysteresis loop. The shape of the $\tau - \gamma$ curve determines the degree of reduction of shear modulus with shear strain, and the area of the hysteresis loop represents the amount of strain energy dissipated during the cycle. The dissipated energy implies the degree of material damping at this strain level.

In a dynamic analysis involving hysteretic non-linearity, a rigorous method of analysis in modelling the shear stress-strain behaviour is to follow the actual loading-unloading-reloading curve. This method has been successfully applied in 1-D ground motion analyses (Finn et al., 1977, Lee and Finn, 1978) and 2-D plane strain analyses (Finn et al., 1986). However this method requires updating the tangential shear modulus for all soil
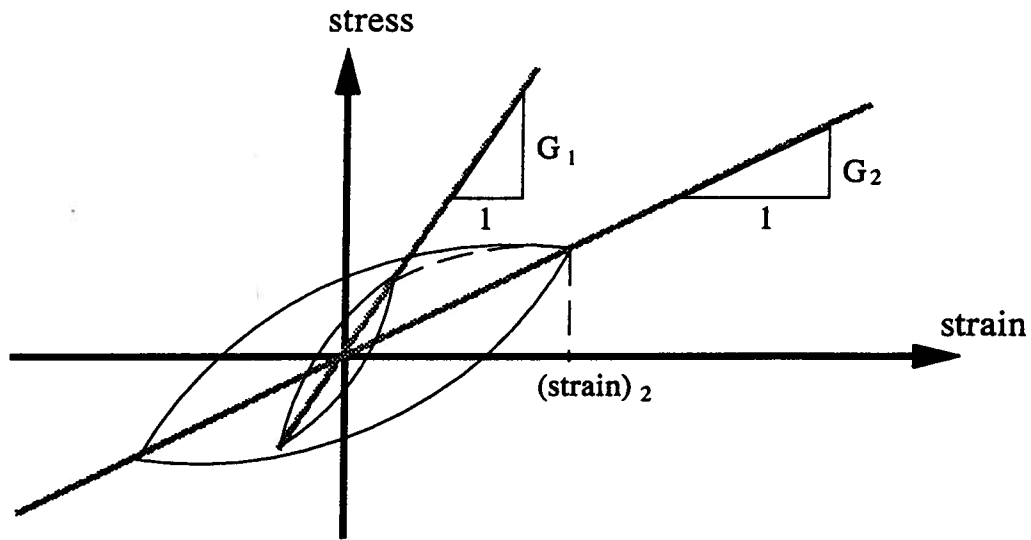
Figure 8.1: Hysteretic stress - strain relationships at different strain amplitudes

elements and building up stiffness matrix in every time step of integration. This procedure is too time-consuming for 3-D analysis.

The equivalent linear method is employed in PILE3D to model the soil non-linear hysteretic behaviour. The equivalent linear method was initially proposed by Seed and Idriss (1967), and it has been widely accepted and used in soil dynamic analyses. The spirit of this method is that the hysteretic behaviour of soil can be approximated by a set of effective shear moduli and viscous damping which are compatible with the levels of shear strains. Figure 8.2(a) shows typical relationships between the ratio G/G_{max} , effective shear modulus G over the shear modulus at very low strain G_{max}, and the effective shear strain. Figure 8.2(b) shows typical relationships between damping ratio and the shear strain.
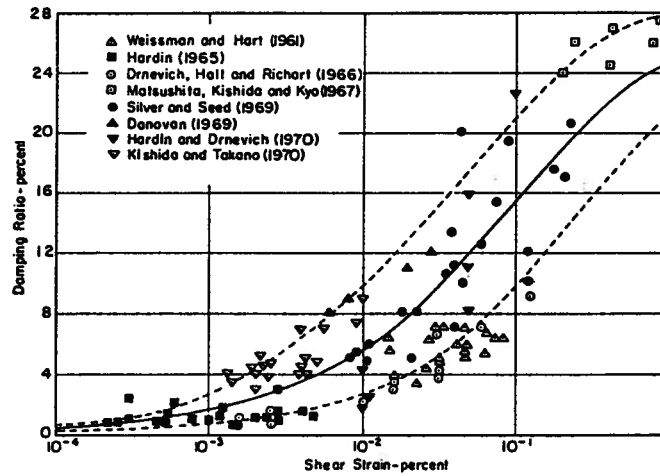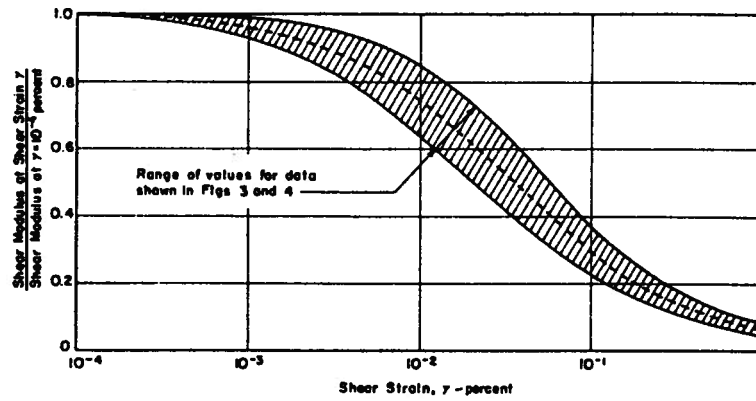
Figure 8.2: Relationships between shear moduli, damping ratios and shear strains (after Seed and Idriss, 1970 & Seed et al.,1986)

The equivalent linear method has been applied in the computer code SHAKE (Schnable et al., 1972) for 1-D ground motion analyses and QUAD-4 (Idriss, 1974) for 2-D plane strain analyses. Here the procedures of this method are incorporated in the quasi-3D dynamic pile-soil interaction analysis. However they are used with some modifications.

In SHAKE, analysis is performed using initial shear moduli and dampings for the entire input acceleration record; then a second analysis is performed for the same acceleration record using constant shear moduli and dampings which are compatible to the effective shear strains obtained from the first analysis. In other words, the shear modulus and damping are determined according to the shear strain using curves such as those shown in Figure 8.2. Iteration process is used to achieve the compatibility between modulus, damping and shear strain. Analyses cease when the differences between the moduli and dampings in the two subsequent analyses are with the desired given values.

There is a disadvantage of the equivalent linear method used in SHAKE. A set of constant values of shear modulus and damping is usually not appropriate to represent the non-linear behaviour of soil within the whole time domain. Especially under earthquake type of loading the level of shear strain usually changes very much from the beginning, through the middle to the end of the time domain. The common-used criterion of taking the effective shear strain equal to 65% of the maximum shear strain may not applicable in many cases.

A procedure of applying the equivalent method based on the periodical level of shear strain is proposed to overcome this problem. This procedure requires no iteration process. Figure 8.3 shows the idea of this method. In this procedure an assumption is made that the effective shear moduli and damping in a period of time ΔT_i remain constant

responses, A
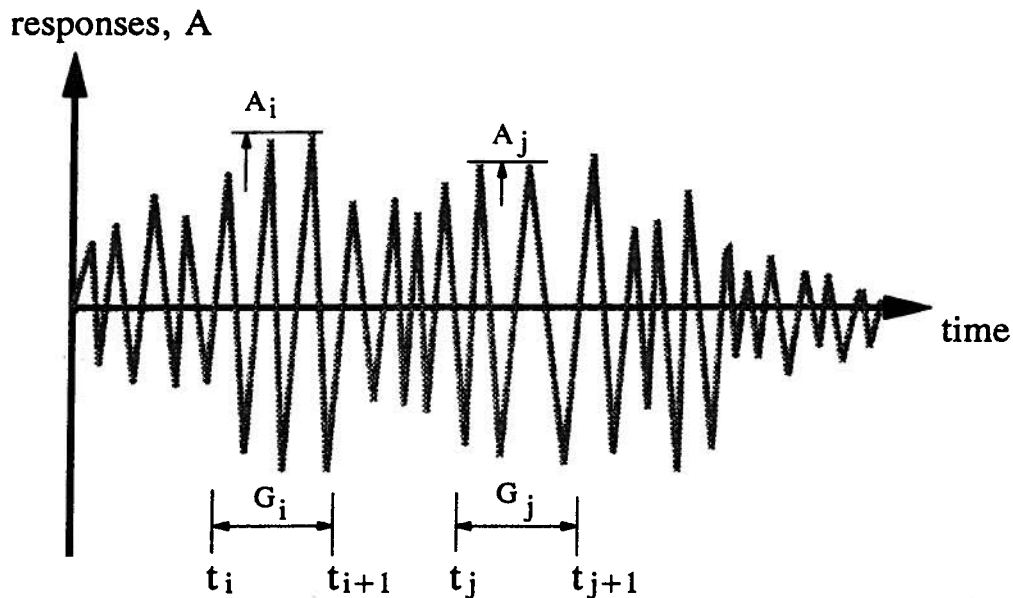
Figure 8.3: The principle of modified equivalent linear method

and are determined by the peak shear strain in the previous period ΔT_{i-1} based on re-
lationships such as those shown in Figure 8.2. The shear moduli and damping ratios in
all soil elements are then determined for the period of time. PILE3D has the capability
allowing the use of different curves input by users.

The selection of the length of time period is based on the fundamental frequency of
the input earthquake motion, and this length can be selected by users. The length of
time period is selected neither too short to take too much computational time nor too
long to lose the accuracy of the analysis. A length between 0.4 second and 1.0 second is
good for the earthquake records used in the analysis presented in the thesis.
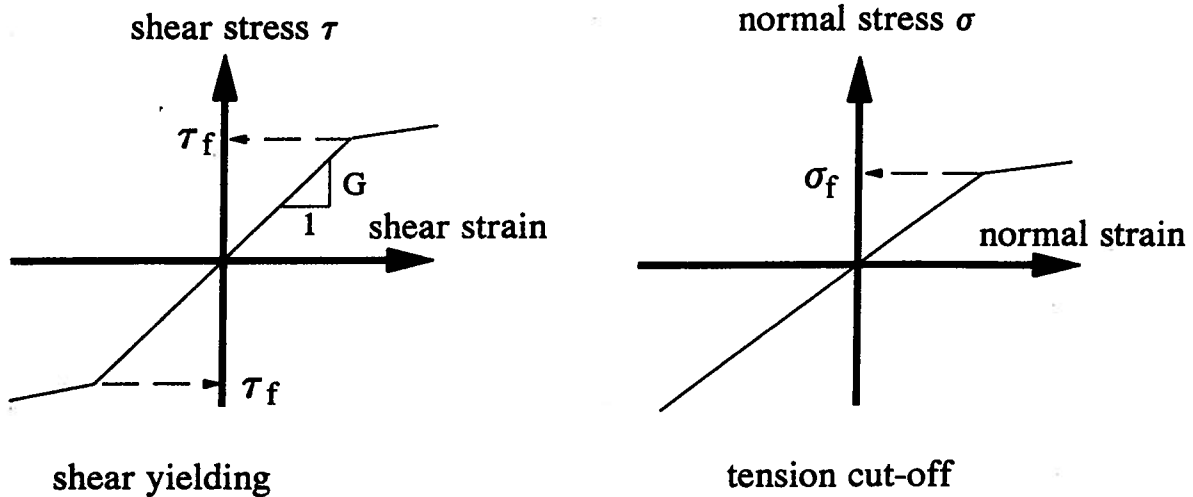
Figure 8.4: Simulations of shear yielding and tension cut-off

8.5   Features in dealing with yielding, tension

Apart from the non-linear shear stress-strain relationship, shear yielding of soil material occurs when the shear stress exceeds the shear strength of the material. When yielding occurs the soil element may develop significantly large shear deformation under very small increment of shear stress. In other words the shear modulus of the soil is significantly reduced due to shear yielding. The shear yielding is prominent near the pile head.

A numerical procedure is included in PILE3D so that the shear modulus is reduced to a very small value when shear yielding occurs. Figure 8.4(a) shows the principle of this procedure. The shear stress used for this purpose is the maximum shear stress in the vertical plane; while the shear strength τ_f is input by users according to the type of soil. The shear strength τ_f may be determined by $c + \sigma'_{vo} \cdot tan\phi$ (c is the cohesion, ϕ is the friction angle, and σ'_{vo} is the effective overburden stress).

On the other hand, cracking or tensile failure may occur when the total lateral normal stress of a soil element exceeds the tensile strength of soil. For sands any tensile stress developing may lead to a tensile failure. When a tensile failure occurs soil has no resistance. A no-tension model shown in Figure 8.4(b) is used to accommodate this phenomenon. One of the criteria built in PILE3D for checking tension is

$$\sigma_{dynamic} > \sigma_N^0 + \sigma_f \tag{8.7}$$

where σ_N^0 is the static lateral stress of the soil element, and σ_f is the tensile strength of soil, and $\sigma_{dynamic}$ is the dynamic lateral stress computed during the analysis.

The options of checking shear yielding and allowing no-tension to develop in soils are available only when a dynamic step-by-step integration procedure is used. These features overcome the difficulties that may be encountered in a pure elastic analysis. In a pure elastic analysis no controls on the shear yielding or the tensile failure can be enforced. The application of these features has been found very effective in eliminating the over-stiffness of soil in the zone near the pile.

8.6 Soil parameters required in PILE3D analysis

The method was developed so that fundamental soil parameters are used.

Shear modulus of soil The key parameter required for this analysis is the low-strain shear modulus G_{max} of soil. The low strain shear modulus is also called the maximum shear modulus. The G_{max} can be determined accurately by measuring the shear wave

velocity V_s of soil, then

$$G_{max} = \rho \cdot V_s^2$$

$$= \gamma/g \cdot V_s^2 \tag{8.8}$$

where ρ is the mass density of soil, and γ is the unit weight of soil and g is the gravity acceleration, 9.81 m/sec^2.

When data on shear wave velocity are not available, empirical equations may be applied to estimate the low strain shear modulus G_{max}. A useful empirical equation proposed by Hardin and Drnevich (1972) is of the form

$$G_{max} = 320.8 \frac{(2.973 - e)^2}{1 + e} (\frac{\sigma'_m}{P_a})^{0.5} (OCR)^k \tag{8.9}$$

in which

e = void ratio;

OCR = overconsolidated ratio;

k = a constant dependent on the plasticity of the soil;

Pa = atmospheric pressure, 101.3 kPa;

σ'_m = current mean normal effective stress.

The Hardin and Drnevich equation is applicable for both sands and clays. For clays it is recommended that the equation be used when the void ratio is in the range of 0.6 to 1.5. The variation of constant k with plasticity index PI is given in Table 8.8.

For most practical purposes, Seed and Idriss (1970) proposed another useful expression for estimating G_{max} of granular soils (sands and gravels)

Table 8.8: Relationship between Hardin and Drnevich constant k and plasticity index PI (after Hardin and Drnevich, 1972)

PI	0.0	20	40	60	80	>100
k	0.0	0.18	0.30	0.41	0.48	0.50

$$G_{max} = 1000\,(k_2)_{max}(\sigma'_m)^{0.5}......in\,psf\,\,units \tag{8.10}$$

The coefficients $(k_2)_{max}$ was found to vary from about 30 for loose sands to about 75 for dense sands. Values of $(k_2)_{max}$ for relatively dense gravels are generally in the range of about 80 to 180.

A useful relationship between $(k_2)_{max}$ and SPT $(N_1)_{60}$ values was proposed by Seed et al. (1986)

$$(k_2)_{max} = 20\,(N_1)_{60}^{\frac{1}{3}} \tag{8.11}$$

For clays the maximum shear modulus may be calculated based on the undrained shear strength, S_u, using the equation

$$G_{max} = K_{clay} \cdot S_u \tag{8.12}$$

in which K_{clay} is a constant for a given clay. From Seed and Idriss (1970) the typical values of K_{clay} vary between 1000 to 3000.

Damping ratio and other parameters   The second input required in the analysis is the relationship between damping ratio and the shear strain of soil. Although variation
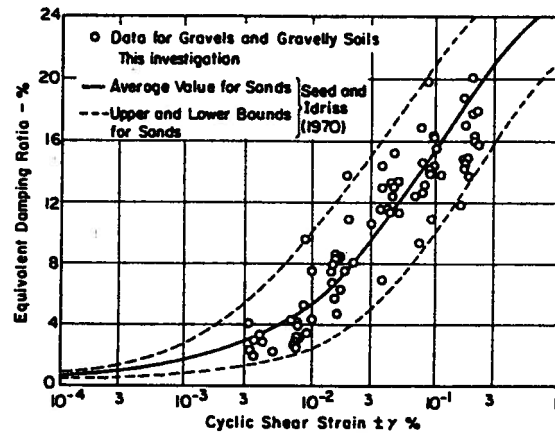
Figure 8.5: Comparison of damping ratios for sands and gravelly soils (after Seed et al., 1986)

may be expected for specific soil material, typical values of damping ratios as function of shear strain were given by Seed et al. (1986) for sands and gravelly soils, and they are shown in Figure 8.5. Other parameters required in the analysis are Poisson's ratio and shear strength of soil.

8.7 Aspects relative to analysis of pile group

The program PILE3D has the capability of simulating the dynamic response of a pile group supporting a rigid pile cap. Analysis is done in a fully coupled manner. The rigid pile cap is represented by a concentrated mass at the centre of gravity of the pile cap, and the mass is rigidly connected to the piles by a massless rigid bar.

Figure 8.6 shows the principle for modelling a pile cap in PILE3D. The pile cap is modelled as a rigid body in the analysis. The motions of the pile cap are represented

A
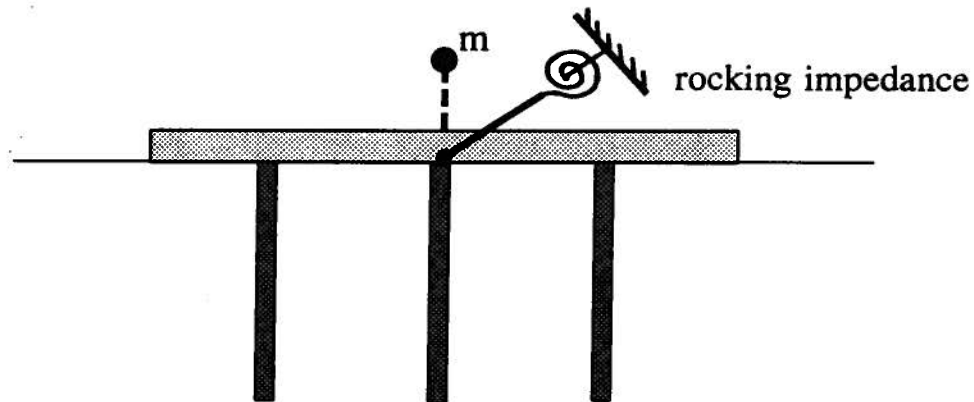
Figure 8.6: A diagram showing the representation of pile group supporting structure

by the motions of the pile nodes which are connected to the bottom of the pile cap. These nodes are called the pile head nodes. The pile head nodes have identical deflections (translations and rotations in the vertical plane) as the pile cap does. Therefore a principal restraining pile head node can be used to represent the motions of all pile head nodes or of the pile cap. In the finite element analysis the translation and rotation of all pile head nodes in the group are restrained to the principal pile head node. In this way, identical deflections of all pile head nodes are achieved. The mass of the pile cap is connected to the principal pile head node so that all pile head nodes share the same mass, stiffness and deflections.

On the other hand, under seismic loading the pile cap rotation is primarily resisted by the rocking impedance of the pile group. The rocking impedance is induced by the vertical resistance of the piles. In the proposed quasi-3D analysis the rocking impedance cannot be included directly because the vertical and horizontal motions are uncoupled.

The rocking impedance of the the pile group is included in the analysis by using the following procedures.

The rocking stiffness and damping is updated at selected times during the horizontal mode analysis by using PILE3D in the vertical mode. The procedure for computing rocking impedance K_{rr} has been given in chapter 7. The rocking impedance is computed using the current values of strain dependent shear moduli and damping ratio of soil. The current rocking impedance (stiffness and damping) is then transferred to the pile cap as rotational stiffness and damping.

The rocking impedance of pile group is important to the dynamic response under horizontal shaking, and it has been properly treated in the dynamic analysis of pile group using PILE3D.

Chapter 9

Analyses of Centrifuge Tests of Pile Foundations

9.1 Introduction

In this chapter the proposed quasi-3D finite element method of analysis is used to analyze the non-linear response of model pile foundations subjecting to horizontal loading in centrifuge tests. Centrifuge tests on a single pile and a 2x2 pile group are analyzed using the computer program PILE3D. The computed results are compared with those measured in the centrifuge tests. The ability of the proposed model for simulating the non-linear response of pile foundations is evaluated.

During strong shaking, the shear modulus and damping ratio of soil medium change with time, which causes corresponding changes in the dynamic impedances of pile foundations. These variations in dynamic impedances with time during strong shaking are evaluated for the model pile foundations. This is the first time that the time-histories of dynamic impedances have been calculated.

9.2 Dynamic analysis of centrifuge test of a single pile

9.2.1 Description of centrifuge test on a single pile

A centrifuge test on a single pile was carried out at the California Institute of Technology (Caltech) by B. Gohl (1991). Detailed data on the centrifuge test are given by Gohl

148

(1991). Details of the test may also be found in a paper by Finn and Gohl (1987). A centrifuge acceleration of 60g was used for the test.

Figure 9.1 shows the soil-pile-structure system used for the single pile test. The effect of the super-structure was simulated by clamping a rigid mass at the pile head. The pile head mass was instrumented using a non-contact photovoltaic displacement transducer and an Entran miniature accelerometer. The locations of the accelerometer and light emitting diode (L.E.D.) used by the displacement sensor are shown in Figure 9.1. The pile head displacements were measured with respect to the moving base of the soil container. The prototype parameters of the single pile test is shown in Figure 9.2. The model pile has a unit weight of 74.7 kN/m^3. The prototype pile has an outer diameter $d_{outer} = 0.5712$ m and an inner diameter $d_{inner} = 0.5412$ m. The flexural rigidity of the prototype pile is 172,614 $kN.m^2$.

The sand used for the centrifuge test was a loose sand with a void ratio $e_0 = 0.78$ and a mass density $\rho = 1.50 Mg/m^3$. The friction angle of the sand was determined to be $30°$. Gohl (1991) has showed that the low strain shear moduli of the sand foundation vary as the square root of the depth, and that they can be quantitatively evaluated by using the Hardin and Black (1968) equation

$$G_{max} = 3230 \frac{(2.973 - e_0)^2}{1 + e_0} (\sigma'_m)^{0.5} \qquad (9.1)$$

where e_0 is the in-situ void ratio of the sand and σ'_m is the mean normal effective confining stress in kPa. The mean normal effective confining stress is computed from the effective vertical stress σ'_v
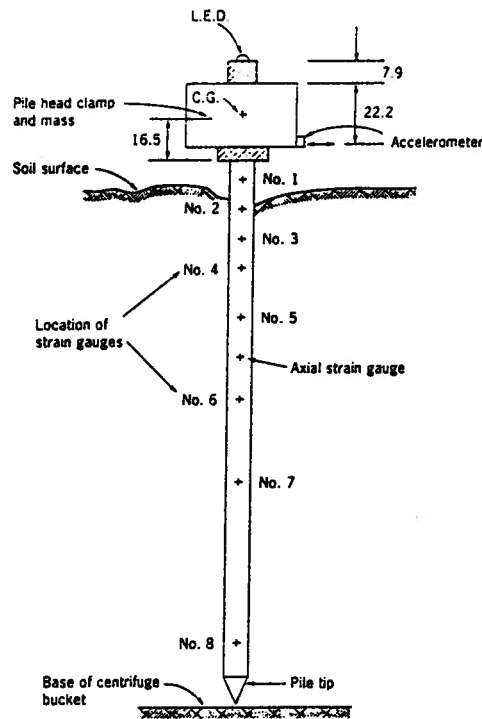
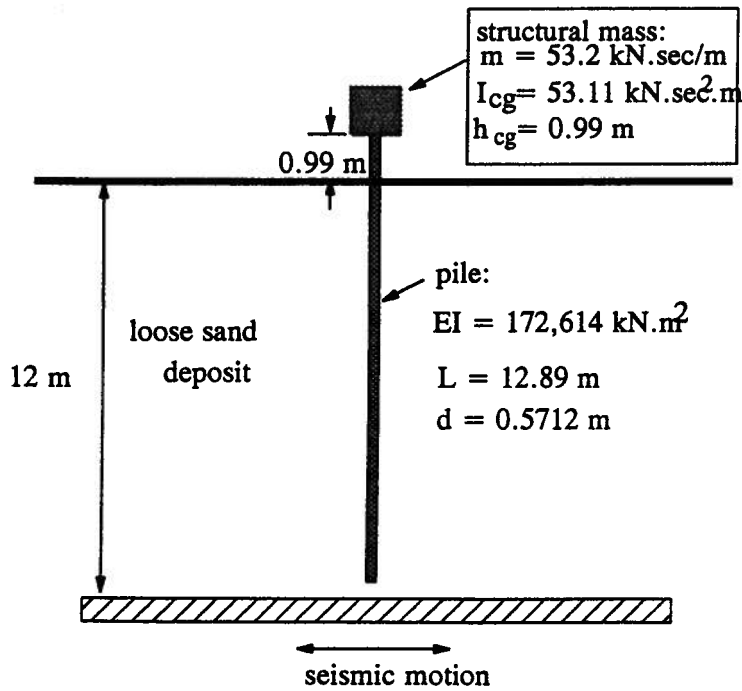Figure 9.1: The layout of the centrifuge test for a single pile

Figure 9.2: The prototype model of the single pile test

$$\sigma'_m = \frac{1 + 2K_0}{3}\sigma'_v \tag{9.2}$$

Using $e_0 = 0.78$ and a lateral stress coefficient $K_0 = 0.4$ for the loose sand, Gohl showed that measured shear wave velocities and those computed by using the Hardin and Black equation are in good agreement.

A horizontal acceleration motion is input at the base of the system. The peak acceleration of the input motion is 0.158g. During the centrifuge test, accelerations at the free field surface and at the pile head and displacements at the top of the super-structure were recorded. Dynamic moments at the selected locations along the pile shown in Figure 9.1 were also recorded during the test.

The computed Fourier amplitude ratios of the pile head response and the free field motion with respect to the input motion are given in Figure 9.3(a) and Figure 9.3(b), respectively. The natural frequency of the free field acceleration is estimated to be 2.75 Hz, and the fundamental frequency of the pile to be 1.1 Hz. The period of the pile response is much longer than the period of the free field motion.

9.2.2 Dynamic analysis of the single pile

The centrifuge test of single pile is analyzed at the prototype scale. Figure 9.4 shows the finite element model used in the analysis. The sand deposit is divided into 11 layers. A decreasing thickness of layer is used toward the soil surface. This arrangement would allow more detailed modelling of the stress and strain field where lateral soil-pile
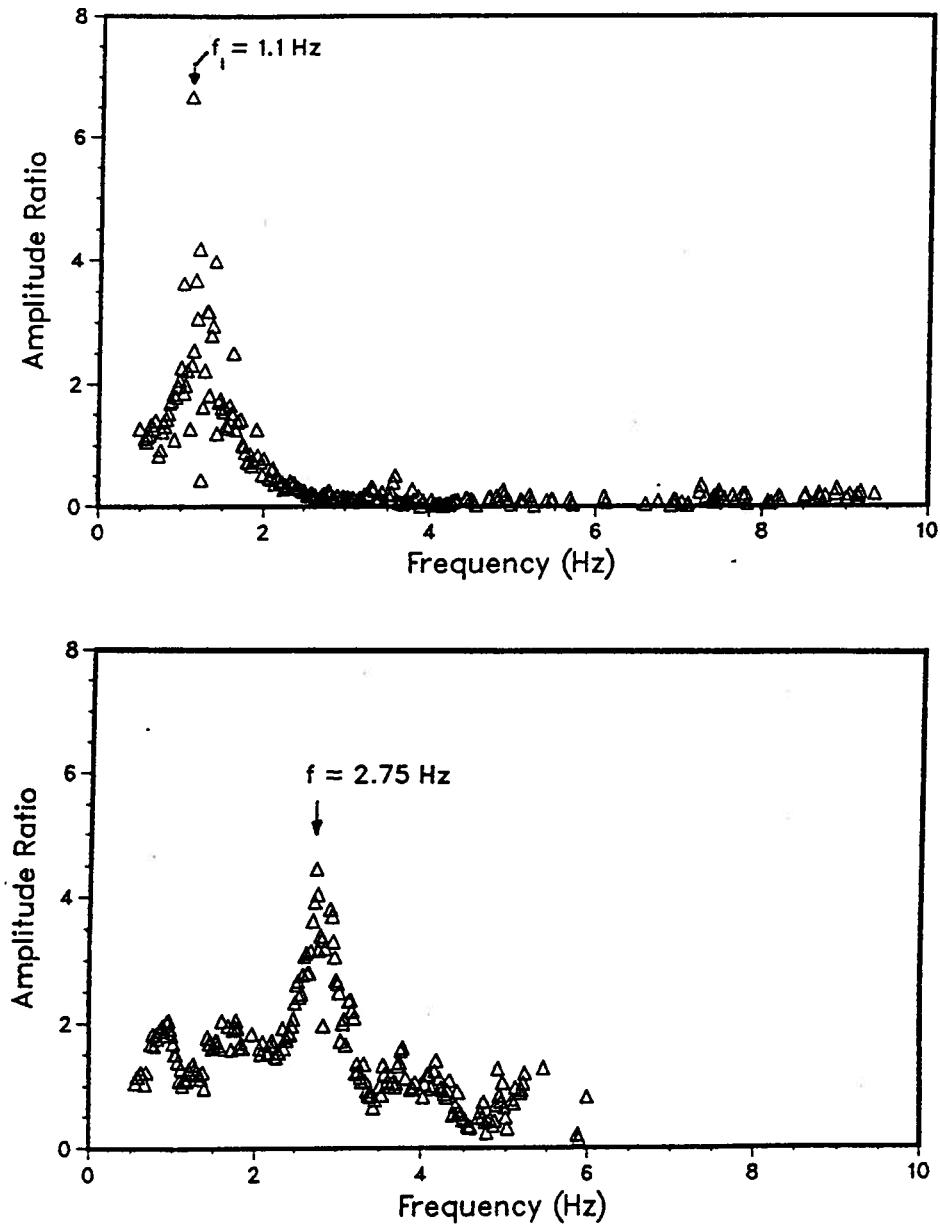
Figure 9.3: Computed Fourier amplitude ratios (a) pile amplitude ratio (APH/AFF) (b) free field amplitude ratio (AFF/AB) (after Gohl, 1991)
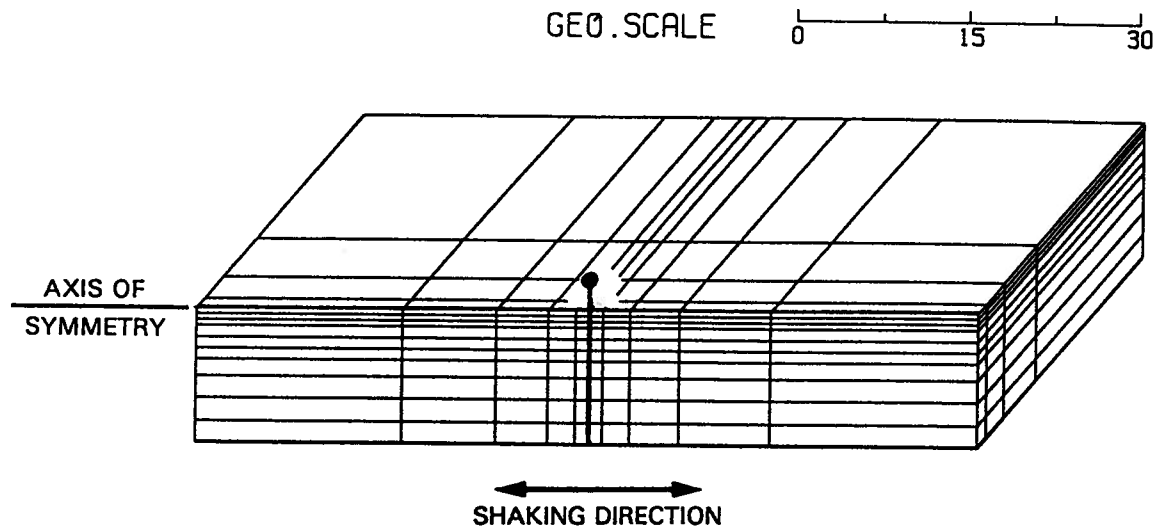
Figure 9.4: The finite element modelling of centrifuge test

interaction is strongest. The pile is modelled using 15 beam elements including 5 elements above the soil surface. The super-structure mass is treated as a rigid body, and its motion is represented by a concentrated mass at the centre of gravity. A very stiff beam element with flexural rigidity 1000 times that of the pile was used to connect the mass and the pile head. The motion of any point in the rigid super-structure can be determined according to its geometric relationship to the reference point, the pile head. The present finite element mesh consists of 666 nodes and 456 elements.

The finite element analysis was carried out in the time domain. The non-linear analysis was performed to account for the changes of shear moduli and damping ratios due to dynamic shear strains. According to Gohl (1991), the shear-strain dependency of the shear modulus and damping ratio used in the analysis is shown in Figure 9.5. The maximum shear modulus G_{max} was calculated according to Eq. 9.1. The maximum damping ratio of the loose sand was taken as 25% following Gohl (1991).
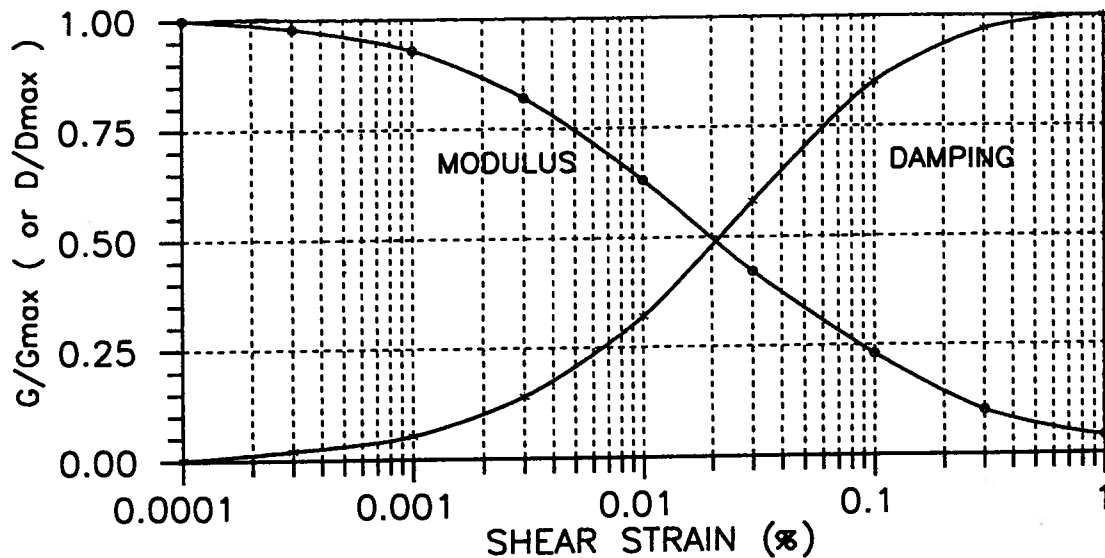
Figure 9.5: The relationships between shear modulus, damping and the shear strain for the loose sand

Results of analysis The computed and measured accelerations in the free field and at the pile head are shown in Figure 9.6 and Figure 9.7, respectively. There is good agreement between the measured and the computed accelerations.

The computed and measured time histories of displacements at the top of the structure are plotted in Figure 9.8. The computed displacements are smaller than the measured displacements in the first 10 sec of motion. However, the computed peak displacement is 56 mm compared to the measured peak displacement of 67 mm, with an error of about 16%. The frequency content of the displacement response has been captured satisfactorily by the analysis.

The computed time histories of moments in the pile at the soil surface and at a depth
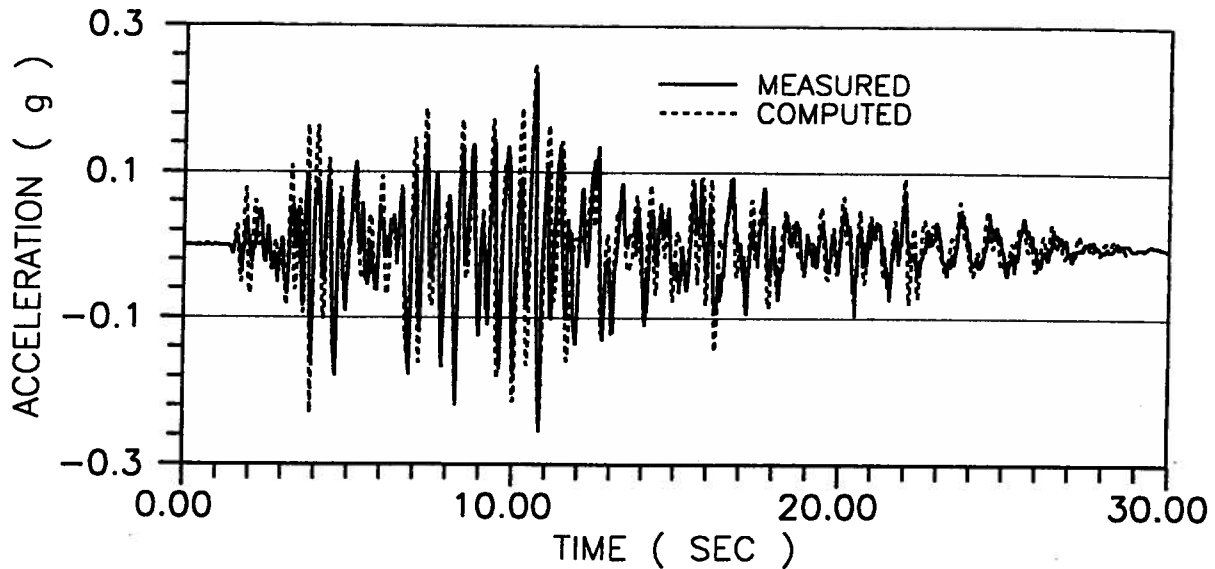
Figure 9.6: The computed versus measured acceleration response at the free field

of 3 m (near point of maximum moment) are plotted against the measured time histories in Figure 9.9 and Figure 9.10, respectively. Satisfactory agreement between the computed and the measured moments is observed in the range of larger moments.

The distributions of the computed and measured bending moments along the pile at the instant of peak pile deflection are shown in Figure 9.11. The computed moments agree very well with the measured moments. The bending moments increase to a maximum at a depth of 3.5 diameters, and then decrease to zero at a depth around 12.5 diameters. The moments along the pile have same signs at any instant time, suggesting that the inertial interaction caused by the pile head mass was dominant and the pile was vibrating in its first mode. The measured peak moment is 325 kN.m, whereas the computed peak moment is 344 kN.m with an error of 6% overestimate.
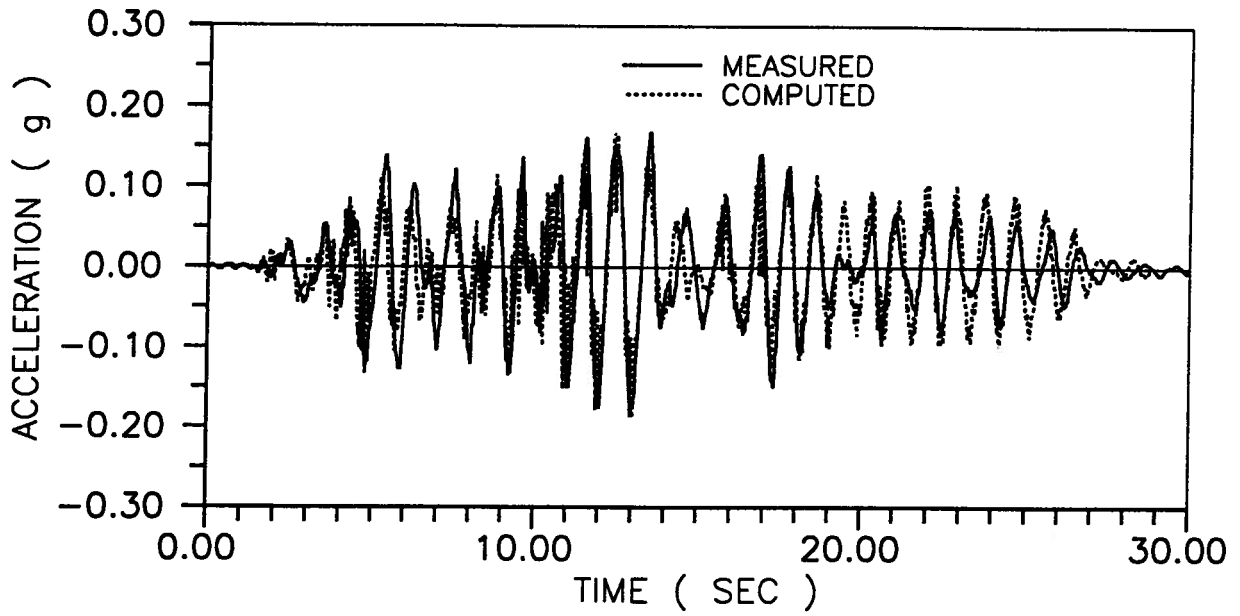
Figure 9.7: The computed versus measured acceleration response at the pile head
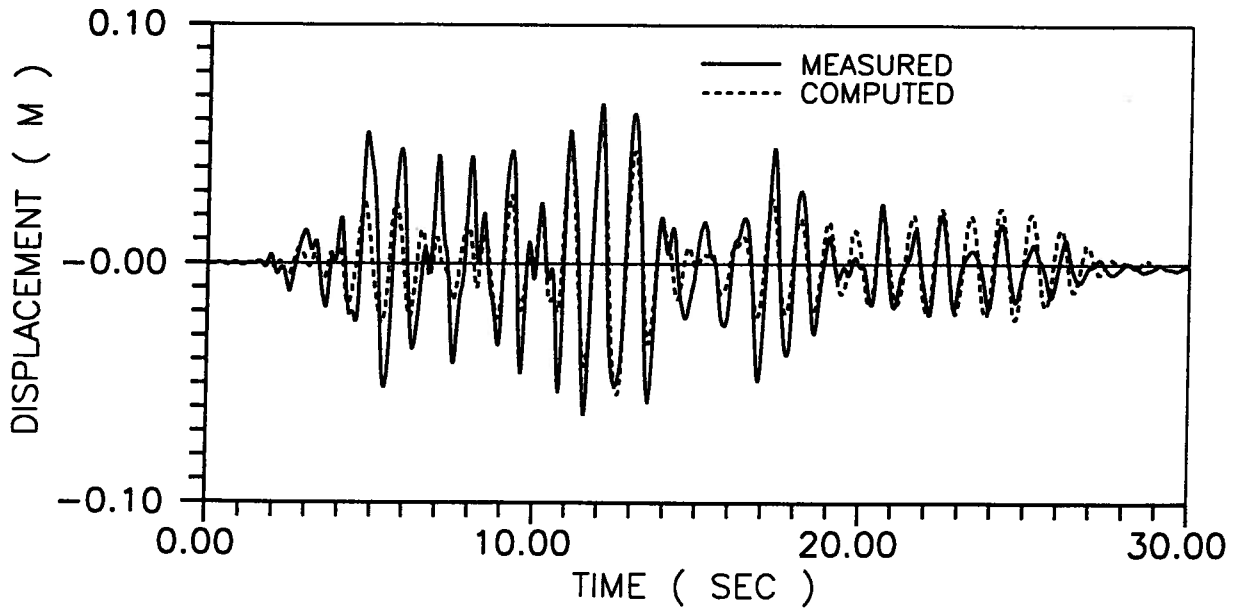
Figure 9.8: The computed versus measured displacement response at the top of the structure
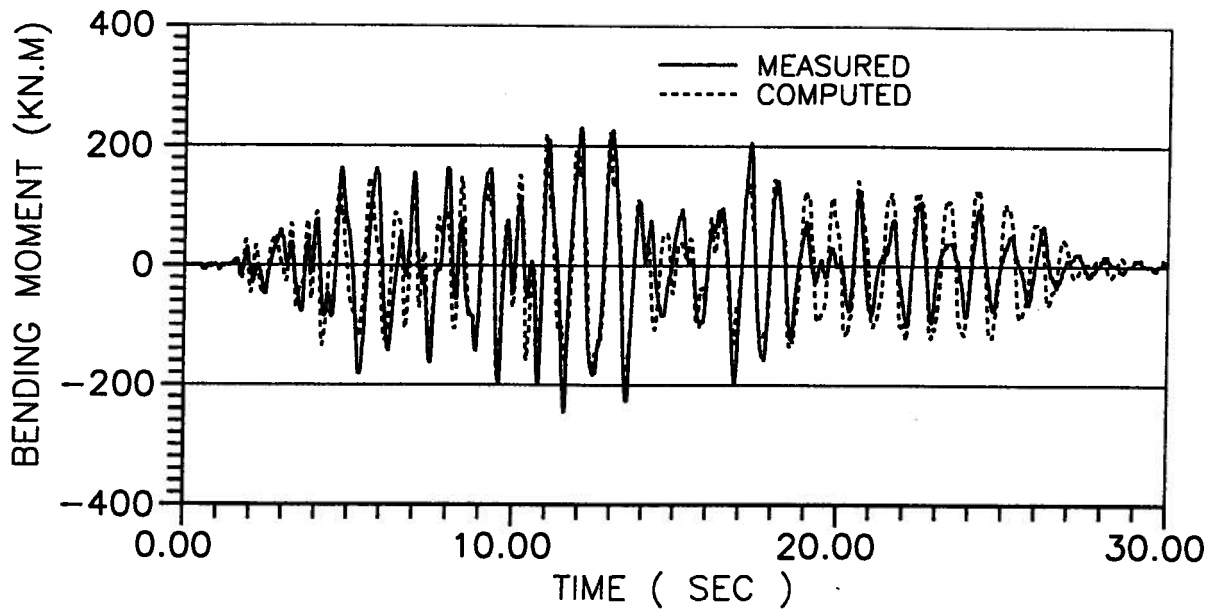
Figure 9.9: The computed versus measured moment response at the soil surface
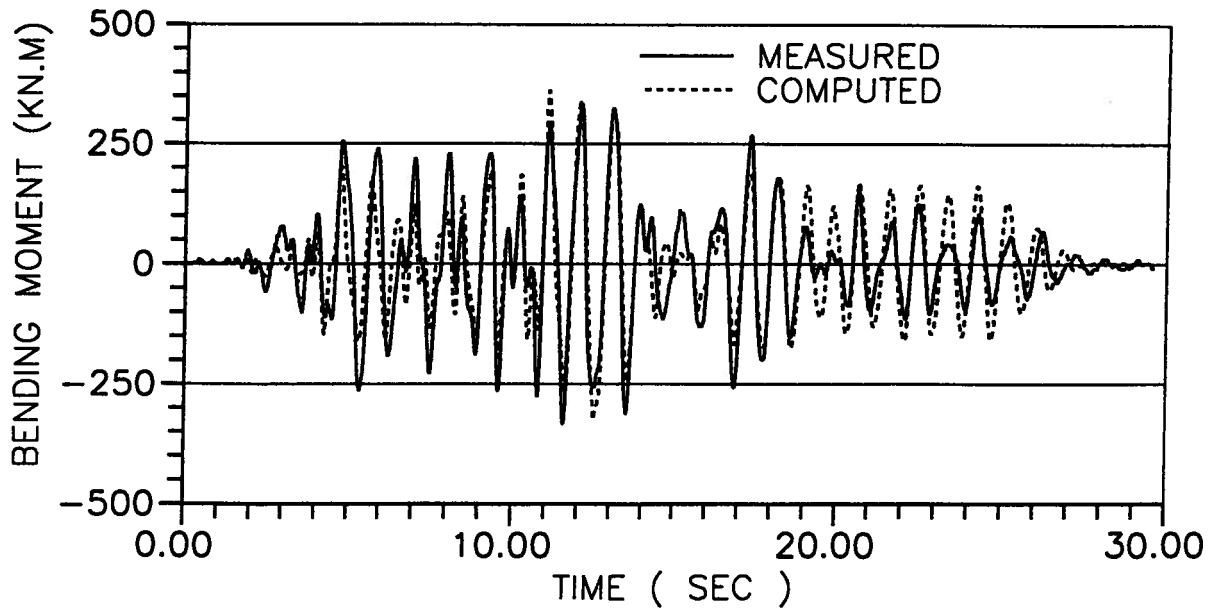
Figure 9.10: The computed versus measured moment response at depth D=3m
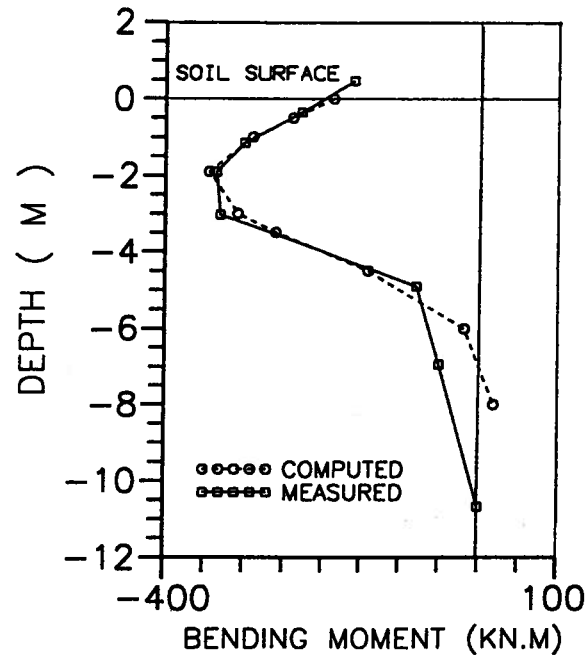
Figure 9.11: The computed versus measured moment distribution of the pile at peak pile deflection

9.2.3 Non-linear pile impedances

Under earthquake loads the shear moduli and damping ratios of soil vary with both the time and the location. The proposed non-linear analysis is capable of tracing the variation of soil properties at any instant during shaking. As examples of this feature, distributions of soil shear moduli at depths of 0.25 m and 2.10 m are plotted in Figure 9.12 at an instant t=12.58 sec, and in Figure 9.13 at another instant t=17.11 sec. It is seen that at a certain depth such as 2.10 m the soil shear moduli in the near field of the pile are much less than the shear moduli in the far field.

At any instant during shaking, a set of soil properties are determined for each soil element. Therefore the dynamic impedances of the pile foundation can be evaluated corresponding to soil properties at this instant. The variation of dynamic impedances of pile foundations with time during shaking is evaluated. These non-linear pile impedances

single pile at 12.58 sec

initial shear modulus 12945 kPa
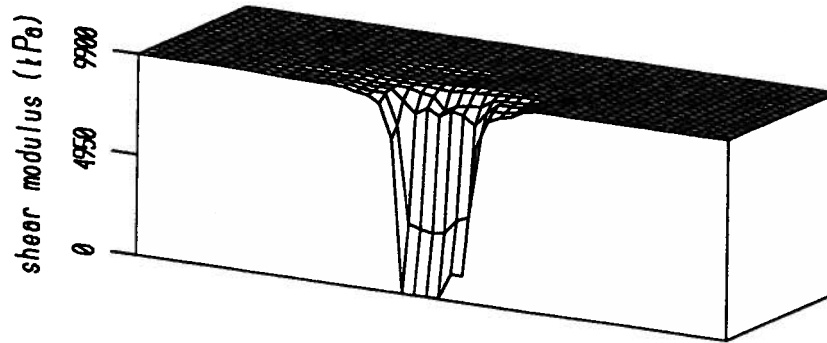
(a) at depth 0.25 m

initial shear modulus 36610 kPa
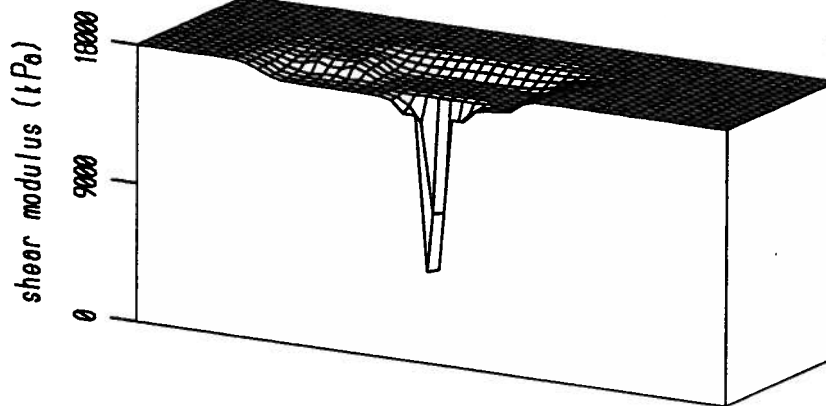
(b) at depth 2.10 m

Figure 9.12: 3-D plots of the distribution of shear moduli at t=12.58 sec

single pile at 17.11 sec

initial shear modulus 12945 kPa

(a) at depth 0.25 m

initial shear modulus 36610 kPa
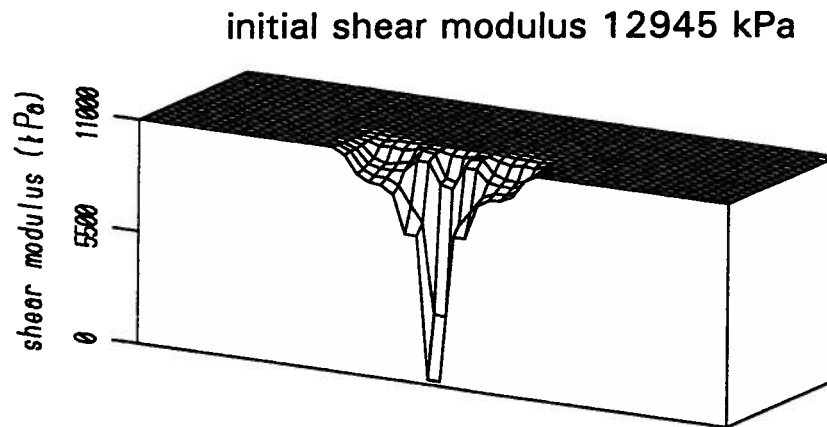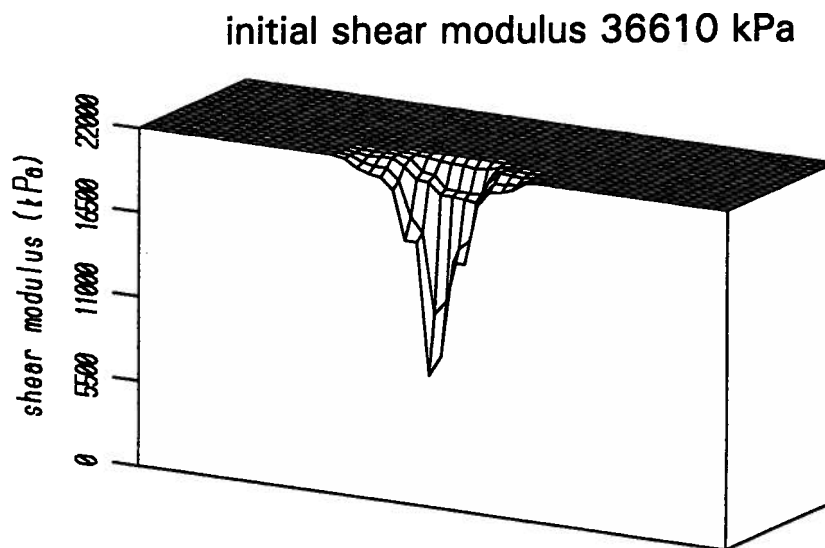
(b) at depth 2.10 m

Figure 9.13: 3-D plots of the distribution of shear moduli at t=17.11 sec

include effect of pile-soil kinematic interaction and inertial interaction from the super-structure.

Dynamic impedances under an earthquake motion The concept of dynamic impedance is formulated to reflect the complex force-deflection relationship of a pile foundation under harmonic pile head loading at a specific excitation frequency. This concept is well suited for the dynamic analysis of a machine foundation which is normally excited at specific frequencies. However under earthquake excitation, the pile foundations do not usually vibrate at a constant frequency. Strictly speaking, the concept of dynamic impedance does not apply directly in dynamic analyses of pile foundations involving earthquake motions.

Conventionally dynamic impedances are used in sub-structuring analysis of pile supporting structures. Pile head impedances are usually computed at the dominant frequency of excitation appropriate to an earthquake motion. In normal design prior to an earthquake event, it would appear logical to select the fundamental frequency of the pile as the frequency of interest, provided the earthquake motions are expected to contain significant frequency contents around the fundamental frequency of the pile. An alternative technique is to explore variations of dynamic stiffness and damping of the pile foundation in the frequency range of an earthquake motion, such as from 0 Hz to 10 Hz. The latter approach is used in this study to look into the characteristics of dynamic stiffness and damping as functions of frequency.

The dynamic impedances (stiffness k_{ij} and damping C_{ij}) of the single pile are computed using program PILIMP. These impedances are determined at the ground surface.

Excitation frequencies of 1.91 Hz, 6.0 Hz and 10 Hz are selected to explore the effect of excitation frequency on dynamic impedances of pile foundations. Frequency is limited to the 0-10 Hz range considered appropriate for seismic loading.

Stiffnesses of the pile foundation during shaking At the excitation frequency f=1.91 Hz, the dynamic stiffnesses of the pile decrease dramatically as the level of shaking increases (Figure 9.14). The dynamic stiffnesses experienced their lowest values in the 10 to 14 seconds range when the maximum accelerations occurred at the pile head. It can be seen that the translational stiffness k_{vv} decreased more than the rotational stiffness $k_{\theta\theta}$ or the cross-coupling stiffness $k_{v\theta}$. At their lowest levels, k_{vv} decreased to 20,000 kN/m which is only 13.8 % of its initial stiffness of 145,000 kN/m. $k_{v\theta}$ decreased to 45,000 kN/rad which is 36% of its initial stiffness of 125,000 kN/rad. $k_{\theta\theta}$ showed the least effect of shear strain. It decreased to 138,000 kN.m/rad which is 63.6% of its initial stiffness of 217,000 kN.m/rad. The stiffnesses rebounded when the level of shaking decreased with time. Representative values of the pile stiffnesses $k_{vv}, k_{v\theta}$ and $k_{\theta\theta}$ for the use in a structural analysis might be selected as 40,000 kN/m, 65,000 kN/rad and 160,000 kN.m/rad, respectively, on the basis of the time histories shown in Figure 9.14. These stiffnesses are 27.6%, 52% and 73.7% of their original stiffnesses.

The variations of translational stiffness k_{vv} and rotational stiffness $k_{\theta\theta}$ with time at different excitation frequencies are shown in Figure 9.15. It can be seen that the excitation frequency has little influence on the dynamic stiffness of the pile foundation for frequency less than 10 Hz. The dynamic stiffnesses of the pile foundation may be considered independent of frequency under seismic loading.
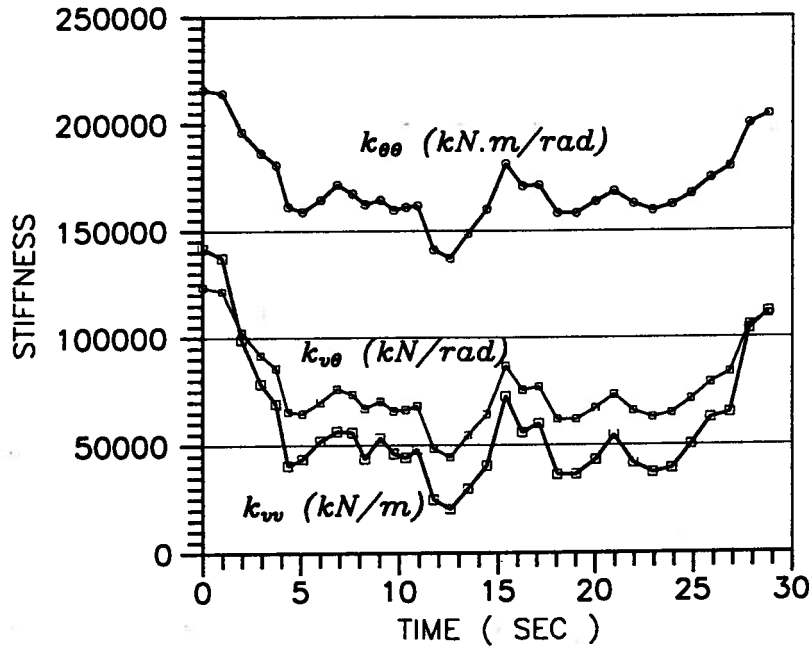
Figure 9.14: Variation of stiffnesses $k_{vv}, k_{v\theta}, k_{\theta\theta}$ of the single pile at f=1.91 Hz
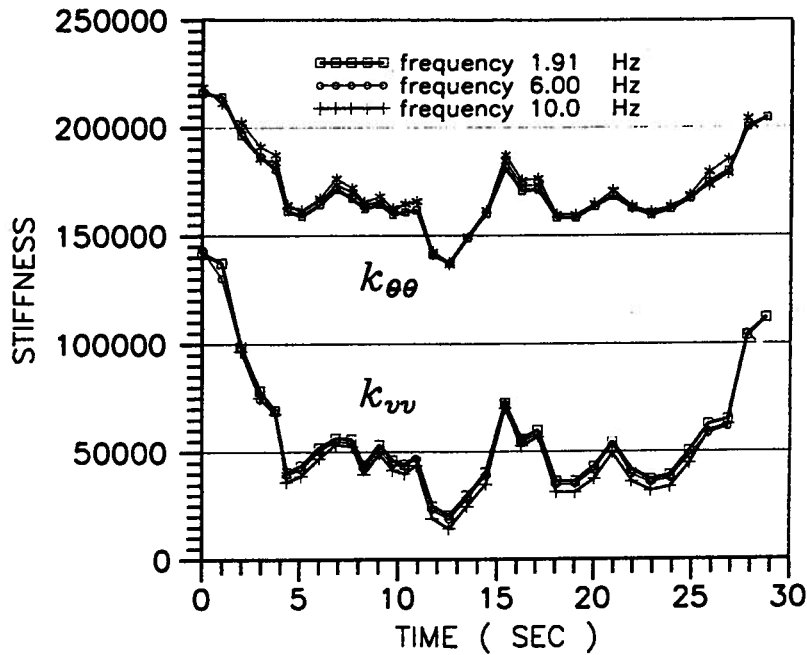
Figure 9.15: Variation of stiffnesses k_{vv} and $k_{\theta\theta}$ with time under different excitation frequency
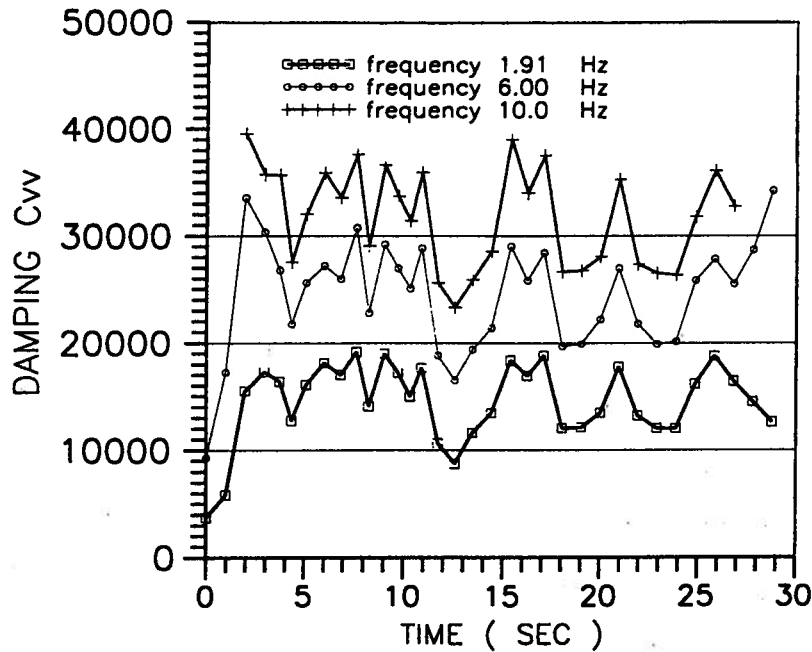
Figure 9.16: Variation of translational damping C_{vv} versus time under different frequency

Dampings of the pile foundation during shaking The variatin of damping with the excitation frequency is different from that of the stiffness. The values of dampings usually increase with the excitation frequency due to the frequency-dependent radiation damping. Figure 9.16 shows typical variations of the translational damping C_{vv} versus time as the excitation frequency increases. It is seen that the amount of incremental damping due to the change of frequency is roughly proportional to the amount of incremental frequency. Same patterns are observed for the cross-coupling damping $C_{v\theta}$ and the rotational damping $C_{\theta\theta}$. Under these observations and due to the fact that hysteretic damping is independent of frequency ω, the following expression is proposed to represent dampings C_{ij} of pile foundations under seismic loading

$$C_{ij} = C_{ij}^h + R_{ij}\,\omega^{0.75} \tag{9.3}$$

where C_{ij}^h represents the frequency-independent hysteretic damping, and R_{ij} is the
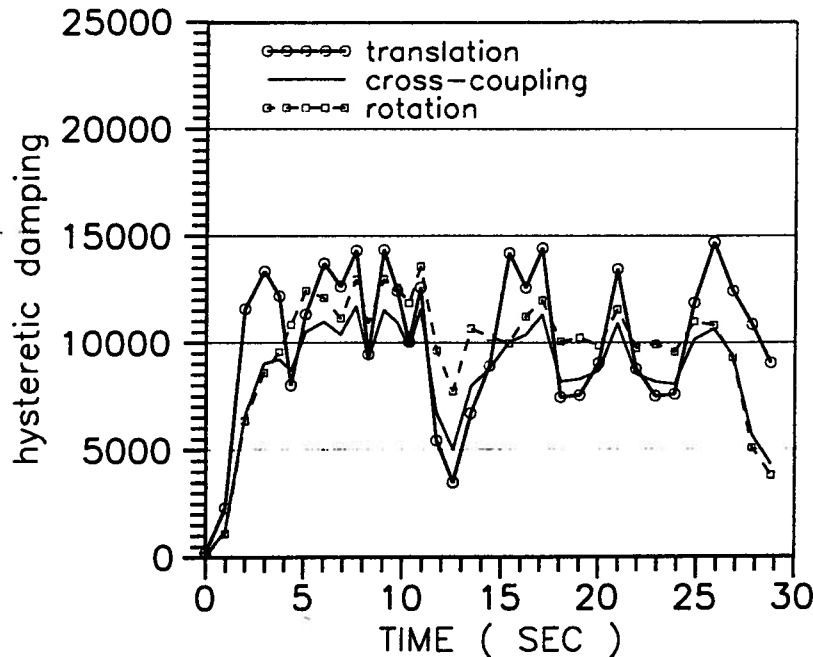
Figure 9.17: Variation of hysteretic dampings C_{vv}^h, $C_{v\theta}^h$ and $C_{\theta\theta}^h$ of the single pile radiation damping constant, ω is the excitation frequency $\omega = 2\pi f$.

The hysteretic damping C_{ij}^h were determined by using very low excitation frequency (such as f=0.01 Hz) when computing impedances. Figure 9.17 shows the variations of hysteretic damping contributions C_{vv}^h (translation), $C_{v\theta}^h$ (cross-coupling) and $C_{\theta\theta}^h$ (rotation) with time. The rotational hysteretic damping is less sensitive to the change of shaking level than the other two hysteretic dampings. Representative values of 12,000 kN/m, 11,000 kN/rad, and 12,000 kN.m/rad may be selected to represent the hysteretic dampings of C_{vv}, $C_{v\theta}$ and $C_{\theta\theta}$, respectively.

The radiation damping constants R_{ij} are computed using Eq. 9.3. As expected the radiation damping constants R_{ij} fall into a relatively narrow zone in the time domain when the frequency changes from 1.91 Hz to 10 Hz. Figure 9.18 shows the translational radiation damping constant R_{vv} with time for the three frequencies analyzed. A value of
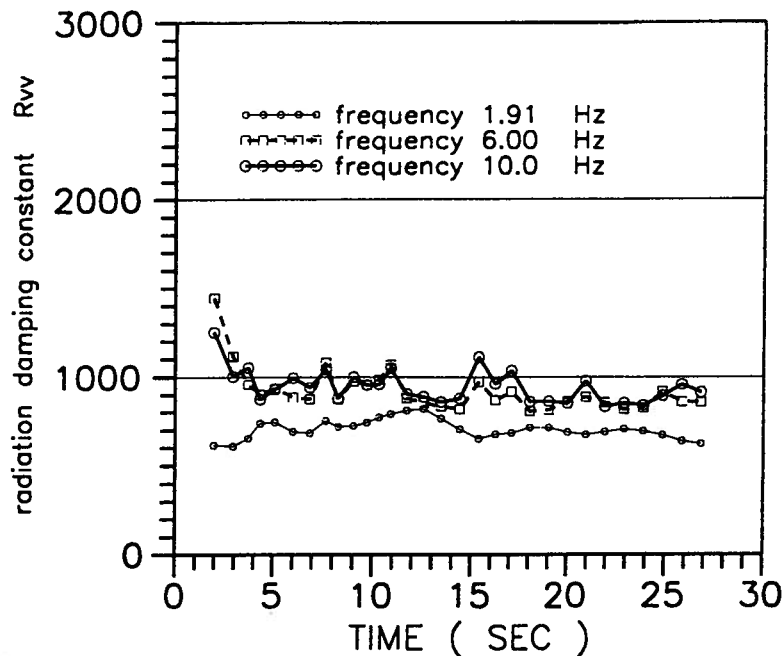
Figure 9.18: Variation of radiation damping constant R_{vv} at different frequencies

850 of R_{vv} is typical for representing the translational radiation damping. Applying the same concept, a value of 600 is found typical for both $R_{v\theta}$ and $R_{\theta\theta}$.

The results of studies on pile impedances are summarized in Table 9.1. Since the damping C_{ij} are functions of excitation frequency the resulting damping coefficients $(c_{ij} = C_{ij}/\omega)$ are different at different excitation frequencies. For instance at $\omega = 12$ rad/sec (f=1.91 Hz), the damping coefficients $c_{vv}, c_{v\theta}, c_{\theta\theta}$ have values of 1457 kN.sec/m, 1239 kN.sec/rad and 1322 kN.m.sec/rad, respectively. However the corresponding damping coefficients change to 741 kN.sec/m, 604 kN.sec/rad and 635 kN.m.sec/rad if the excitation frequency changes to 31.41 rad/sec (f = 5 Hz).

Effect of structural mass on pile impedances In the analysis described early the effect of the structural mass on the dynamic impedances has been included. The heavy structural mass would significantly increase the level of non-linearity of soil in the near

Table 9.9: Parameters of dynamic impedances of single pile

	Average stiffness	Minimum stiffness	Hysteretic damping C_{ij}^h	Radiation damping constant R_{ij}
$k_{vv}(kN/m)$	40,000	20,000		
$C_{vv}(kN/m)$			12,000	850
$k_{v\theta}(kN/rad)$	65,000	45,000		
$C_{v\theta}(kN/rad)$			11,000	600
$k_{\theta\theta}(kN.m/rad)$	160,000	138,000		
$C_{\theta\theta}(kN.m/rad)$			12,000	600

field, and thus significantly affect the dynamic impedances. It is important to include the structural mass at the pile head in the analysis so that the non-linear behaviour of soil can be adequately modelled.

Studies were conducted to explore the effect of structural mass on dynamic stiffnesses of pile foundations. The centrifuge tests presented early were re-analyzed by not taking the structural mass into account. A set of time-dependent shear moduli and damping ratios of soil were obtained. Dynamic impedances of the pile foundation were computed again using the new sets of soil properties. The effect of the structural mass on dynamic stiffnesses of the pile foundation is illustrated in Figure 9.19. The translational and rotational stiffnesses are used to display this effect.

The dynamic stiffnesses of the pile foundation with the full structural mass are much less than those without structural mass. This is because soils in the near field of the pile are much more strongly mobilized when the structural mass is present during shaking.
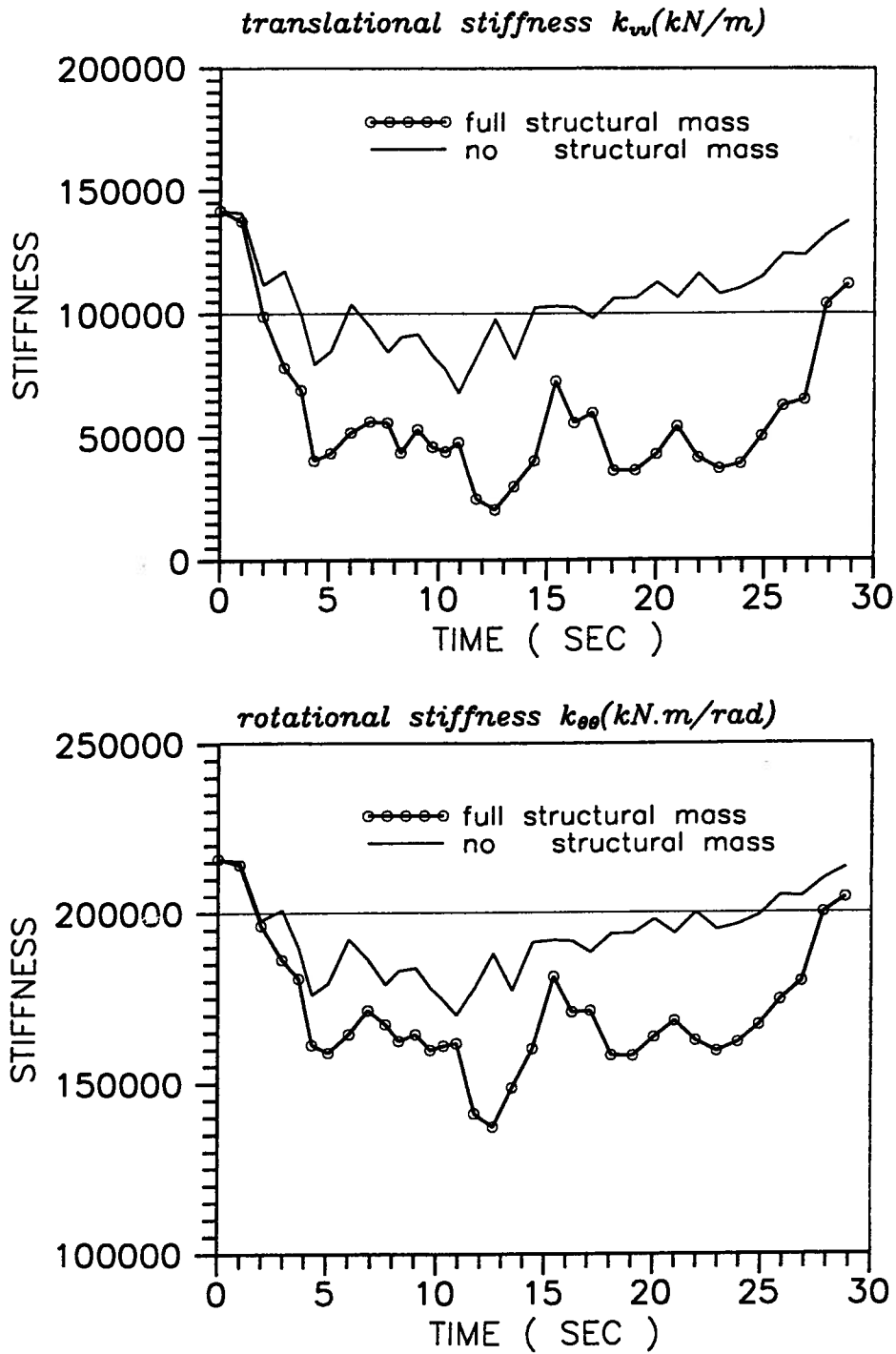
Figure 9.19: Comparison of dynamic stiffnesses of pile foundations with full structural mass and without structural mass

9.2.4 Computational times

The non-linear analysis was carried out in the time domain. The average CPU time using a PC-486(33MHz) computer needed to complete one step integration is 7.0 sec for the finite element grid shown in Figure 9.4, and 3 hours of CPU time are required for an input record of 1550 steps. The computation time is much shorter for a linear elastic analysis when the shear moduli of soil foundation remain constant through the tMime domain.

The average computational time for computing the dynamic impedances using PILIMP is 50 seconds for one set of soil properties. The total computational time required to generate curves as shown in Figures 9.14 is about 30 minutes.

9.3 Dynamic analysis of centrifuge test of a pile group

9.3.1 Description of centrifuge test on a 4-pile group (2x2)

A centrifuge test on a 4-pile (2x2) group was conducted by Gohl and reported by Gohl (1991) and Finn and Gohl (1987). The test setup is shown in Figure 9.20. The piles were set in a 2x2 arrangement at a centre to centre spacing of 2 pile diameters or 1.14 m. The properties of piles in the group are same as those of the single pile. Two of the four piles were instrumented. The piles in the group were rigidly clamped to a stiff pile cap, and four cylindrical masses were bolted to the cap at locations shown in the Figure 9.20. The top of the pile cap was the location where the four pile heads were clamped to the structural mass. A pile cap accelerometer and a displacement L.E.D. were placed at locations shown in the figure. The displacement L.E.D. was located 46 mm (2.76 m in prototype scale) above the four pile heads.

After being converted to the prototype scale, the pile cap has a mass of 220.64 $kN.sec^2/m$ and a mass moment of inertia about centre of gravity $I_{cg} = 715.39\ kN.sec^2.m$. The centre of gravity was 0.96 m above the pile-head. The piles had a free standing length of 1.21 m above the soil surface.

The sand used for the pile-group test was a dry dense sand with a void ratio $e_0=0.57$ and a mass density $\rho = 1.70 Mg/m^3$. The friction angle of the dense sand was $45°$. Gohl (1991) showed that the small strain shear modulus G_{max} can be evaluated using the Hardin and Black equation (Eq. 9.1) with a lateral stress coefficient $K_0 = 0.6$.

The four pile group was shaken by a simulated earthquake acceleration motion. Peak accelerations of up to 0.14g were applied to the base of the foundation and were dominated by frequencies in the range of 0 to 5 Hz. The free field accelerations were strongly amplified through the sand deposit to values of up to 0.26g at the surface. Pile cap accelerations of up to 0.24g and displacements up to 60 mm were recorded during the test. Residual displacements of up to 10 mm remained at the end of earthquake motion.

9.3.2 Dynamic analysis of the pile group

In the analysis, the pile cap was treated as a rigid body. Hence all pile heads, which were rigidly connected to the bottom of the pile cap, had identical translational and rotational deflections as the pile cap. In the finite element analysis, restrained nodes are used to impose the identical motions on the nodes. This technique of restraining nodes has been described in the earlier chapter and was applied in the analysis of pile groups.
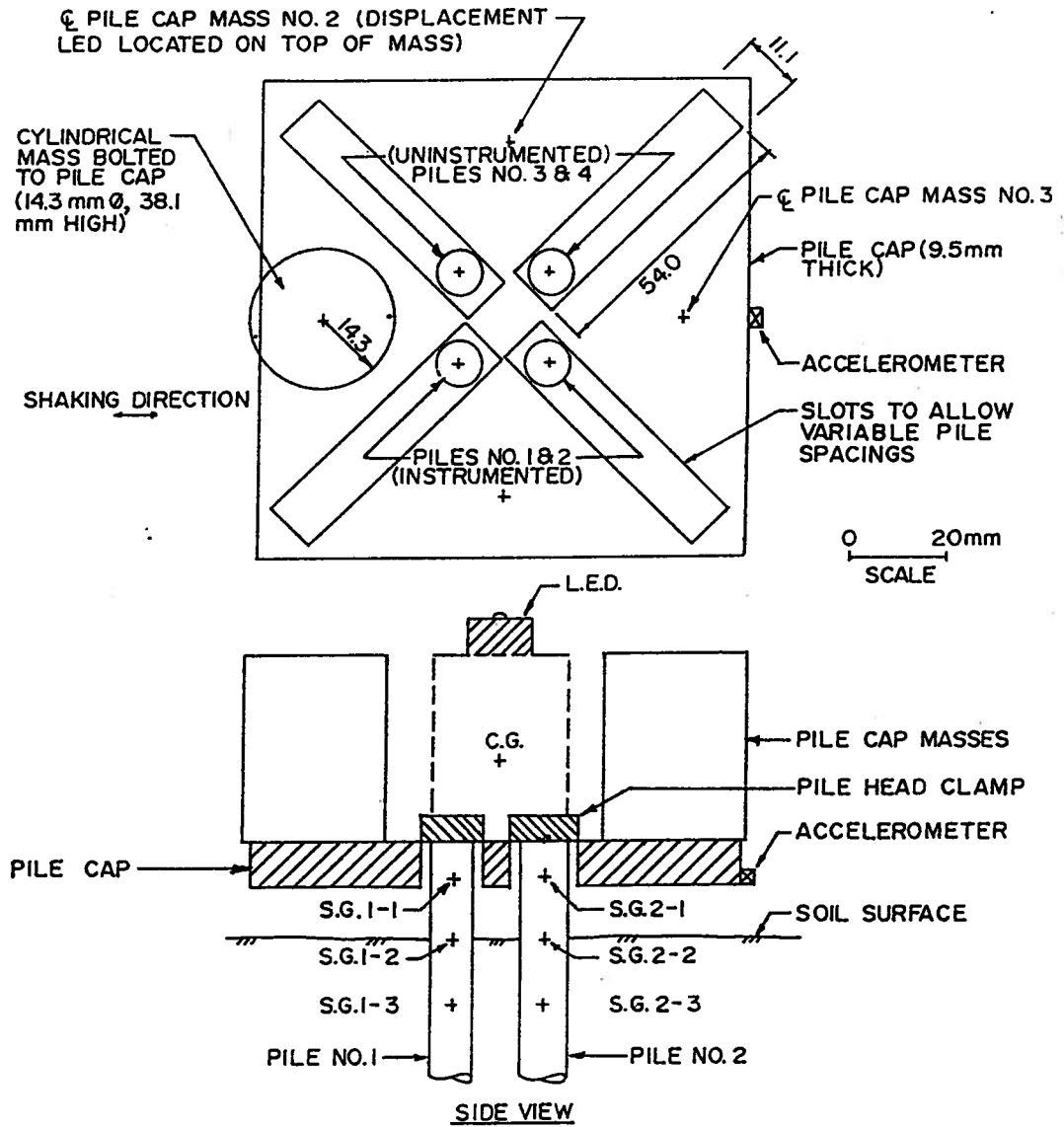
Figure 9.20: The layout of centrifuge test for 4-pile group (after Gohl, 1991)

Another important issue in the analysis of pile groups is to incorporate rocking stiffness and damping into the analysis of horizontal motions. In the proposed quasi-3D analysis, the horizontal motions are uncoupled with the vertical motions. The rocking stiffness induced by the vertical resistance of piles can not included directly in the quasi-3D analysis of horizontal motions. However the rocking impedances (resistance) may significantly restrain the rotational motions of the pile heads, and the effect of rocking impedances on the horizontal motions must be taken into account. The rocking impedances may be even larger than the rotational impedances from the pile heads, especially when the pile spacing is large.

The rocking impedances of the pile cap are included in the analysis of pile groups. They are computed by performing a separate quasi-3D analysis in the vertical mode during the analysis in the horizontal mode. This impedance calculation is made using the current values of strain dependent shear moduli and damping ratios of soil. The theory and procedures for computing such rocking impedances have been given in chapter 7. After the rocking impedances were computed for each time period, they are transferred to the pile cap as rotational stiffness and damping.

The finite element mesh used for the pile group analysis is shown in Figure 9.21. The mesh used in the present analysis has 947 nodes and 691 elements. The sand foundation was modelled by 11 horizontal layers with a smaller thickness toward the sand surface. Each pile was modelled using 15 beam elements including 5 elements for the part above soil surface. A very stiff massless beam element was used to connect the structural mass to the pile heads.

The analysis was carried out using the non-linear option to simulate the changes of

GEO.SCALE
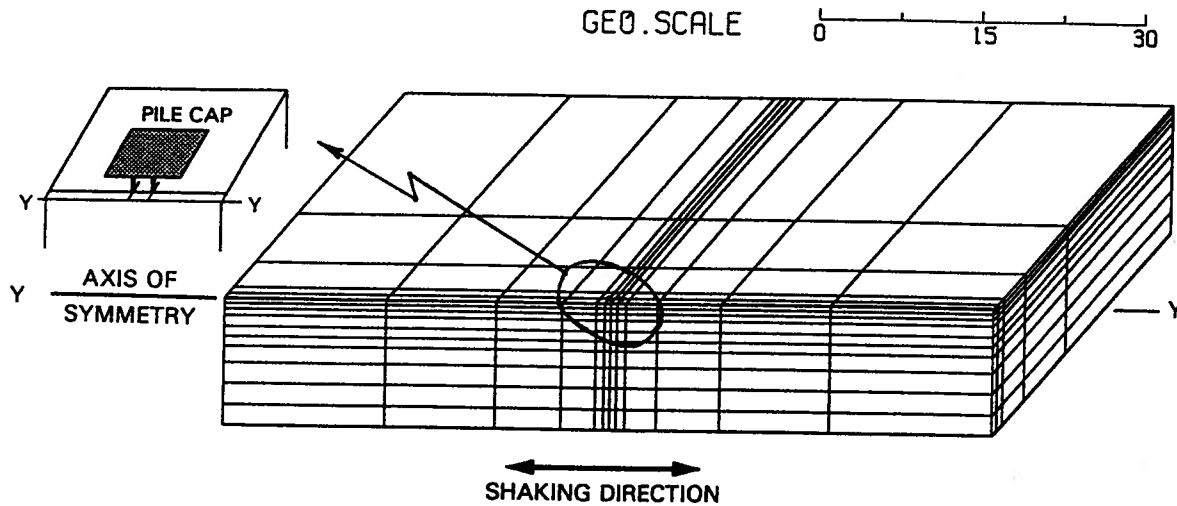
Figure 9.21: Finite element modelling of the 2x2 pile group

shear moduli and damping of soil with the shear strain. According to Gohl (1991), the shear-strain dependency of current shear moduli G and damping ratio D of the dense sand are shown in Figure 9.22. The small strain shear moduli G_{max} are functions of the overburden stresses and are estimated according to Eq. 9.1. The maximum hysteretic damping ratios D_{max} of the sand foundation are taken as 25 % following Gohl (1991).

Results of analysis Fig.9.23 shows the computed acceleration response at the pile cap versus the measured acceleration response. There is fairly good agreement between the measured and the computed accelerations. The computed peak acceleration at the pile cap is 0.23g which agrees very well with the measured peak acceleration of 0.24g.

The computed displacement at the top of the structural mass matches fairly well with the measured displacement in the first 11 secs of motion (Figure 9.24). The computed displacement response did not show any residual displacement; whereas the measured
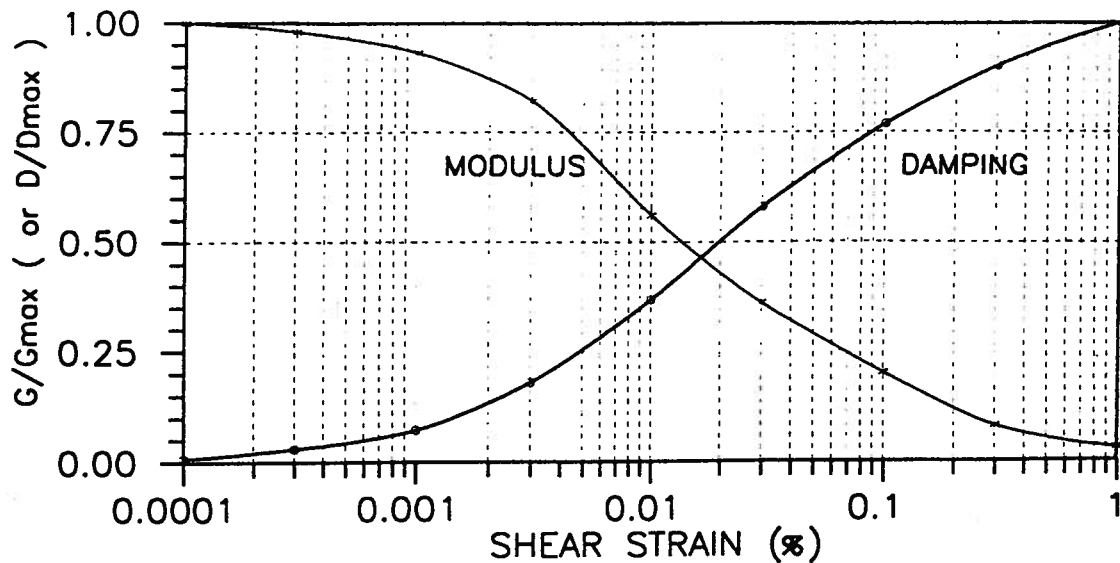
Figure 9.22: The relationships between shear modulus, damping and the shear strain for the dense sand

displacement response showed a permanent residual displacement of about 10 mm at the end of earthquake motion. This is because the analysis is carried out using the equivalent linear elastic approach.

The computed moment time history in the instrumented pile at a depth of 2.63 m in the area of maximum moment is plotted against the measured moment time history in Figure 9.25. There is good agreement between the measured and the computed moments. The distribution of computed and measured bending moments along the pile at the instant of peak pile cap displacement are shown in Figure 9.26. The computed moments agree reasonably well with the measured moments, especially in the range of maximum moments. The computed peak moment is 203 kN.m compared to a measured peak moment of 220 kN.m.
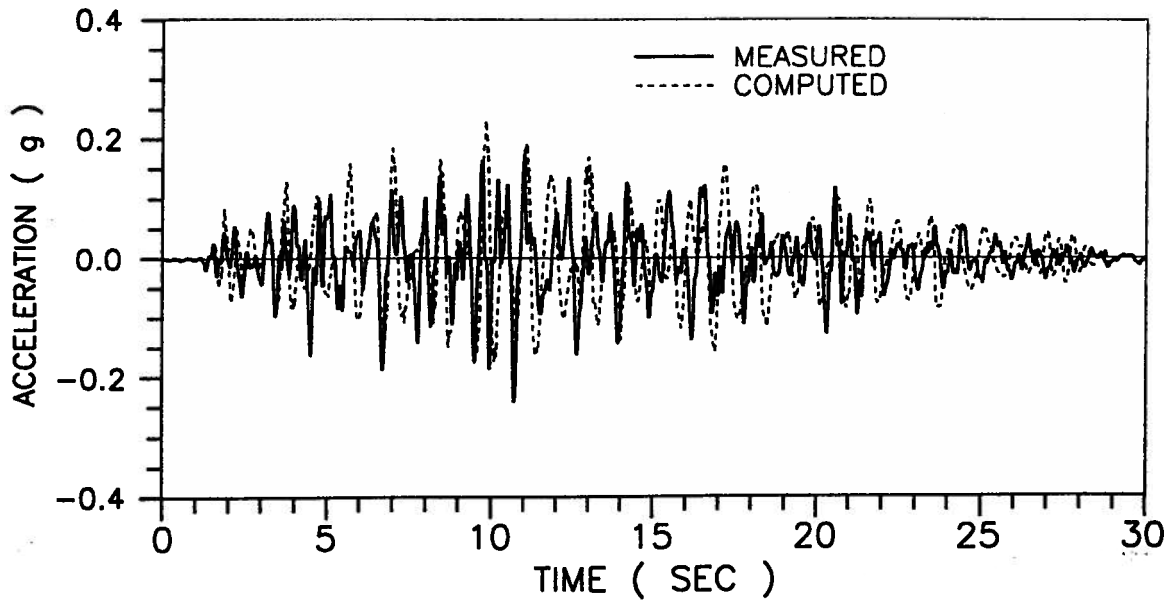
Figure 9.23: The computed versus measured acceleration responses at pile cap
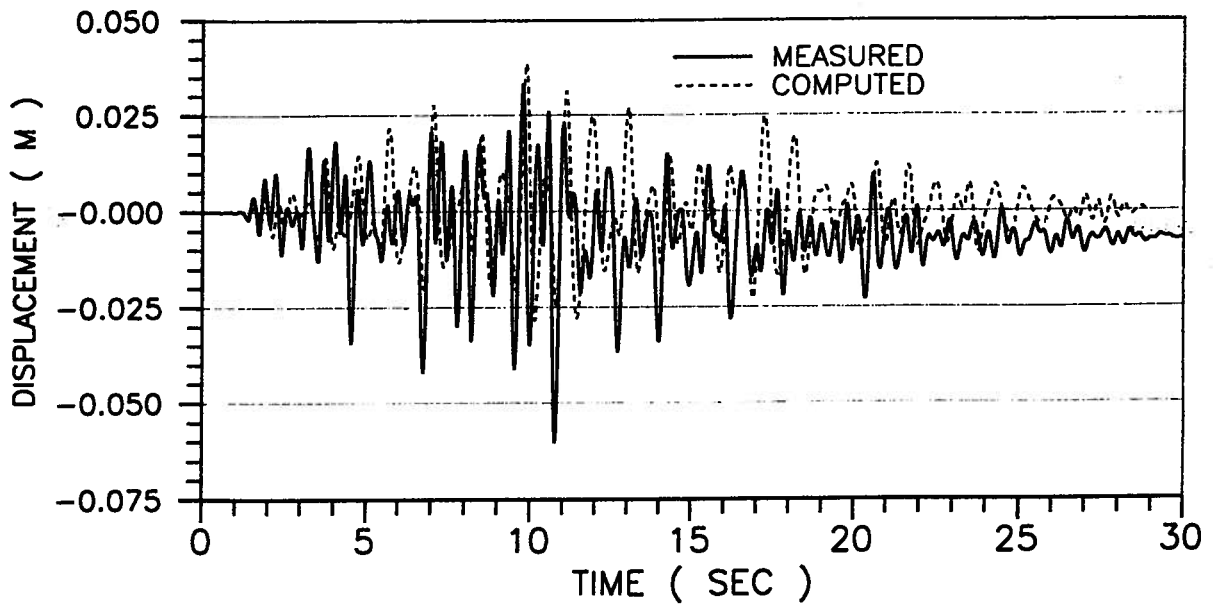
Figure 9.24: The computed versus measured displacement at top of structural mass
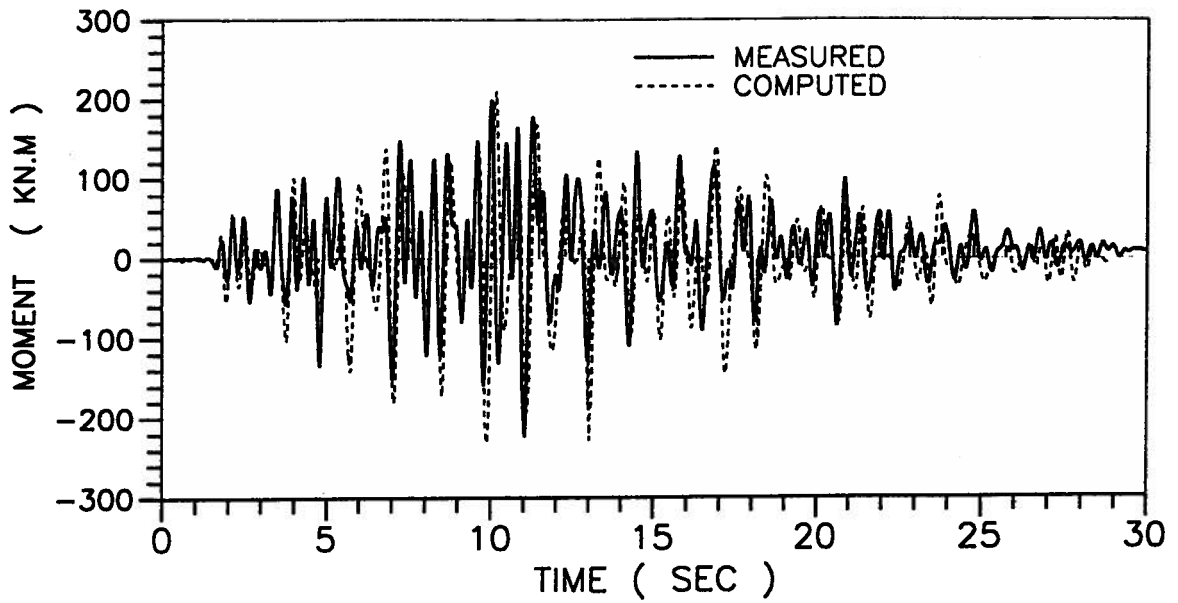
Figure 9.25: The computed versus measured moment at depth D=2.63 m
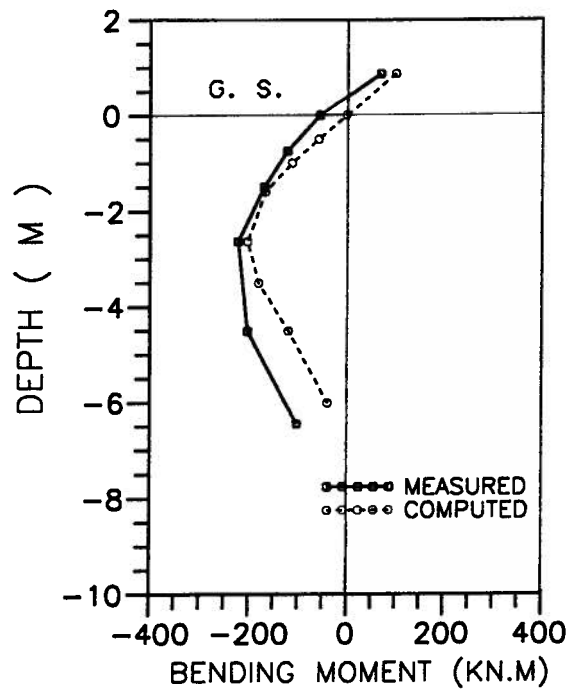
Figure 9.26: Distribution of moments at peak pile cap displacement
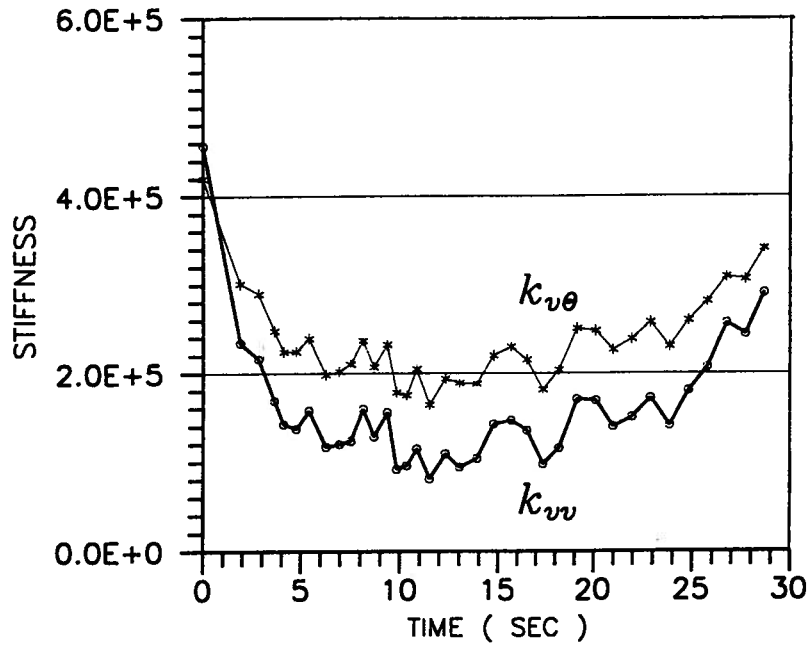
Figure 9.27: Variation of stiffnesses $k_{vv}, k_{v\theta}$ of the 4-pile group at f=1.91 Hz

9.3.3 Non-linear impedances of the 4-pile group

Applying the same technique as used in the analysis of single pile, dynamic impedances of the 4-pile group are evaluated. To illustrate the results of this analysis, the translational stiffness k_{vv} and the cross-coupling stiffness $k_{v\theta}$ of the 4-pile group are presented.

The variations of stiffnesses k_{vv} and $k_{v\theta}$ of the 4-pile group with time are shown in Figure 9.27 at an excitation frequency f=1.91 Hz. The dynamic stiffnesses of the 4-pile group k_{vv} and $k_{v\theta}$ were reduced dramatically at times when strong ground motions occurred. k_{vv} decreased to 80,000 kN/m from its initial stiffness of 460,000 kN/m; whereas $k_{v\theta}$ decreased to 160,000 kN/rad from its initial stiffness of 420,000 kN/rad. The stiffnesses k_{vv} and $k_{v\theta}$ were reduced to about 17% and 38% of their initial stiffnesses.

Part III

Summary and Suggestions for Future Work

Chapter 10

Summary and Suggestions for Future Work

10.1 Dynamic thrusts on rigid walls

Approximate methods for determining the dynamic thrusts against rigid walls subjected to horizontal dynamic loads were presented. Analytical solutions were obtained for the dynamic thrusts against rigid walls.

Calibration was made by comparing the approximate 1-g static solutions with Wood's exact 1-g static solution. Results showed that the proposed model using the shear beam analogy produces best approximation to solution of the rigid-wall problem. The computed total static thrusts are about 5% less than those from Wood's solution for any L/H ratio, in which H is the height of the wall and L is the half length of the soil backfill confined by two vertical rigid walls.

Dynamic analyses have been performed for wall-soil systems with uniform backfills and subjected to both sinusoidal motion and earthquake motion. The wall-soil systems with semi-infinite backfills are approximated by using L/H=5.0; the wall-soil systems with finite backfills are represented by using L/H=1.5.

Under sinusoidal motion, at resonant conditions the peak dynamic thrusts are $2.4\rho H^2 A_{max}$ for L/H=5.0 and $3.0\rho H^2 A_{max}$ for L/H=1.5. The static thrusts are $1.0\rho H^2 A_{max}$ for

L/H=5.0 and $0.86\rho H^2 A_{max}$ for L/H=1.5. Therefore, their corresponding dynamic amplification factors are 2.4 for L/H=5.0 and 3.5 for L/H=1.5. These results strongly suggest that the use of a static force for dynamic loading may result in serious underestimate of the dynamic thrusts against rigid walls.

The earthquake motions are represented by the scaled records of the El Centro and the Loma Prieta ground motions. The results of analyses show that the peak dynamic thrusts are $1.30\rho H^2 A_{max}$ for L/H=5.0 and $1.38\rho H^2 A_{max}$ for L/H=1.5. Their corresponding dynamic amplification factors are about 1.3 for L/H=5.0 and 1.6 for L/H=1.5. The dynamic amplification factors under earthquake motions are about 50% of that under sinusoidal motions.

Finite element formulations for evaluating the dynamic thrusts against rigid walls with non-homogeneous soil profiles have been presented. Comparisons with close-form solutions showed that the dynamic thrusts can be predicted accurately using the proposed finite element method of analysis.

An efficient computer program SPAW has been developed for determining the dynamic thrusts and moments against rigid walls. The program was designed for dynamic analysis of rigid walls with arbitrary non-homogeneous soil layers under sinusoidal motions and earthquake motions. A finite element mesh necessary for the analysis has been embedded in SPAW so that only the properties of soil layers are required for input. The computational time for a dynamic time-history analysis is only few minutes in a PC486 33MHz computer.

For soil profiles with linear variation of shear modulus with depth, the analyses revealed that the peak dynamic thrust at resonance is $1.56\rho H^2 A_{max}$ for sinusoidal motions. The peak dynamic thrust reduces to $1.0\rho H^2 A_{max}$ for the scaled El Centro input. For soil profiles with parabolic variation of shear modulus with depth, the peak dynamic thrust at resonance is $1.87\rho H^2 A_{max}$ for sinusoidal motions. The peak dynamic thrust reduces to $1.18\rho H^2 A_{max}$ for the El Centro input.

Because the static force is about $0.71\rho H^2 A_{max}$ for linear soil profiles and $0.82\rho H^2 A_{max}$ for parabolic soil profiles. The corresponding dynamic amplification factors are 2.3 for sinusoidal motions and 1.4 for earthquake motions. The dynamic thrust at resonance for sinusoidal motions are about 60% greater than that for earthquake motions with same peak acceleration.

Results from the equivalent linear elastic analyses show that the non-linearity of soils has significant effects on the dynamic thrusts. For parabolic soil profiles the peak dynamic thrust of a wall-soil system under strong shaking (0.35g) due to non-linear effect is about 25% higher than that obtained using the linear elastic analysis. This result was obtained using the scaled El Centro input as the base motion. For wall-soil systems that have different soil profiles or that are subjected to other earthquake motions, the finite element program SPAW can be readily applied to evaluate the dynamic response of the systems.

The conclusions made on the study of dynamic thrusts on rigid walls are presented as follows:

1. The proposed simplified wave equation has been successfully applied to determine the dynamic thrusts and moments acting on rigid walls. It implies that the dynamic motions of soil structure under horizontal motions are mainly governed by the waves in the horizontal directions.

2. It is recommended that the mode superposition method be used to determine the peak dynamic thrusts against rigid walls. The use of the absolute summation of modal thrust is suggested when the response spectrum method is selected, especially at low frequency ratios.

3. When wall-soil systems are subjected to dynamic loading, the total thrusts computed using the 1-g static solution should not be used to represent the peak dynamic thrust. The use of static solution may cause significant error of dynamic thrust especially at resonance. A dynamic analysis is required under dynamic loading.

4. The height of the resultant dynamic thrust is generally suggested to be at 0.6H above the base of the wall for a wall height of H. However for non-homogeneous soil profiles, such as linear soil profiles or parabolic soil profiles, the height may decrease to about 0.5H.

5. The peak dynamic thrusts become large when the soil profile becomes more uniform. Under sinusoidal motions, the peak dynamic thrusts at resonance are $1.56\rho H^2 A_{max}$, $1.87\rho H^2 A_{max}$ and $2.40\rho H^2 A_{max}$ for linear, parabolic and uniform soil profiles, respectively. For scaled El Centro input, the peak dynamic thrusts are $1.00\rho H^2 A_{max}$, $1.18\rho H^2 A_{max}$ and $1.30\rho H^2 A_{max}$ for linear, parabolic and uniform soil profiles, respectively. These results are obtained for wall-soil systems with L/H=5.0 and λ=10%.

6. The effect of soil non-linearity on the dynamic thrust seems to be significant for

rigid walls. A 25% increase of peak dynamic thrust may be expected for wall-soil systems subjected to earthquake motions with peak accelerations in the order of 0.35g, compared to results from a linear elastic analysis.

Suggestions For future research, studies should be focused on including the effects of seismic pore water pressures in a saturated backfill on the dynamic thrusts. The development of pore water pressure may significantly reduce the shear moduli of soils. Also one should be aware of that the mechanism of liquefaction in soil layers confined by rigid walls is different from that in a free field. The shear strains of soils are much less especially in the area near the wall.

10.2 Dynamic analyses of pile foundations

A quasi-3D finite element method of analysis has been proposed to determine dynamic response of pile foundations subjected to horizontal loading. The proposed model is based on a simplified 3-D wave equation. The 3-dimensional dynamic response of soil is simulated by displacements in the horizontal shaking direction. Displacements in the vertical direction and in the horizontal cross-shaking direction are neglected. The use of the proposed simplified wave equation greatly saves the computing space and computing time for the finite element analysis. However it maintains adequate accuracy in the modelling of the dynamic response of pile foundations.

The proposed quasi-3D theory is first incorporated using the finite element method in the frequency domain. This formulation is used for the analysis of elastic response of pile foundations. Elastic solutions of Kaynia and Kausel (1982) have been used to validate the proposed model for elastic response. Dynamic impedances of single piles and 2x2 pile groups have been computed and compared with those obtained by Kaynia

and Kausel (1982). Also kinematic interaction factors of single piles have been computed and compared with those obtained by Fan et al. (1991) who used solutions by Kaynia and Kausel. The computed results from the proposed quasi-3D model agreed well with the results by Kaynia and Kausel.

Full scale vibration tests of a single pile and a 6-pile group have been analyzed using the proposed quasi-3D model. For the single expanded base pile, the computed fundamental frequency of the pile cap system was 6.67 Hz, which agreed well with the measured fundamental frequency of 6.5 Hz. The computed damping ratio is 6% compared to a measured damping ratio of 4%. For the 6-pile group supporting a transformer bank, the computed fundamental frequencies of the transformer-pile cap were 3.74 Hz and 4.63 Hz in the NS and EW directions, respectively, which agreed well with the measured fundamental frequencies of 3.8 Hz and 4.6 Hz in the corresponding two directions. The computed damping ratios of the system in the two directions were 9% and 9%, compared to measured damping ratios of 6% and 5%. The damping ratios were overestimated using the proposed model.

The proposed quasi-3D method is also formulated in the time domain using the finite element method. This formulation is targeted for the analyses of non-linear response of pile foundations under earthquake loading. The time-domain analysis allows modelling the variations of soil properties with time under earthquake loading.

The procedures of non-linear time-domain analysis are incorporated in the computer program PILE3D. In PILE3D, the shear stress-strain relationship of soil is simulated to be either linear elastic or non-linear elastic. When the non-linear option is used, the shear modulus and the hysteretic damping are determined using a modified equivalent

linear approach based on the computed levels of dynamic shear strains. Features such as shear yielding and tension cut-off are incorporated in PILE3D as well. The dynamic response of pile groups can also be effectively modelled using PILE3D.

Centrifuge tests of a single pile and a 2x2 pile group have been analyzed using the proposed quasi-3D finite element method of analysis. The ability of the program PILE3D to model the dynamic response of the pile supported structures under moderately strong shaking has been proven adequate for engineering purpose. These studies suggest that the shear-strain dependent shear moduli and damping ratios of soil is modelled adequately in the analysis by using the modified equivalent linear approach. Also the approximate method for modelling the shear yielding and the tension cut-off seems to yield satisfactory results.

The other important feature of the proposed method is that the time histories of dynamic impedances of single piles and pile groups can be computed. This is the first time that this has been done.

The results of analyses showed that stiffnesses of the pile foundations decrease with the level of shaking; the dampings of the pile foundations increase with the level of shaking. In a seismic event, the translational stiffness k_{vv} decreases the most due to the shear strain dependency of the stiffness; the rotational stiffness $k_{\theta\theta}$ shows the least effect of shear strain. At the moderately strong shaking of the centrifuge tests, the translational stiffness would decrease to as much as 15% of its initial stiffness; however the rotational stiffness decreases to about 60% of its initial stiffness. The variation of the cross-coupling stiffness $k_{v\theta}$ is around 50% of its initial stiffness.

The dynamic stiffnesses of pile foundations are little affected by the excitation frequencies in the range of earthquake loadings, $f \leq 10Hz$. However the damping usually increases with excitation frequency. The damping can be represented by the hysteretic and radiation damping components. The coefficient of equivalent viscous damping can be determined according to the damping at any specific frequency. Generally viscous damping coefficients decrease with excitation frequency.

The quasi-3D finite element method has been proven to be a very cost-effective method. Using a PC-486 (33MHz) computer, 3 hours of CPU time are required to conduct the non-linear analysis of a single pile for an input record of about 30 seconds. For the same length of input record, 30 minutes of CPU time is required for computing the pile impedances associated with the time-dependent soil properties.

Studies presented in this thesis lead to general conclusions on dynamic response of pile foundations as follows:

1. The proposed quasi-3D finite element method of analysis is an effective approach for determining elastic response of pile foundations and analyzing non-linear response of pile foundations under earthquake loading. The simplified 3-D wave equations of motion greatly reduce the computing time of the finite element analysis. The error of results caused by the quasi-3D model is minor especially at low frequencies such as those in an earthquake motion.

2. A quasi-3D finite element program PILIMP has been developed for analyses of elastic response of single piles and pile groups. Analyses are performed in the frequency domain. The proposed model has been validated using the elastic solutions from

Kaynia and Kausel (1982) and data from full scale vibration tests of a single pile and a 6-pile group.

3. A quasi-3D finite element program PILE3D has been developed for the analyses of non-linear response of single piles and pile groups. Analyses are performed in the time domain. The characteristics of soil non-linearity with strains is modelled using the modified equivalent linear approach. Other features such as the modelling of shear yielding and tension cut-off are incorporated in PILE3D. The program is applicable for analyses of single piles as well as pile groups.

4. The proposed model for modelling non-linear response of pile foundations under earthquake loading has been validated using data from centrifuge tests of a single pile and 2x2 pile group. Satisfactory results have been obtained.

5. Time-dependent variations of dynamic impedances of pile foundations during shaking can be evaluated and have been demonstrated for the model pile foundations used in the centrifuge tests. The results of analyses showed that stiffnesses of pile foundations decrease with the level of shaking. The translational stiffness k_{vv} decreases the most at high strain level; the rotational stiffness $k_{\theta\theta}$ decreases the least. However, the damping of pile foundations increases with the level of shaking.

Suggestions for future work For future research on dynamic response of pile foundations, studies should be focused on including the effects of seismic pore water pressures on the response of pile foundations. This next step is very important because pile foundations are often used at potentially liquefiable sites.

Bibliography

[1] American Petroleum Institute (1986). " Recommended Practice for Planning, Designing and Constructing Fixed Offshore Platforms," 16th edition, Dallas, TX.

[2] Angelides, D.C., and Roesset J.M., (1981). "Non-linear Lateral Dynamic Stiffness of Piles," ASCE, Jour. of the Geotech. Engineering Division, vol. 107, no. GT11, pp.1443-1460

[3] Arnold, P., Idriss, I.M., Reimer, R.B., Beebe, K.E., and Marshall, P.W. (1977). " A Study of Soil-Pile-Structure Systems in Severe Earthquakes," OTC 2749, 9th Offshore Technology Conference, Houston, Texas, pp. 189-198.

[4] Bea, R.G., Litton, R., Nour-Omid, S. and Chang, J.Y. (1984). "A Specialized Design and Research Tool for the Modelling of Near-Field Soil Interactions," OTC 4806, 16th Offshore Technology Conference, Houston, Texas, pp. 249-252.

[5] Brown, D.A. and Shie, C.F. (1991). "Modification of p-y Curves to Account for Group Effects on Laterally Loaded Piles." Geotechnical Engineering Congress 1991, ASCE, Geotechnical Special Publication No. 27, vol. 1, pp. 479-490.

[6] Clough, R.W. and Penzien, J., (1975). Dynamics of Structures. McGraw-Hill Book Company.

[7] Crouse, C.B. and Cheang, L., (1987). " Dynamic Testing and Analysis of Pile-Group Foundations." Dynamic Response of Pile Foundations - Experiment, Analysis and Observation, ASCE Geotech. Special Publication No. 11, 79-98.

[8] Davies, T.G., Sen, R., and Banerjee, P.K. (1985). " Dynamic Behaviour of Pile Groups in Inhomogeneous Soil," J. Geotech. Eng., ASCE, Vol. 111, No. 12, pp. 1365-1379.

[9] El-Marsafawi, H., Kaynia, A.M., and Novak, M. (1992a). " Interaction Factors and the Superposition Method for Pile Group Dynamic Analysis," Research Report, GEOT-1-1992, Univ. of Western Ontario, London, Ontario.

[10] El-Marsafawi, H., Kaynia, A.M., and Novak, M. (1992b). " The Superposition Approach to Pile Group Dynamics," Geotechnical Special Publication No. 34, ASCE, New York, N.Y., pp. 114-136.

[11] El Sharnouby, B. and Novak, M., (1986). "Flexibility Coefficients and Interaction Factors for Pile Group Analysis." Can. Geotech. J., 23, 441-450.

[12] Fan, K., Gazetas, G., Kaynia, A., Kausel, E., and Shahid, A., (1991). "Kinematic Seismic Response of Single Piles and Pile Groups." Jour. of Geotech. Engineering Division, ASCE, Vol 117(12), 1860-1879.

[13] Finn, W.D. Liam, Lee, K.W. and Martin, G.R. (1977)." An Effective Stress Model for Liquefaction", Journal of the Geotech. Engineering Division, ASCE, June, 517-533.

[14] Finn, W.D. Liam, and Gohl, W.B., (1987)." Centrifuge Model Studies of Piles under Simulated Earthquake Loading," Dynamic Response of Pile Foundations - Experiment, Analysis and Observation, ASCE Geotech. Special Publication No. 11, 21-38.

[15] Finn, W.D. Liam, M. Yogendrakumar, N. Yoshida and H. Yoshida. (1986). "TARA-3: A Program for Nonlinear Static and Dynamic Effective Stress Analysis," Soil Dynamics Group, University of British Columbia, Vancouver, B.C., Canada.

[16] Gazetas, G. (1984). "Seismic Response of End-Bearing Piles," Soil Dynamics and Earthquake Engineering, Vol.3, No.2, pp. 82-94.

[17] Gazetas, G., Fan, K. and Kaynia, A. (1993). "Dynamic Response of Pile Groups with Different Configurations," Soil Dynamics and Earthquake Engineering, No. 12, pp.239-257.

[18] Gazetas, G. and Dobry, R., (1984). " Horizontal Response of Piles in Layered Soils," ASCE, Jour. of the Geotech. Engineering Division, Vol. 110, No.1, pp.20-41

[19] Gazetas, G. and Makris, N. (1991a). "Dynamic Pile-Soil-Pile Interaction. Part I: Analysis of Axial Vibration," Earthquake Engineering Structure Dynamics, Vol. 20, No.2, pp.115-132.

[20] Gazetas, G., Fan, K., Kaynia, A.M. and Kausel, E. (1991b). " Dynamic Interaction Factors for Floating Pile Groups," J. Geotech. Eng., ASCE, Vol. 117, No. 10, pp.1531-1548.

[21] Gazetas, G.,Fan, K., Tazoh, T., Shimizu, K., Kavvadas, M. and Makris, N. (1992). " Seismic Pile-Group-Structure Interaction," ASCE National Convention, proc. specialty session on "Piles Under Dynamic Loads," Geotech. Special Publication No. 34, pp. 56-94.

[22] Gazioglu, S.M. and O'Neil M.W. (1984). " Evaluation of P-Y Relationships in Cohesive Soils," from "Analysis and Design of Pile Foundations," proc. of a symp. sponsored by the ASCE Geotechnical Engineering Division, ASCE National Convention, San Francisco, Calif. Oct. 1-5, 1984, pp. 192-214.

[23] Gohl, W.B., (1991)." Response of Pile Foundations to Simulated Earthquake Loading: Experimental and Analytical Results," Ph.D. Thesis, Dept. of Civil Engineering, Univ. of British Columbia, Vancouver, B.C., Canada.

[24] Hardin, B.O., and Drnevich, V.P., (1972)." Shear Modulus and Damping in Soils: Design Equations and Curves," Jour. of Soil Mech. and Found. Div., ASCE, 98(7), 667-692.

[25] Hardin, B.O., and Black, W.L., (1968)." Vibration Modulus of Normally Consolidated Clay," ASCE, J. Soil Mechanics and Foundations Division, Vol. 94, 353-369.

[26] Idriss, I.M., et al., (1973)." A Computer Program for Evaluating the Seismic Response of Soil Structures by Variable Damping Finite Element Procedures," Report

No. EERC 73-16, Earthquake Engineering Research Centre, University of California, Berkeley, Calif., July.

[27] Idriss, I.M., Seed, H.B., and Serff, N., (1974). "Seismic Response by Variable Damping Finite Elements" Jour. of Geotech. Engineering Division, ASCE, 100(1), 1-13.

[28] Kaynia, A.M., (1982). " Dynamic Stiffness and Seismic Response of Pile Groups," MIT Research Report R82-03, Cambridge, MA, USA.

[29] Kaynia, A.M. and Kausel, E., (1982). "Dynamic Behaviour of Pile Groups." Proc. of Conf. on Numerical Methods in Offshore Piling, Univ. of Texas, Austin, Texas, USA, 509-532.

[30] Lee, M.K.W., and Finn, W.D. Liam (1978). "DESRA-2: Dynamic Effective Stress Response Analysis of Soil Deposits with Energy Transmitting Boundary Including Assessment of Liquefaction Potential," Soil Mechanics Series Report No. 38, Dept. of Civil Engineering, University of British Columbia, Vancouver, Canada.

[31] Matlock, H., Foo, S.H.C., and Bryant L.M., (1978a). " Simulation of Lateral Pile Behaviour Under Earthquake Motion," Proc. Earthquake Engineering and Soil Dynamics, ASCE Specialty Conference, Pasadena, Calif., pp. 601-619.

[32] Matlock, H., Foo, S.H.C., and Cheang L.C., (1978b). " Example of Soil Pile Coupling Under Seismic Loading," proc. 10th Annual Offshore Technology Conference, Houston, Texas, paper no. OTC 3310.

[33] Matlock, H., and Foo, S.H.C. (1980) " Axial Analysis of Piles Using a Hysteretic Degrading Soil Model," Proc. Int. Symp. Numer. Methods Offshore Piling, Institute of Civil Engineers, London, pp. 127-133.

[34] Matuo, H., and Ohara, S. (1960) " Lateral Earthquake Pressure and Stability of Quay Walls During Earthquakes," Proceedings, Second World Conference on Earthquake Engineering, Vol. 2.

[35] Mononobe, N., and Matuo, H. (1929) " On the Determination of Earth Pressure during Earthquakes," Proceedings, World Engineering Conference, Vol 9.

[36] Murchison, J.M. and O'Neil M.W. (1984). " Evaluation of P-Y Relationships in Cohesionless Soils," from "Analysis and Design of Pile Foundations," proc. of a symp. sponsored by the ASCE Geotechnical Engineering Division, ASCE National Convention, San Francisco, Calif. Oct. 1-5, 1984, pp. 174-192.

[37] Newmark, N.M., (1959). " A Method of Computation for Structural Dynamics," Jour. of the Engineering Mechanics Division, ASCE, Vol. 85, EM3, July.

[38] Nogami, T. and Chen, H.L., (1987). "Prediction of Dynamic Lateral Response of Non-linear Single Pile by Using Winkler Soil Model," Dynamic Response of Pile Foundations - Experiment, Analysis and Observation, ASCE Geotech. Special Publication No. 11, pp.39-52.

[39] Nogami, T., and Novak, M., (1977). " Resistance of Soil to a Horizontally Vibrating Pile," J. Earthquake Engineering and Structural Dynamics, Vol.5, pp.249-261.

[40] Novak, M., Nogami, T., and Aboul-Ella, F. (1978). " Dynamic Soil Reactions for Plane Strain Case," ASCE, J. Engineering Mechanics Division, vol. 104, no EM4, pp.953-959

[41] Novak, M. and Sheta, M. (1980). " Approximate Approach to Contact Effects of Piles," Proc. "Dynamic Response of Pile Foundations: Analytical Aspects," ASCE National Convention, Oct. 30,1980, ed. M.W. O'Neil and R. Dobry

[42] Novak, M., Sheta, M., El-Hifnawy, L., El-Marsafawi, H. and Ramadan, O., (1990) "DYNA3, A Computer Program for Calculation of Foundation Response to Dynamic Loads. Users Manual." Geotech. Research Centre, The University of Western Ontario, London, Ontario, Canada.

[43] Novak,M. and Sheta, M. (1982). "Dynamic Response of Piles and Pile Groups," Proc. 2nd International Conference on Numerical Methods in Offshore Piling, U. of Texas, Austin, Apr. 29-30,1982, pp.489-507

[44] Novak, M., (1974). " Dynamic Stiffness and Damping of Piles," Canadian Geotech. Jour., Vol. 11, No.4, 574-598.

[45] Novak, M., Nogami, T. (1977). " Soil Pile Interaction in Horizontal Vibration," Earthquake Engineering Structural Dynamics, Vol. 5,263-282.

[46] Novak, M.,(1991). " Piles under Dynamic Loads." State of the Art Paper, 2nd Int. Conf. on Recent Advances in Geotech. Earthquake Engineering and Soil Dynamics, Univ. of Missouri-Rolla, Rolla, Missouri, Vol. III, 250-273.

[47] Novak, M. and Aboul-Ella, F. (1978a). "Impedance Functions of Piles in Layered Media," J. Eng. Mech. Div. ASCE, June, Vol.104, no. EM3 pp.643-661.

[48] Novak, M. and Aboul-Ella, F. (1978b). " Stiffness and Damping of Piles in Layered Media," Proc. Earthq. Eng. & Soil Dyn., ASCE Specialty Conf., Pasadena, CA, June 19-21, pp.704-719.

[49] Okabe, S. (1926) "General Theory of Earth Pressure," Journal, Japanese Society of Civil Engineers, Vol. 12, No. 1.

[50] Penzien, J., (1970). "Soil-Pile Foundation Interaction," from "Earthquake Engineering," ed. R.L. Wiegel, Prentice-Hall Inc. Englewood Cliffs, New Jersey, pp. 349-381.

[51] Poulos, H.G. (1971). "Behaviour of Laterally Loaded Piles. II- Pile Groups," Journal of the Soil Mechanics Division, ASCE, Vol. 97, No. SM5, pp. 733-751.

[52] Poulos, H.G. (1975). "Lateral Load Deflection Prediction for Pile Groups," Journal of the Geotechnical Engineering Division, ASCE, No. GT1, pp. 19-34.

[53] Poulos, H.G. (1979). "Groups Factor for Pile-Deflection Estimation," Journal of the Geotechnical Engineering Division, ASCE, No. GT12, pp. 1489-1509.

[54] Poulos, H.G. and Davis, E.H., (1980). Pile Foundation Analysis and Design. John Wiley & Sons.

[55] Prakash, S. and Sharma, H.D., 1990. Pile Foundation in Engineering Practice. John Wiley & Sons, Inc.

[56] Rayleigh, L., Theory of Sound, Vol. I, Dover Publications Inc., New York, N.Y., 1945.

[57] Roesset, J.M. and Angelides, D. (1980). " Dynamic Stiffness of Piles," from "Numerical Methods in Offshore Piling," Institution of Civil Engineering, pp.75-81

[58] Schnabel, P.B., Lysmer, J., and Seed, H.B., (1972). "SHAKE: A Computer Program for Earthquake Response Analysis of Horizontally Layered Sites," Report No. EERC 72-12, Earthquake Engineering Research Centre, University of California, Berkeley, Calif., Feb..

[59] Scott, R.F. (1973) "Earthquake-Induced Earth Pressures on Retaining Walls," Proceedings, Fifth World Conference on Earthquake Engineering, Rome, Italy.

[60] Seed, H. B., and Whitman, R. V. (1970) " Design of Earth Retaining Structures for Dynamic Loads," Lateral Stresses in the Ground and Design of Earth-Retaining Structures, ASCE.

[61] Seed, H.B., Wong, R.T., Idriss, I.M., and Tokimatsu, K., (1986). " Moduli and Damping Factors for Dynamic Analyses of Cohesionless Soils," Jour. of Geotech. Engineering Division, ASCE, 112(11), 1016-1032.

[62] Seed, H.B., and Idriss, I.M. (1967) " Analysis of Soil Liquefaction: Nigatta Earthquake," Jour. Soil Mechanics and Foundation Division, ASCE, Vol. 93, No. SM3, pp. 83-108.

[63] Seed, H.B., and Idriss, I.M. (1970) " Soil Moduli and Damping Factors for Dynamic Response Analyses," Report No. ERRC 70-10, Earthquake Engineering Research

Center, University of California, Berkeley, California, December

[64] Stevens, J.B. and Audibert, J.M.E. (1979). " Re-examination of P-Y Curve Formulations," 11th Offshore Technology Conference, Houston, Texas, pp. 397-401.

[65] Sy, A., (1992). " An Alternative Analysis of Vibration Tests on Two Pile Group Foundations," Piles under Dynamic Loads, ASCE Geotech. Special Publication No. 34, 136-152.

[66] Sy, A. and Siu, D., (1992). " Forced Vibration Testing of An Expanded Base Concrete Pile," Piles under Dynamic Loads, ASCE Geotech. Special Publication No. 34, 170-186.

[67] Tajimi, H. (1966;1969). " Earthquake Response of Foundation Structures", Rep. of Fac. Sci. Eng., Nihon University, 1966.3, 1.1-3.5 (in Japanese). See also Tajimi, H. " Dynamic Analysis of a Structure Embedded in an Elastic Stratum", Proc. 4th WCEE, Chile.

[68] Veletsos, A.S. and Younan, A.H. (1994). "Dynamic Soil Pressures on Rigid Vertical Walls," International Journal of Earthquake Engineering and Structural Dynamics, Vol. 23, No.3, pp275-301.

[69] Wilson, E.L., Farhoomand, L., and Bathe, K.J., (1973). "Nonlinear Dynamic Analysis of Complex Structures," International Journal of Earthquake Engineering and Structural Dynamics, Vol. 1, No.3, Jan.-March.

[70] Wood, J. H. (1973) " Earthquake-Induced Soil Pressures on Structures ," Ph.D thesis submitted to the California Institute of Technology, Pasadena, Calif., USA.

[71] Yan, L. (1990). "Hydraulic Gradient Similitude Method for Geotechnical Modelling Tests with Emphasis on Laterally Loaded Piles." Ph.D. Thesis, Faculty of Graduate Studies, Univ. of British Columbia, Vancouver, Canada

[72] Yegian, Y. and Wright, S. (1973). "Lateral Soil Resistance-Displacement Relationships for Pile Foundations in Soft Clays," OTC 1893, 5th Offshore Technology

Conference, vol. 2, pp.663-671.

Derivation of Equations for the Proposed Model: Rigid-Wall Problem

The proposed model is an extension of the classic shear beam model to include horizontal normal stresses in the direction of shaking.

The shear stress τ_{xy} is given by

$$\tau_{xy} = G(\frac{\partial u}{\partial y} + \frac{\partial v}{\partial x})$$ (.1)

In the shear beam $\frac{\partial v}{\partial x} = 0$

$$\tau_{xy} = G\frac{\partial u}{\partial y}$$ (.2)

The normal stress σ_x in the direction of shaking is determined using the assumption $\sigma_y=0$

$$\sigma_y = \frac{2G}{1 - 2\nu}[(1 - \nu)\frac{\partial v}{\partial y} + \nu\frac{\partial u}{\partial x}] = 0$$ (.3)

Therefore

$$\frac{\partial v}{\partial y} = -\frac{\nu}{1 - \nu}\frac{\partial u}{\partial x}$$ (.4)

The normal stress σ_x in the direction of shaking is given by

$$\sigma_x = \frac{2G}{1 - 2\nu}[(1 - \nu)\frac{\partial u}{\partial x} + \nu\frac{\partial v}{\partial y}]$$ (.5)

Substituting for $\frac{\partial v}{\partial y}$

$$\sigma_x = \frac{2}{1 - \nu}G\frac{\partial u}{\partial x}$$ (.6)

Substituting Eq. .2 and Eq. .6 into the equilibrium equation

$$\frac{\partial \sigma_x}{\partial x} + \frac{\partial \tau_{xy}}{\partial y} = \rho \frac{\partial^2 u}{\partial t^2} \qquad (.7)$$

one finds that

$$\frac{2}{1-\nu}\frac{\partial^2 u}{\partial x^2} + G\frac{\partial^2 u}{\partial y^2} = \rho \frac{\partial^2 u}{\partial t^2} \qquad (.8)$$

Therefore by comparison with Eq. (3.6) and (3.7)

$$\theta = \beta = \frac{2}{1-\nu} \qquad (.9)$$

Eq. .8 satisfies equilibrium but does not satisfy second order compatibility.